NORTHWESTERN UNIVERSITY

Isocitrate Dehydrogenase 3 and One-Carbon Metabolism:

Defining a Novel Role for Isocitrate Dehydrogenase 3 in Glioblastoma

A DISSERTATION

SUBMITTED TO THE GRADUATE SCHOOL

IN PARTIAL FULLFILLMENT OF THE REQUIREMENTS

for the degree

DOCTOR OF PHILOSOPHY

Field of Driskill Graduate Training Program in Life Sciences

By

Jasmine L. May

EVANSTON, ILLINOIS

September 2018

ABSTRACT

Isocitrate Dehydrogenase 3 and One-Carbon Metabolism:

Defining a Novel Role for Isocitrate Dehydrogenase 3 in Glioblastoma

Jasmine L. May

Glioblastoma (GBM) is a highly malignant brain tumor that accounts for the most commonly diagnosed type of primary brain tumors in adults. It has a poor prognosis of only 15 months from the time of diagnosis. The gold standard therapy regimen consists of radiotherapy and the chemotherapeutic temozolomide. Both of these therapies can have major side effects and no major strides have been made to improve the therapeutic options or outcomes. Many researchers have been investigating GBM to discover druggable targets that might have fewer side effects and improve disease prognosis. Of late many researchers have been investigating a group of enzymes called isocitrate dehydrogenase (IDH) enzymes. They are a key group of enzymes important for the conversion of isocitrate (ICT) to α-ketoglutarate (α-KG). IDH1 carries out this conversion in the cytosol supplying α-KG. α-KG is important for fatty acid synthesis and to act as a co-factor for other enzymes that regulate histone methylation and protein degradation. IDH2 and IDH3 carry out the reaction as part of the tricarboxylic acid (TCA) cycle. Therefore, IDH2 and IDH3 are important for energy production in the mitochondria. IDH1 and IDH2 have frequently been found to be mutated in the setting of GBM, in particular in secondary GBM, GBM that develops from low grade gliomas, while wild type IDH1 is more commonly found in primary GBM, GBM that arises de novo. Recently our lab determined that wild type IDH1 promotes primary GBM growth and receptor tyrosine kinase inhibitor resistance. While IDH1

and IDH2 has been the focus in GBM research, very little has been discovered with regards to IDH3. Interestingly IDH3 is rarely found mutated in the setting of GBM and the reason for this has remained unclear. Unique to IDH3 compared to its family members is that IDH3 is a heterotetramer, composed of four subunits, two α, one β, and one γ subunit. Its main function is as part of the TCA cycle to convert ICT to α-KG, like IDH2, but some researchers have hinted at alternative functions, including one that may involve a nuclear role for IDH3, in particular for the α subunit (IDH3α). My research focuses on confirming nuclear localization of IDH3α and elucidating the role that it plays at the nucleus. Through a non-biased approach we have identified a novel interactor, cytosolic serine hydroxymethyltransferase (cSHMT), with IDH3α. We have determined that IDH3α regulates cSHMT activity, promoting thymidylate synthesis at the nuclear lamina. In the absence of IDH3α expression we observed decreased proliferation, increased sensitivity to the anti-folate chemotherapeutic methotrexate (MTX), and increased flux of folate metabolites through the methionine pathway, ultimately leading to an overall increase in DNA methylation. These effects result in decreased tumor growth and thus increased survival *in vivo* and the epigenetic changes caused a deregulation of pathways like the cAMP mediated signaling and regulation of epithelial-to-mesenchymal transition pathways. Thus, we have discovered a novel role for IDH3α in GBM pathogenesis and in general cellular physiology. Based off our research IDH3α appears to be a novel metabolic target for future therapies that may improve GBM patient outcomes.

ACKNOWLEDGEMENTS

I am in absolute shock and awe that I have made it to this point but I definitely could not have come this far without the help of the following people. First off, I greatly thank Dr. Alexander Stegh for being willing to take me on as a student. This was going to be my first foray into the world of cellular biology, coming from a chemical engineering lab background, but he was always very patient with me. He was a fantastic mentor as I worked my way through this treacherous PhD life. I hope to take that same sense of calm and insightfulness that he demonstrates on a daily basis as I progress through my career and mentor students.

Secondly, I would like to thank my lab mates. Thank you to Fotini Kouri. She was a godsend in lab. Again, since I had hardly any cellular biology experience she was extraordinarily patient with me as she introduced me to different experimental techniques. She is one of the nicest people I know and no matter what I was going through or struggling with, she always took time out of her busy schedule to help me muddle through a problem. She certainly laid the foundation upon which I could build a successful PhD career. Next, I would like to thank Andrea Calvert. She was my first introduction to the Stegh lab and I was completely floored by her organizational skills and her ability to multitask. She was an inspiration to me and I worked to achieve the same level of focus and organization. Then I would like to thank Lisa Hurley and Serena Tommasini-Ghelfi. I have never enjoyed conducting animal experiments but it is a necessary evil to bring better therapeutic treatments to patients. Lisa and Serena were kind enough to conduct these

experiments on my behalf so that I could create a more cohesive and translational argument as to the possible implications of my research on the general patient population. I would also like to thank a new member to our lab, Kevin Murnan. It's been great having him in the lab. He is a great resource when discussing fields of research I am unfamiliar with, to bounce ideas of off, and to vent to when experiments just don't work out.

I would also like to thank the key members of the core facilities at Northwestern. This was a project that required a lot of collaboration with members from many of the facilities. In particular I would like to thank Young Ah who helped me start the project in a non-biased manner with the mass spec work. I dread mass spec and with your staff and expertise I was able to start off my project with a great lead. I would also like to thank Dr. Horbinski and those at the Nervous System Tumor Bank and the Mouse Histology and Phenotyping Laboratory for all of the histology processing and analysis which helped to connect the *in vitro* and *in vivo* experiments with the patient population I wish to help. Then I would like to thank Dina from the Nikon core. You helped me with my immunofluorescence protocol and prevented me from making avoidable errors so that I had strong data. Lastly, I would like to thank Paul, Suchitra, and Carolina from the flow core. I would not have been able to generate any of my necessary cell models without your expertise. With these models I was able to build on the data from the Proteomics and Nikon cores and better understand the mechanism of my protein and flesh out the rest of my thesis. I would also like to thank Dr. Davuluri and Yanrong for their thorough analysis of the methylation

and RNA-seq data sets. Finally I will thank Dr. Locasale and Dr. Liu for their work on the metabolic flux experiments out of Duke University.

In addition to the people I worked with I would like to thank my family. My parents-in-law were always checking in on me to make sure I was still alive and amazed that I was making my way through this program. My mother always encouraged me to keep pushing forward one day at a time and to not get frustrated at myself. She always told me to be patient with myself and as long as I was giving it 110% how to realize when I needed to step away from a problem and return to it with a clearer head. Finally, I would like to thank my loving husband. He has been fantastic throughout this whole experience. He was always there for me to vent my frustrations, to cheer me up when an experiment failed, and to proof-read my writing because he is definitely the better writer between the two of us. He also was always there with a home cooked meal if I had a long hard day at work or with takeout if neither of us wanted to deal with it. This whole program would have been immensely harder without him in my life and I thank him so much for sticking with me through it all. I would also be remiss if I didn't thank my dog Marshmallow (Marshie). She always affectionately met me at the door and cheered me up no matter what sort of day I had.

DEDICATION

This dissertation is dedicated to my father. Through his encouragement of academics and in particular the sciences he laid the groundwork for me to be successful today. Also, by witnessing his battle with glioblastoma he inspired me to combat this deadly disease, clinically and scientifically, to improve the lives that come after him.

Thank you for all that you have done and continue to do.

TABLE OF CONTENTS

LIST OF FIGURES

CHAPTER 1: INTRODUCTION

1.1 Opening

Mutation or transcriptional up-regulation of isocitrate dehydrogenases 1 and 2 *(IDH1* and *IDH2)* promote cancer progression through metabolic reprogramming and epigenetic deregulation of gene expression. Here, we demonstrate that IDH3α, a subunit of the IDH3 heterotetramer, is elevated in Glioblastoma (GBM) patient samples compared to normal brain tissue, and promotes GBM progression in orthotopic glioma mouse models. IDH3α loss-of-function reduces tricarboxylic acid (TCA) cycle turn over, and inhibits oxidative phosphorylation. In addition to its impact on mitochondrial energy metabolism, IDH3a binds to cytosolic serine hydroxymethyltransferase (cSHMT). This interaction enhances nucleotide availability during DNA replication, while absence of IDH3α promotes methionine cycle activity, *S*-adenosyl methionine generation and DNA methylation. Thus, the regulation of one-carbon metabolism via a nuclear IDH3α-cSHMT signaling axis represents a novel mechanism of metabolic adaptation in GBM.

1.2 Glioblastoma

1.2.1 Overview

Glioblastoma (GBM) is a World Health Organization (WHO) grade IV brain tumor (Louis et al., 2007). GBM is diagnosed by the presence of several prevailing characteristics of GBM tumors, via immunohistochemistry: high mitotic activity, pseudopalisading necrosis, infiltrative cells, intravascular microthrombi, and microvessel proliferation (Olar and Aldape, 2014) and

sometimes with the assistance of functional MRI and diffusion weighted imaging (Wen and Kesari, 2008). GBM is the most commonly diagnosed malignant central nervous system tumor in adults, 46.1%, with an incidence of rate of 3.19/100,000 (Ostrom et al., 2013). GBM is also the deadliest with a 15 month prognosis from diagnosis when treated, 3 months if left untreated (Ostrom et al., 2016, Malmstrom et al., 2012). This dismal prognosis is due to the rate of recurrence, 7 months post diagnosis. Recurrence occurs due to the aggressive growth and invasive behavior of GBM, even without the presence of metastasis, which is a rare occurrence (Lun et al., 2011, Franceschi et al., 2016). Patients may present with headaches, focal neurologic deficits, confusion, memory loss, personality changes, nausea, vomiting and/or seizures. Most of these symptoms are due to the increase in intracranial pressure from the growing tumor and the inflammatory response (Behin et al., 2003). The mean age of diagnosis is about 64 years old, with a higher prevalence in Caucasians versus African Americans, Asians, and Latinos, and a higher rate in men versus women (1.5:1) (Ostrom et al., 2016).

There are a few different environmental factors that have been linked to an increased prevalence of brain tumors which include therapeutic ionizing radiation, vinyl chloride, pesticides, smoking, petroleum refining, and working in the synthetic rubber manufacturing industry (Wrensch et al., 2002). Genetically a few conditions predispose patients to the development of GBM like Li-Fraumeni syndrome, Lynch Syndrome, Turcot Syndrome, Nevoid basel cell carcinoma syndrome, Tuberous sclerosis complex, and if patients carry the Neurofibromatosis 1 & 2, or Multiple Endocrine Neoplasia type 1 mutation (Farrell and Plotkin, 2007). Yet many of these

factors predispose patients to developing many different types of cancers in general. No risk factors have been conclusively linked to brain tumors/GBM specifically.

GBM can present as the initial tumor, primary GBM, or as the result of a lower grade glioma, secondary GBM, which is less common (Ohgaki, 2009, Wen and Kesari, 2008). Primary GBMs account for 80% of all GBM cases and mainly arise in older patients, average age of 62, with rates being highest from 74 to 85 years of age, versus secondary which arises in younger patients, average age of 45 (Ohgaki and Kleihues, 2007, Ohgaki et al., 2004, Kleihues and Ohgaki, 2000, Ostrom et al., 2016).

Although many researchers have worked hard to understand and characterize this disease there are few therapies that are available to patients. The typical therapy course for patients diagnosed with GBM consists of maximal surgical resection followed by radiotherapy combined with either temozolomide (TMZ) or carmustin wafers (Stupp et al., 2009, Stupp et al., 2005) and followed up with six cycles of TMZ treatment (Stupp et al., 2005). Surgery is important for relieving the increase in intracranial pressure due to the growing tumor mass and it has been improved upon with the addition of fluorescence guidance (Stummer et al., 2006, Lacroix et al., 2001). With the addition of post-operative radiotherapy, increasing overall survival to 10.4%, and then TMZ, increasing to 26.5%, this shifted the median overall survival from 12.1 to 14.6 months (Stupp et al., 2005). The use of carmustin wafers has fallen out of favor due to side effects which include delayed wound healing, intracranial edema, cerebrospinal fluid leakage, intracranial infection,

and seizures (Wen et al., 2006). These treatments have been the standard of care for the past 10 years with very little change in the overall 5 year survival rate, which is only about 5.1% of patients (Ostrom et al., 2016). This disappointing result is believed to be due to the occurrence of drug resistance in these tumors (Stupp et al., 2009). The TMZ regimen can lead to a hypermutated phenotype in gliomas which may promote the development of drug resistance genes (Hunter et al., 2006, Cahill et al., 2007). For example, one group found that after treatment with TMZ there was an induction of Epidermal Growth Factor Receptor (EGFR) vIII and EGFR expression both of which have been demonstrated to increase drug resistance (Munoz et al., 2014).

As an alternative approach, and as a way to avoid drug resistance, a newly approved device has come onto the market which produces alternating electric fields of low intensity and intermediate frequency which interferes with cell division and eventually leads to cell apoptosis (Kirson et al., 2007). The device is placed onto a shaved scalp and powered by a battery pack, both worn for 18 hours, at a minimum, at a time (Stupp et al., 2017). A prospective, randomized phase 3 clinical trial was conducted on both patients with newly diagnosed and patients with recurrent GBM. While usage of the device led to an increase in overall survival in newly diagnosed patients with GBM, 20.5 months versus 15.6 months in the control group treated only with concomitant radiochemotherapy (Stupp et al., 2017), there was no significant difference for those patients with recurrent GBM outside of reduced side effect profiles for the device versus typical chemotherapy regimens for recurrent GBM (Stupp et al., 2012). Even with these demonstrated

improvements utilization has been slow due to the nature of the treatment. Patients must shave their head and patients saw the greatest benefit when they wore the device for longer than 18 hours, both of which can be deterrents for patient acceptance (Stupp et al., 2017). Therefore, further work still needs to be done. There are arguments to focus on the development of GBM to know what initiating events and cells must be targeted and with this understanding improve early detection.

1.2.2 Origin and cellular makeup of GBM

GBMs are typically of astrocytic origin, astrocytes being a type of glial cell or support cell for the nervous system, and as mentioned previously can arise either as primary or "de novo," without a lower grade precursor tumor, or as secondary GBM, arising from a lower grade glioma which could also be of oligodendrocytic origin, another glial cell (Namiki, 1981). Within GBMs there are several different cell populations, due to the outgrowth of heterogenous clones (Greaves and Maley, 2012, Navin et al., 2011, Shapiro et al., 1981), which contribute to its growth and maintenance. This heterogeneity is key to GBM survival. Each clonal population is unique and provides different supportive features to the tumor. Studies have shown that when separate clones are isolated from the tumor they show differences in invasive (Fidler and Kripke, 1977) and drug resistance (Yung et al., 1982) potential.

In addition to these different subtypes of tumor cells, detailed later on, there is a small population of cells called glioma initiating cells (GICs), which are theorized to contribute to tumor recurrence, via their self-renewal ability, (Huang et al., 2010, Singh et al., 2004) while also being

resistant to radiotherapy (Bao et al., 2006) due to selective activation of DNA damage response pathways (Dean et al., 2005). GICs also tend to be resistant to standard chemotherapy, partially due to upregulation of multidrug resistance protein-1 (MRP1) transporters (de Faria et al., 2008) and p-glycoprotein (Pgp) (Linnet and Ejsing, 2008). Due to all of these characteristics GICs are a key cell population in GBM tumors that must be therapeutically targeted to advance the current GBM treatment regimen.

GICs are identified by several characteristics: when they express the neural stem cell marker CD133, can propagate in culture as neurospheres, can be differentiated into the cell types found within the original tumor, and when intracranially injected into mice can proliferate to reform the original tumor (Singh et al., 2003, Singh et al., 2004). Using these characteristics, scientists have developed protocols for isolating these cells from patient tumors for the purpose of studying them in culture. These cell systems have contributed to our improved understanding of GBM pathogenesis.

Within the tumor, GICs are typically found in perivascular and hypoxic regions (Wei et al., 2011, Zhu et al., 2011). Interestingly both under situations of cellular hypoxia and at baseline, GICs typically express hypoxia inducible factors (HIFs), which promote the survival and expansion of GICs while also aiding in the maintenance of stemness (Seidel et al., 2010). Evidence demonstrating that a hypoxic environment supports GIC growth shows that stemness could be induced in non-GICs if they experienced hypoxic stress (Pistollato et al., 2010, Seidel et

al., 2010). Along with hypoxia induced stress other stressors, i.e. – acidic environment, chemotherapeutic treatment, and radiotherapy have all shown to induce stemness in non-GICs illustrating the importance of maintaining the GIC population in tumor pathogenesis (Auffinger et al., 2014, Dahan et al., 2014, Hjelmeland et al., 2011). These stressors all arise as a tumor grows, eventually out growing its blood supply, and undergoes treatment. Therefore, the development of GICs in the tumor seems to be an adaptive response to maintain and promote tumor propagation.

In addition to the upregulation of HIF factors GICs also commonly utilize different cellular pathways to reinforce their stem cell functions. One group found that inhibition of Bone Morphogenic Protein signaling by Gremlin1 promotes stemness and increases tumor formation *in vivo (Yan et al., 2014)*. Similarly, Ephrin type-A receptor 3 was found to inhibit MAPK signaling, promoting Nuclear Factor-κB transcriptional activity leading to proliferation and neurosphere maintenance and growth (Day et al., 2013). Another group determined that Notch regulation by Spy1 promotes symmetric cell division and decreased differentiation (Lubanska et al., 2014). Lastly, Achaete-scute homolog 1 represses Dickkopf-related protein 1, allowing for Wnt signaling to progress through Lymphoid enhancer-binding factor 1 maintaining the tumorigenecity of the GICs (Rheinbay et al., 2013). All of these genetic alterations contribute to the GICs ability to promote recurrence after therapy. Some of these pathways promote redundant functions, illustrating the plasticity of GICs and the difficulty in targeting them via one pathway to induce stasis or apoptosis. Lastly, all of these results may be due to the different *in vitro*

conditions used to study the GICs and demonstrates the importance of the tumor microenvironment in maintaining the GIC niche.

In addition to the tumor forming cells within the tumor microenvironment there are also supportive cells that have been found to aid in tumor growth, maintenance, angiogenesis, and drug resistance. These cells may have been attracted to the tumor through molecules secreted by the tumor or may have been incorporated into the tumor as the tumor grew. There are many different cell types including glial cells like astrocytes, oligodendrocytes, and microglia, immune cells like macrophages and T regulatory cells (Tregs), neurons, pericytes, and endothelial cells. Oligodendrocytes, through the release of heparin binding-EGF (Ramnarain et al., 2006) and glial cell line derived neurotrophic factor (Song and Moon, 2006), can stimulate glioma motility which may contribute to invasion (Du and Dreyfus, 2002). Astrocytes and microglia have been shown to degrade the extracellular matrix, promoting invasion and cellular proliferation (Rao, 2003, Le et al., 2003). M2 variant macrophages have been shown to be anti-inflammatory (Sica et al., 2008), versus their M1 counterparts, and along with microglia promote angiogenesis (Zeisberger et al., 2006, Tsai et al., 1995). Specifically, macrophages and microglia can stimulate the tumor, via interleukin 1β, to secrete Vascular Endothelial Growth Factor (VEGF) to attract endothelial cells, which then attract pericytes, to form a blood supply for the tumor (Watters et al., 2005). These pericytes also lower the vessel response to inhibitors of VEGF (Franco et al., 2011), which have become a treatment option for cerebral edema in recurrent GBM (Friedman et al., 2009). In addition to VEGF secretion, GBM tumors will secrete indoleamine 2,3-

dioxigenase to attract Tregs to the tumor microenvironment so that the Tregs may then suppress an anti-tumor inflammatory response (Wainwright et al., 2012).

More and more it is being recognized that the title of glioblastoma applies to a set of tumors that have very distinct developmental paths, like primary versus secondary, and behave differently as they grow with a very heterogeneous cell population. The biggest differentiating factor that has been used and studied to further define these subgroups of glioblastoma has been analyzing the genetic makeup of these different tumors.

1.2.3 Genetic Alterations in GBM

To discover new therapeutic avenues many research groups have attempted to find genetic alterations that can be exploited for better targeted therapies. Some of the major hurtles for therapy development include the blood brain barrier, which restricts passage of drugs to the intrathecal area (Zhan and Lu, 2012), GICs (Huang et al., 2010, Ahmed et al., 2013), and the heterogeneity within GBM tumors, as discussed above (Nicholas et al., 2011). By differentiating between different subgroups of GBM, based off genetic alterations targeted therapies can be specifically catered to that particular tumor subtype with improved efficacy. For example, it is now clinically relevant to screen all GBM tumors for the methylation status of O^6-methylguanine-DNA methyltransferase (MGMT) (Hegi et al., 2004). MGMT is a DNA repair protein that specifically removes alkyl groups from the O6 position in guanine in DNA. Therefore, this mechanism of action can reverse the alkylating properties of TMZ, preventing the induced DNA damage and resultant cell death (Hegi et al., 2005). When the *MGMT* promoter is

methylated, there is no expression of the MGMT protein. The reverse is true when the *MGMT* promoter is unmethylated (Nakagawachi et al., 2003). Therefore, by screening for MGMT methylation status it is possible to determine a patient's tumor's response to TMZ therapy (Hegi et al., 2004). In addition to MGMT status being relevant for TMZ therapy it has also been found to be predictive of a patient's response to radiotherapy (Rivera et al., 2010). MGMT promoter methylation can be found in approximately 50% of all newly diagnosed GBM cases (Mellai et al., 2012). Thus, MGMT has become a key prognostic marker in GBM and illustrates the importance of genetic testing in improving patient care. In addition to MGMT status there are specific genetic alterations seen in primary or secondary GBM. In primary GBM a common genetic alteration is EGF receptor amplification versus in secondary, which tends to have *TP53* inactivating mutations. In on study, only 1 out of 49 GBM tumors had both genetic alterations

indicating that these alterations are most often mutually exclusive, and therefore are useful markers of GBM type (Watanabe et al., 1996). Now it has been demonstrated that primary and secondary GBMs arise due to different genetic alterations and thus why their associated mutations tend to be mutually exclusive of the others (Ohgaki et al., 2004). The most common genetic alterations associated with primary GBM, in addition to EGFR overexpression and absence of IDH1 mutations, are phosphate and tensin homology gene (*PTEN*) mutations, loss of heterozygosity (LOH) 10q, and p16 deletions (Ohgaki and Kleihues, 2007). In secondary GBMs, along with *TP53* and IDH1 mutations, there are alpha thalassemia/mental retardation syndrome X-link (ATRX) mutations (Ohgaki and Kleihues, 2007, Ohgaki et al., 2004). The most differentiating

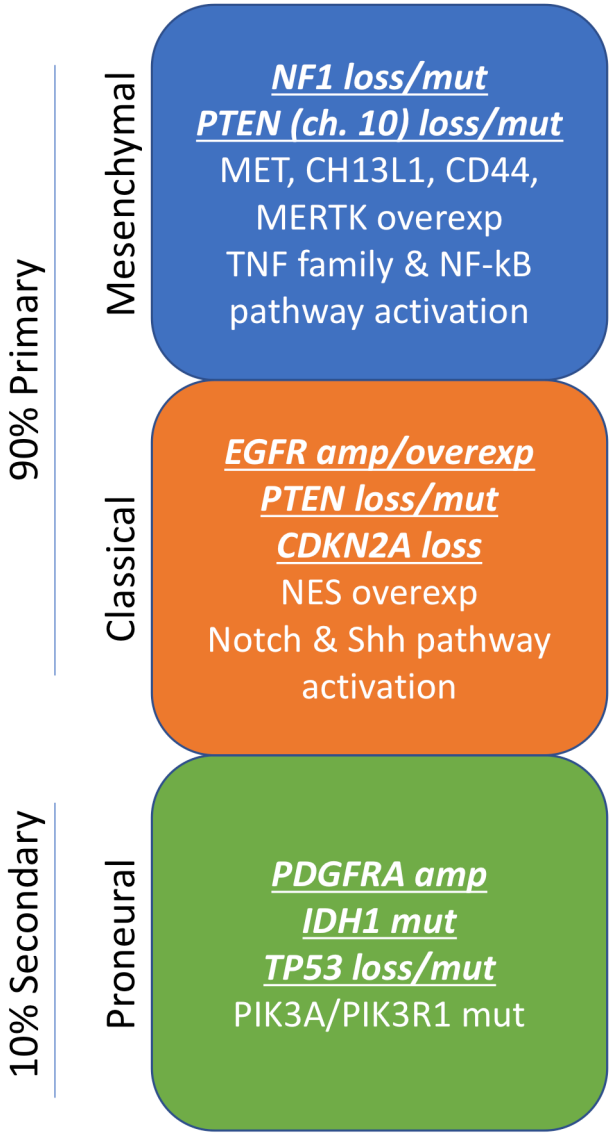

Fig. 1. GBM subtypes with associated genetic aberrations.
Based off the work done by the Verhaak and Cho groups (Verhaak et al., 2010, Wang et al., 2017).

factor between primary and secondary GBM, which has been discovered recently, is IDH1 mutation status (Balss et al., 2008, Watanabe et al., 2009, Yan et al., 2009b).

In addition to primary and secondary GBM classification Verhaak et al 2010 used The Cancer Genome Atlas to create subtypes with improved clinical relevance (Verhaak et al., 2010). The main subtypes they delineated are mesenchymal, the most invasive and thus the one with the shortest overall survival, classic, and proneural, which is commonly associated with secondary GBMs and is the least aggressive. The mesenchymal subtype typically has mutations in NF1 and PTEN, classical has amplification of EGFR and loss of chromosome 10, and proneural has focal amplification of PDGFRA, p53 mutations, and IDH1 mutations. IDH1 mutation is so common in proneural that the subtype classification can practically be determined by IDH1 status alone (Verhaak et al., 2010). Primary GBM can be categorized into all three of Verhaak's subtypes, while secondary GBM exclusively develops into the proneural (Van Meir et al., 2010). Interestingly more than one of these subtypes can be found within the tumor, either as non-GICs or GICs, again demonstrating the heterogeneity of GBMs (Mao et al., 2013). Recently WHO developed new classifications for GBM based off recent molecular research and now to improve diagnostic, treatment, and prognostic abilities and outcomes GBM will be subclassified into IDH1 wild type (IDH1wt) or IDH1 mutant (IDH1mut) (Louis et al., 2016).

Most of these genetic aberrations fall in similar functional categories or pathways. The typical progression of gliomagenesis is an activating mutation which contributes to aberrant

proliferation, which can include mutations in EGF, PDGF, or loss of PTEN, resulting in increased PI3K/Akt pathway activation. Then there are mutations that follow, with a common one being in VEGF, to promote endothelial cell migration, proliferation, increase vascular permeability, and that are antiapoptotic (Louis, 2006). A few of these alterations are starting to be investigated as drug targets with EGFR antagonists, mTOR inhibitors, and anti-angiogenesis agents (Villano et al., 2009).

While allowing for better phenotypic classification, commonly found mutations and genetic alterations in GBM are starting to be implicated in one of the newest hallmarks of cancer, metabolic adaption (Hanahan and Weinberg, 2011). These alterations arise due to a need for increased products for cellular replication (Calvert et al., 2017), energy maintenance, or due to the tumor microenvironment, i.e. handling the stressors of hypoxia (Zhang et al., 2017, Velpula et al., 2013). Genetic alterations in Ras, PI3K/Akt (Elstrom et al., 2004), HIF1α (Velpula et al., 2013), and SREBP-1 (Guo et al., 2014), to name a few, have all been implicated in changing the metabolic landscape in GBM. In addition to these, IDH1 expression and IDH1 and 2 mutations also lead to metabolic alterations in GBM (Dang et al., 2009, Krell et al., 2011, Turcan et al., 2012, Ward et al., 2012, Yan et al., 2009b).

While mutations have been found in both IDH1 and IDH2 in the setting of GBM no mutations have been observed that affect IDH3 expression status or function (Krell et al., 2011). Some researchers believe this is due to the fact that IDH3 is unable to produce 2-hydroxyglutarate (2-

HG) when mutated like IDH1 and IDH2 (Dang et al., 2009). Thus they believe that inactivation of IDH conversion activity, leading to decreased α-KG levels, and production of 2-HG promotes gliomagenesis (Krell et al., 2011), indicating that IDH1/2 mutation may be an initiating event.

1.3 Isocitrate Dehydrogenase Enzymes

Isocitrate dehydrogenase (IDH) enzymes are a group of enzymes responsible for the conversion of isocitrate to α-ketoglutarate (α-KG) and carbon dioxide (CO_2). They reduce either nicotinamide adenine dinucleotide phosphate (NADP+) to NADPH or nicotinamide adenine dinucleotide (NAD+) to NADH. IDH1 is NADP+ dependent and resides in the cytoplasm and the peroxisomes, IDH2 is NADP+ dependent and along with IDH3, which is NAD+ dependent, resides in the mitochondria to execute the reaction within the tricarboxylic acid cycle (TCA cycle) (Reitman and Yan, 2010, Minard and McAlister-Henn, 1999). IDH1 and IDH2 are homodimeric, and are very similar in structure and protein sequence, while IDH3 is a heterotetramer consisting of two α, one β, and one γ subunit (Xu et al., 2004). In addition to their differences in overall structure IDH1 and IDH2 execute the conversion reaction differently from IDH3. IDH1 and 2's reaction involves an intermediate structure, unlike IDH3, and they can carry out the conversion in the reverse, thus allowing for production of 2-HG, specifically the D-enantiomer, when mutated (Dang et al., 2009, Keum and Choi, 2015).

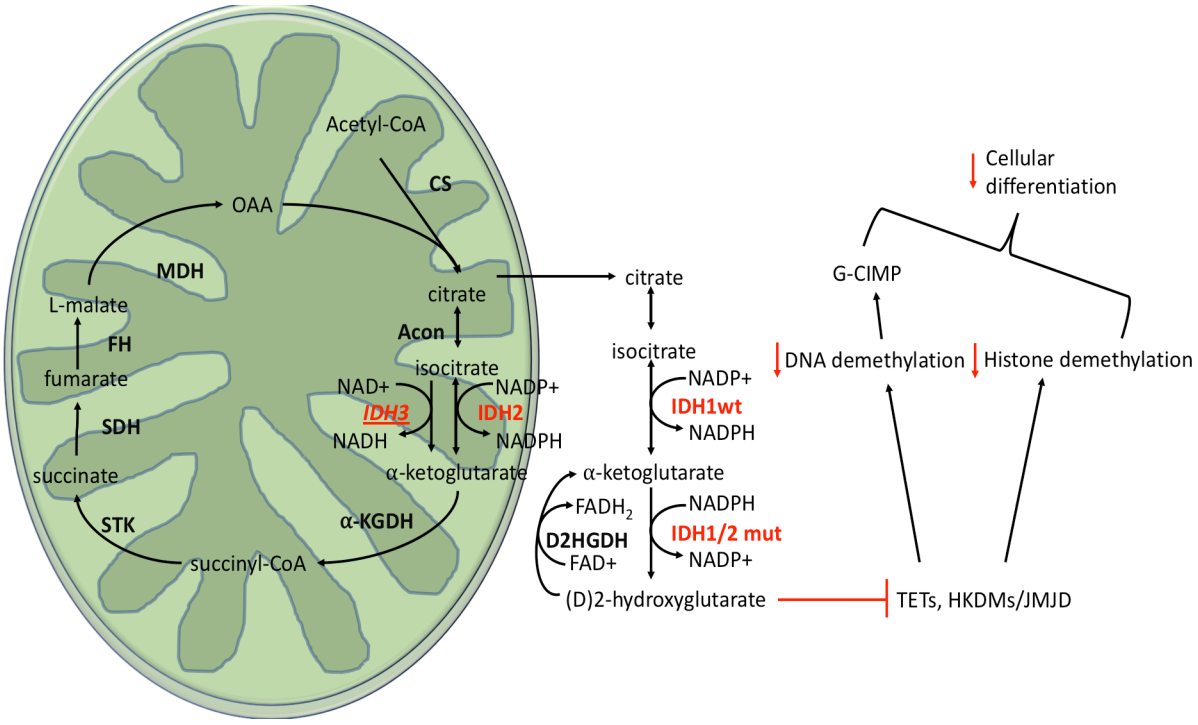

Fig. 2. IDH mechanism of action and impact on cellular physiology.
This figure illustrates the TCA cycle which IDH2 and IDH3 are a part of and the mechanism IDH1 conducts in the cytosol. It also shows the effects of IDH1/2 mut on D2-HG production and downstream effects. OAA = oxaloacetic acid; CS = citrate synthase; Acon = aconitase; α-KGDH = α-ketoglutarate dehydrogenase; STK = succinate thiokinase; SDH = succinate dehydrogenase; FH = fumarate hydratase

1.3.1 IDH1/2 mutation

These IDH1 and 2 mutants are commonly found in GBM along with acute myeloid leukemia (AML), chondrosarcomas, and intrahepatic cholangiocarcinoma (Dang et al., 2010, Krell et al., 2011, Amary et al., 2011, Borger et al., 2012) but IDH3 mutations are not seen. Research suggests that IDH1/2 mutation may be an initiating event in gliomagenesis (Juratli et al., 2012b). Typically, the mutation is somatic, heterozygous, mutually exclusive, and involves a single amino acid residue substitution, most often affecting the arginine residue at codon 132 in IDH1 or codons 140 or 170 in IDH2 (Duncan et al., 2012, Kranendijk et al., 2010, Pietrak et al., 2011,

Yang et al., 2012). These codons are located within the isocitrate binding site of IDH1 and 2 (Losman and Kaelin, 2013). In both gliomas (Yan et al., 2009b) and AML (Patel et al., 2012) IDH1/2 mutation is associated with better prognoses. Patients with IDH1mut gliomas have a median overall survival of 31 months versus patients with IDH1wt gliomas with a median of 15 months (Juratli et al., 2012a, Combs et al., 2011). Some researchers postulate that this may be in part due to IDHmut gliomas being more responsive to chemotherapy, with clinicians starting to predict chemosensitivity based off IDH mutational status (SongTao et al., 2012, Houillier et al., 2010).

The mutation is considered both a loss and gain-of-function mutation since IDH1/2mut have a decreased affinity for their normal substrate, isocitrate, and an increased affinity for the product NADPH thus promoting 2-HG production (Dang et al., 2009). Typically, 2-HG is in the micromolar range and formed due to metabolism errors within the cell. Whenever this happens FAD-dependent 2-hydroxyglutarate dehydrogenases (L/D2HGDH) convert 2-HG to α-KG (Van Schaftingen et al., 2013). When IDH1 or 2 are mutated 2-HG levels can rise to the millimolar (Dang et al., 2016). In conjunction with this rise in 2-HG levels in some cases of solid tumors expressing the IDH1/2 mutant 2-HG can be found circulating in the blood and correlate with the level of tumor burden (Borger et al., 2014).

1.3.2 Effects of 2-HG

2-HG is structurally similar to α-KG therefore 2-HG can interact with those enzymes that utilize α-KG as a co-factor, di-oxygenases (Xu et al., 2011). These enzymes are important in regulating

protein degradation and the methylation status of histones and DNA. Thus, IDH1 and 2 mutations have been commonly associated with genome wide hypermethylation, CpG Island Methylator Phenotype (CIMP), due to inhibition of the histone lysine demethylases and the TET family DNA hydroxylases (Figueroa et al., 2010, Yan et al., 2009a), which can alter the epigenome. For example, MGMT promoter methylation is frequently seen in conjunction with IDH1/2 mutation (Horbinski, 2013). This hypermethylation phenotype leads to alterations in gene expression and has been implicated in the ability of GICs to maintain a de-differentiated state, thereby supplying the tumor with the ability to recur after tumor resection, radiotherapy, and chemotherapy. Due to these downstream and widespread effects, 2-HG is considered to be an oncometabolite (Gross et al., 2010). In addition to the mutant form of IDH1, under hypoxic conditions IDH1wt is also found to be able to produce 2-HG thus still having the same downstream effects (Kinnaird et al., 2016, Lee and Kim, 2016, Nakazawa et al., 2016).

Due to the downstream effects of 2-HG production promoting characteristics to support tumor growth by IDH1/2mut, but IDH1/2mut also being associated with better survival, investigations have been carried out to look exclusively at the tumorigenic potential of 2-HG, separate from IDH1/2 mutational status and what other factors may be needed to be coexpressed to promote tumorigenesis. With regards to D2HG, even at elevated levels, causing hydroxyglutaric aciduria, due to mutations in the D2HGDH, no associated tumors have been found. Whereas in cases with elevated L2HG there have been reports of increased brain tumors in children with hydroxyglutaric aciduria (Kranendijk et al., 2010). Due to the catalytic pocket of IDH1/2, when

mutated these enzymes only produce the D2HG form (Dang et al., 2009). If tumor development were just due to IDH mutants forming the 2HG oncometabolite it would be expected that other tumors may contain mutations in the L/D2HGDHs. Yet mutations in these enzymes have not been found in tumors to date. Studies have been done on IDH1/2 mutations in isolation in both the blood and brains of mice. In both instances abnormalities in development and normal physiology occur but there is no tumorigenesis. Therefore, IDH mutations must be tumorigenic only in the presence of other mutations (Sasaki et al., 2012a, Sasaki et al., 2012b). As a result of D2HG inhibition of α-KG dependent dioxygenases, required for DNA demethylation (i.e. -TET1/2 and KDM/JMJDs), DNA hypermethylation can rarely be reversed. At inhibitor concentrations where DNA hypermethylation can be reversed those concentrations have surpassed those that cause tumor growth inhibition (Rohle et al., 2013). Therefore, DNA hypermethylation may contribute to tumorigenesis but it is not the main driver. Thus alone IDH1/2mut, D2HG, or the resultant DNA hypermethylation phenotype cannot initiate gliomagenesis but must occur alongside driver mutations to impact progression.

In the absence of an *IDH1* point mutation, primary GBM are characterized by transcriptional up-regulation of wild-type IDH1. Genetic and pharmacologic inactivation of IDH1 decreases GBM cell growth, promotes a more differentiated tumor cell state, increases apoptosis in response to targeted therapies, and prolongs survival of animal subjects bearing patient-derived xenografts (PDXs) (Calvert et al., 2017). On molecular levels, IDH1 inhibition reduces α-KG and NADPH levels, which is paralleled by deficient carbon flux from glucose or acetate into lipids, exhaustion

of reduced glutathione, increased levels of reactive oxygen species (ROS), and enhanced histone methylation and differentiation marker expression (Calvert et al., 2017). These results demonstrate the advantage of retaining wild type IDH1. Another group found that IDH1mut with associated 2-HG increases and CIMP status had methylation of the tissue factor promoter, tissue factor being an initiator of thromboses development, while 2-HG also inhibited platelet clotting, leading to decreases in thromboses compared to IDH1wt tumors (Unruh et al., 2016). This phenotype may also contribute to the better survival of GBM IDH1/2mut tumor bearing patients compared to those with IDH1wt tumors.

When we conducted our own study of IDH expression in GBM we found in the TCGA dataset that IDH3 was the only IDH enzyme downregulated in GBM versus normal controls. Since our previous research demonstrated the value of IDH1 expression in gliomagenesis we wondered what effects IDH3 downregulation may have and if downregulation promoted tumor growth in GBM.

1.4 Isocitrate Dehydrogenase 3

With defined roles for IDH1 and IDH2 in cancer progression evolving, our understanding of how IDH3 affects metabolic adaptation and tumorigenesis can reasonably be described as rudimentary. IDH3 catalyzes an irreversible and rate-limiting step of the TCA cycle, which is tightly regulated through substrate availability (ICT, NAD+, Mg^{2+}/Mn^{2+}), product inhibition (NADH, α-KG) and competitive feedback inhibition (ATP), to avoid unnecessary depletion of ICT and accumulation of α-KG (Qi et al., 2008, Bzymek and Colman, 2007). Each subunit of

IDH3 contributes specific functions to the overall enzyme. Point mutation studies have determined that the α subunit is the key catalytic subunit. When Asp181, Asp230, and Asp 234 are mutated in the IDH3α subunit the IDH3 enzyme loses all ability to convert ICT to α-KG. This is not the case for point mutations in the β or γ subunits (Bzymek and Colman, 2007, Soundar et al., 2006). The β and γ subunits are more important for improving the affinity IDH3 has for ICT and for binding to cofactors like NAD+ and Mn^{2+} (Bzymek and Colman, 2007, Soundar et al., 2006). When either β or γ have point mutations the Km for isocitrate goes up, indicating a decreased affinity for the substrate and thus decreased efficiency in conducting the reaction but the reaction is still able to progress. Recently, it was discovered that the expression of IDH3α, along with IDH1, was regulated by NF-κB (Zhou et al., 2017), which as mentioned previously has been associated with promoting a stem cell like phenotype in GICs (Day et al., 2013). This research brings into question whether IDH3α is pro- or anti-tumorigenic.

1.4.1 Contribution of IDH3α to disease pathogenesis

Some work has started to come out defining IDH3α's role in neurologic diseases. One group found that families with the hereditary disease retinitis pigmentosa commonly carry a heterozygous loss of function mutation in IDH3B (Hartong et al., 2008). Thus, the authors concluded that IDH2 may be more important for TCA cycle flux throughout the body, the eye being the exception. An additional study also found that IDH2 activity was able to preserve flow through the TCA cycle (MacDonald et al., 2013). This is contrary to the belief that IDH3 is the main contributor to TCA cycle flux since it can contribute to NADH production unlike IDH2. Thus, more work needs to be done to better understand the interplay of IDH2 and 3 in regulating

the TCA cycle. Recently, another group evaluated patients with retinitis pigmentosa accompanied by pseudocoloboma, a scar resembling a congenital malformation affecting the lens, iris, or retina, and identified homozygous germline missense and non-sense mutations in IDH3A gene (Pierrache et al., 2017) further solidifying IDH3's importance in the neurological system particularly the eye, since these patients did not have additional sequelae from the mutation. Another case report found IDH3α to have a homozygous mutation resulting in a histidine substitution for proline at codon 304 (Fattal-Valevski et al., 2017), a mutation also found by the Pierrache et al 2017 group. When investigated using yeast they found that when IDH1 and IDH2 were knocked out in yeast, their growth on ethanol-acetate plates could be rescued by expression of human IDH3α, which is 70% similar to yeast IDH2. Yet when IDH3α Pro304His was expressed, there was no rescue, demonstrating the functional importance of Pro304, in addition to the Asp residues mutated in the earlier studies, to IDH3α function (Fattal-Valevski et al., 2017). Lastly, a group investigating the role of peroxisome proliferator-activated receptor γ coactivator-1α (PGC-1α), a gene frequently reported to be involved in multiple movement disorders, found that decreased PGC-1α led to decreased expression of IDH3α along with several other metabolic enzymes (Lucas et al., 2014). The direct relationship between the two was not determined but the authors concluded that PGC-1α is important in regulating cellular metabolism and when decreased leads to dysfunctional energy production due to decreases in metabolic enzymes like IDH3α (Lucas et al., 2014).

In addition to these neurological outcomes of IDH3 and IDH3α dysfunction and in support of IDH3 having a central role within the TCA cycle, down-regulation of IDH3α, promotes transformation of fibroblasts into cancer-associated fibroblasts (CAFs) by inducing a switch from oxidative phosphorylation to glycolysis (Zhang et al., 2015). Diminished IDH3 activity resulted in reduced α-KG to fumarate and succinate ratio, which inhibits prolyl hydroxylase domain-containing protein 2 (PHD2). PHD2 is important for initiating the degradation of HIF1α. Therefore, when PHD2 is inhibited HIF1α protein levels increase. HIF1α then promotes the up-regulation of glycolytic enzymes and dampens oxidative phosphorylation (Zhang et al., 2015). In contrast in cervical epithelial adenocarcinoma cells and derivative explants down-regulation of IDH3α increased α-KG levels, leading to HIF1α inactivation and inhibition of tumor progression (Zeng et al., 2014). In support of IDH3α pro-tumor effect, IDH3α expression correlated with poor postoperative overall survival of lung and breast cancer patients, pointing to IDH3α as a putative cancer therapeutic target (Zeng et al., 2014). Another group evaluated the effects of chromosomal aneuploidy in colorectal cancer. In trisomies with an additional chromosome 7 or chromosome 13 there was a downregulation of IDH3α in both instances. There was also overlap of pathways involving IDH3α and HMGB1, high mobility group box 1, which is associated with DNA organization and regulates DNA transcription. Therefore, the authors concluded that IDH3α may be involved in genome stability but how it functionally was involved still needed to be investigated (Gemoll et al., 2013). Lastly, in MCF-7 breast cancer cells a group did proteomics studies on mitochondrial and nuclear fractions to determine cellular distributions of proteins between the two compartments since prior work had shown that the mitochondrial

proteome is in flux, not static (Braschi et al., 2010, Chen et al., 2009, Lee et al., 2008, Leigh-Brown et al., 2010, Shen et al., 2012). Experimentally, through cellular subfractionation the researchers were able to identify IDH3α in both the mitochondrial and nuclear fragments (Qattan et al., 2012). All of these studies demonstrate the lack of understanding with regards to IDH3, and in particular IDH3α, and its role in cancer. Discrepancies between studies may result from differences in cell systems, growth conditions/microenvironment, or may hint at IDH3 having unique roles in tumor supportive cells versus tumor cells themselves.

With regard to other disease processes IDH3 has been implicated in the apoptotic response of type 2 alveolar epithelial cells in the setting of acute respiratory distress syndrome (ARDS) and decreased carbon dioxide in the alveolar space. When there is decreased carbon dioxide, as seen in ARDS, researchers found that IDH3 activity increased, resulting in increased NADH production, which increased calcium ion flux into the mitochondria and ROS production, initiating an apoptotic response (Kiefmann et al., 2017). It is possible that the response could also be seen in the setting of cancer if elevated metabolic processes cause an increase in carbon dioxide production.

Outside of these studies others looking at a possible role for IDH3 in human pathophysiology have mainly been correlative or it has come up in large proteomics, metabolomics, and genetics screenings with very little with regards to mechanism. For example, one group found in a large metabolomics study looking at the cerebrospinal fluid of patients with bipolar disorder that

IDH3α was altered in the prefrontal cortex and cerebellum. They also found that there was a correlation between IDH3α expression and the development of bipolar disorder, major depressive disorder, and schizophrenia, but the reasons for this were not further investigated (Yoshimi et al., 2016). Therefore, much work needs to be done to better understand IDH3's physiological and pathophysiological relevance although studies seem to point towards an important role for IDH3 supporting the neurological system. It would be beneficial to generate a global IDH3α homozygous KO model to determine where IDH3α function is necessary and where IDH2 expression is sufficient to support normal cellular metabolism and function. It is possible, based off these studies, that a global IDH3α KO would cause widespread neurological problems, either with development or function.

1.5 Cancer Metabolism

The alterations to physiologically normal metabolism in the setting of cancer have gain more interest over the past few years as possible targets or weaknesses to be exploited by cancer therapy (Hammoudi et al., 2011, Kroemer and Pouyssegur, 2008). The earliest studies looking at cancer cell metabolism resulted in the discovery of the Warburg effect, named after the scientist who defined it. The Warburg effect describes the process of aerobic glycolysis, where tumor cells, even under normoxic conditions, preferentially use glucose to produce lactate versus converting glucose to pyruvate to enter the TCA cycle. Such altered metabolism in cancer cells versus normal cells allowed for the development of positron emission topography, exploiting the increased glucose uptake in cancer cells to image the primary tumor and possible metastatic sites in patients.

In addition to IDH enzymes being connected with the promotion of cancer other metabolism enzymes have also been linked to cancer, either similarly as oncogenes or as tumor suppressors. Even before the IDH1/2 mutation was discovered loss-of-function mutations in fumarate hydratase (FH) and any subunit of the succinate dehydrogenase (SDH) enzyme, enzymes also associated with the TCA cycle as illustrated above, were associated with the development of specific cancers, thereby deeming FH and SDH tumor suppressors (King et al., 2006). More and more it is being acknowledged that there is a relationship between cellular metabolism and cellular proliferation in cancer cells with one set of reactions informing the other, providing feedback with regards to energy for replication, and replication requiring certain metabolites and molecular components.

In addition to disturbances in TCA cycle and ATP production pathways other metabolic pathways are gaining increased interest with respect to cancer research. These pathways support the production of important building blocks for cellular proliferation and to support cellular viability in environments that are typically lacking in exogenous metabolite supplies due to poor vascularization. One metabolic pathway in particular that has gained renewed interest is the one-carbon metabolism pathway.

1.5.1 One-Carbon Metabolism

One-carbon metabolism represents both the folate and methionine synthesis pathways and how those pathways interact. One-carbon metabolism is therefore necessary for the production of

purines, pyrimidines, and for homocysteine recycling to maintain the methylation potential of the cell. All of these functions occur through the exchange of one-carbon groups, methyl groups, which are carried on tetrahydrofolate (THF) and typically supplied by non-essential amino acids, serine and glycine, that can be obtained both exogenously or produced endogenously, *de novo*. THF is produced from dietary folic acid and is the universal methyl group acceptor, which it does so in different forms (formyl-THF, methyl-THF, and methylene-THF). These methyl groups are predominantly donated by serine and glycine in the setting of cancer (Tibbetts and Appling, 2010). Two major sources for providing the different methylated forms of THF reside in the mitochondria and within the cytosol, with each compartment having their own unique set of enzymes to conduct the reactions. Interestingly the protein PGC-1α, not only regulates IDH3α levels, as mentioned previously, but also those enzymes that are important for the mitochondrial production of methylated THF, the conversion of mitochondrial derived formate into 10-formly-THF, methylenetetrahydrofolate dehydrogenase 1 and 2(MTHFD1 and 2), and MTHFD1-like, for use in the cytosol (Audet-Walsh et al., 2016). Understandably these folate and methyl groups are key to cancer growth and progression since they provide the building blocks necessary for cell proliferation, epigenetic regulation, and post-translational modifications.

Serine heavily contributes to one-carbon metabolism and it is important that its levels are carefully regulated to support the nucleotide synthesis of the folate pathway and the methylation potential of the cell through the methionine pathway. Serine contributes to both by aiding in the *de* novo synthesis of ATP which is a necessary purine for DNA synthesis and serves as a

cofactor for the conversion of methionine to SAM (Maddocks et al., 2016). Serine can be produced by the serine synthesis pathway (SSP) which takes 3-phosphoglycerate (3PG) from the glycolysis pathway for serine production. Serine itself can support the function of pyruvate kinase isoform M2 (PKM2), so when serine levels are low activation of PKM2 decreases, slowing down glycolysis so that 3PG can be shuttled into the SSP to increase serine levels (Chaneton et al., 2012, Ye et al., 2012). Serine also supports the production of phospholipids like sphingolipids and phosphatidylserine (Kinney and Moore, 1987). Since serine is so critical in the formation of many different metabolites required for cancer cell proliferation and maintenance cancer cells typically attempt to increase their uptake of exogenous serine and/or increase the *de novo* production of serine by increasing the expression of proteins or their activities in the SSP (Commisso et al., 2013, Snell, 1985). In light of these findings researchers investigated the impact of dietary serine restriction on cancer and preclinical studies demonstrated that serine restriction inhibited tumor growth (Maddocks et al., 2013). In addition to serine, glycine can donate a carbon to THF to produce 5,10-methyleneTHF through glycine dehydrogenase (GLDC), which has also been implicated in tumorigenesis (Jain et al., 2012, Zhang et al., 2012). Also, using the NCI-60 panel glycine was determined to be strongly associated with increased cellular proliferation (Zhang et al., 2012). Not only has glycine been implicated in cell growth but addition of glycine to prostate cancer cells promoted their invasion (Sreekumar et al., 2009). Thus both serine and glycine have been demonstrated to be important for tumorigenesis and highlights the importance of one-carbon metabolism as well.

Focusing on one part of one-carbon metabolism, the importance of folate metabolism in cancer was acknowledged by Sydney Farber when he tried the first chemotherapeutic, which was an anti-folate drug called aminopterin, in a child with leukemia (Farber and Diamond, 1948). The most well-known antifolate is still in use today as a chemotherapeutic, methotrexate. The target of these drugs, discovered at the time, was dihydrofolate reductase (DHFR). DHFR reproduces THF after it is brought into the thymidine synthesis pathway by cSHMT and utilized by thymidylate synthase (TYMS) to produce thymidine. After these initial studies more researchers investigated the role of folate metabolism in cancer progression. Later on, TYMS was determined to be an oncogene, the target of 5-fluorouracil, which is also a commonly used cancer drug today (Rahman et al., 2004). Therefore antifolates decreased the amount of THF to be used by the one-carbon metabolism network by halting thymidine production (Osborn et al., 1958). The cSHMT, TYMS, DHFR complex is enriched at DNA replication forks to supply thymidylate for DNA synthesis (Anderson et al., 2012). In addition to supporting nucleotide synthesis, the folate cycle also contributes to NADPH production via MTHFD1 activity and the breakdown of 10-formylTHF to THF and carbon dioxide (Lewis et al., 2014).

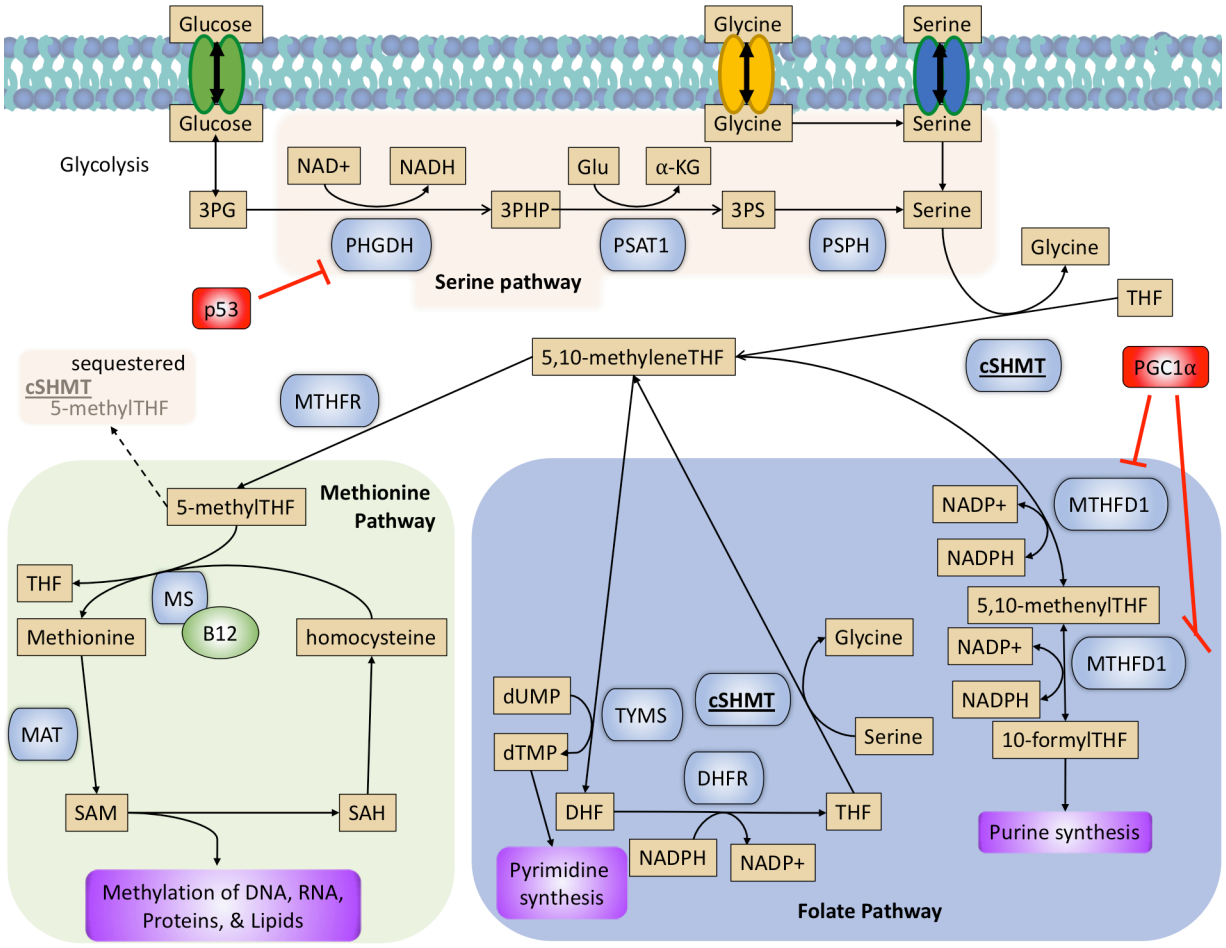

Fig. 3. One-Carbon Metabolism
Here we illustrate the importance of one-carbon metabolism and how it contributes to nucleotide synthesis, via the folate pathway, along with controlling the methylation potential of the cell, via the methionine pathway. [3PG = 3-phosphoglyceric acid; 3PHP = 3-phosphohydroxypyruvate; 3PS = 3 phosphoserine; PSAT1 = phosphoserine aminotransferase 1; PSPH = phosphoserine phosphatase; MAT = methionine adenosyltransferase]

The other part of one-carbon metabolism includes the methionine recycling pathway. This pathway is important for maintaining the methylation potential of the cell. Methionine is converted to SAM with the addition of ATP. Then SAM can be used to methylate DNA, proteins, mRNA, and metabolites and be converted into S-adenosylhomocysteine (SAH). SAM

can also be used as a cofactor in the production of different phosphatidylcholines (Hickman et al., 2011, Kinney and Moore, 1987). The conversion of choline to phosphatidylcholine occurs during the adenylation of methionine to SAM (Aveldano and Bazan, 1983). Flux through the methionine cycle is commonly decreased in cancer cells (Mehrmohamadi et al., 2014, Shlomi et al., 2014). Yet, in GBM, flux through the methionine cycle was found to be important for maintaining cell growth (Palanichamy et al., 2016). This may be due to the contribution of SAM to the production of polyamines which have been demonstrated to support cellular proliferation (Heby and Persson, 1990). Additionally, due to the larger contributions of epigenetic alterations in cancer development the effects of methylation inhibitors, which prevent SAM from donating a methyl group to the DNA, are being investigated (Gnyszka et al., 2013).

1.5.2 Alterations in One-Carbon Metabolism in GBM

As mentioned earlier, like most other cancers GBM tends to rely on the Warburg effect to support rapid cellular proliferation. In addition to the Warburg effect, GBM also still maintains some activity in the TCA and oxidative phosphorylation pathways to provide necessary metabolites to serve other functions throughout the cell. To support both of these metabolic pathways GBM cell are highly glycolytic (Oudard et al., 1996). In agreement with this, astrocytes and other glial cells are highly glycolytic whereas in neurons increased glycolysis tends to cause apoptosis (Herrero-Mendez et al., 2009), further supporting astrocytes and glial cells as being the cells of origin for GBMs. One of the pathways supported by Warburg metabolites is the lipid synthesis pathway, which is key to GBM maintenance and proliferation. When key enzymes, which convert TCA cycle intermediates to lipid synthesis metabolites, are

inhibited GBM growth rate decreases and apoptosis is induced, leading to decreased tumor volume (Mashimo et al., 2014).

Previously, proteins involved in one-carbon metabolism have been implicated in gliomagenesis. PHGDH, an enzyme involved in converting 3-PG from the glycolytic pathway to serine, has been found to be upregulated in gliomas (Liu et al., 2013). The brain is highly reliant on serine since it also functions as a neurotransmitter, but due to the blood brain barrier there is decreased transmission of serine from the plasma to the brain, and if exogenous serine was the only source it would be inadequate to support proper brain function (de Koning and Klomp, 2004). PHGDH-deficient mice have demonstrated severe neurological deficits and cannot survive long after birth (Yoshida et al., 2004). Therefore, upregulation of PHGDH in the setting of GBM seems to be a mechanism by which serine supplies are maintained for the tumor, in an already serine low environment, to support one-carbon metabolism. Upregulation of PHGDH is also not exclusive to GBM. Previously increased PHGDH levels have been found in breast cancers and melanoma (Mullarky et al., 2011, Pollari et al., 2011, Possemato et al., 2011). PHGDH has gained such interest as a cancer promoting gene that small molecule inhibitors are now being developed to target PHGDH and have already shown some success in reduced cancer cell growth *in vitro* and xenograft growth *in vivo* (Mullarky et al., 2016, Pacold et al., 2016).

In addition to alterations to SSP. There is, as mentioned previously, maintained flux through the methionine cycle for maintaining cell growth in GBM (Palanichamy et al., 2016). Methionine

levels themselves, were found to be increased to such an extent in GBM that now PET imaging in GBM is being studied using a methionine-based tracer (Palanichamy and Chakravarti, 2017, Bergstrom et al., 1987).

1.6 cSHMT

cSHMT is important in the folate pathway of one-carbon metabolism. cSHMT is a tetrameric enzyme, made up by a dimer of obligate dimers, each containing an active site for four active sites in total and is reliant on pyridoxal phosphate (PLP) as a co-factor, the active form of vitamin B6 (Zanetti and Stover, 2003). cSHMT is necessary for the production of thymidylate from folate. cSHMT along with TYMS and DHFR are the key enzymes involved in thymidylate synthesis. As mentioned previously, during times of DNA replication cSHMT acts as the scaffold for TYMS and DHFR at DNA replication forks to provide thymidylate (Anderson et al., 2012).

1.6.1 cSHMT physiology and genetic alterations

Since cSHMT plays a key role in allocating folate metabolites for DNA synthesis some groups have looked at the role of cSHMT in neural tube and embryo development, and in adult physiology. When cSHMT is knocked out in adult mice it was found that the SAM/SAH ratio was increased in the liver and there was increased uracil content in the DNA, due to decreased thymidylate synthesis flux (MacFarlane et al., 2008). Also, cSHMT seemed to sequester 5-methylTHF when it was expressed. Thus there was less 5-methylTHF available to recycle into the methionine pathway (MacFarlane et al., 2008). Therefore, cSHMT regulates methionine flux,

not only through 5,10-methyleneTHF usage for the thymidylate pathway but also through 5-methylTHF sequestration. When there is a deficiency in this pathway due to malfunction or inhibition of the enzymes TYMS, DHFR, or cSHMT there is decreased thymidylate production. This leads to inappropriate incorporation of uracil into the DNA causing cell death.

The most common genetic aberration found in cSHMT is a point mutation at site 1420, C → T (C1420T) and is associated with decreased levels of homocysteine (Heil et al., 2001). This polymorphism leads to a cSHMT leucine to phenylalanine substitution at codon 474. This amino acid substitution occurs on the exterior surface of the enzyme and not within the catalytic pocket. Many studies have been done to evaluate the cancer risk associated with cSHMT C1420T with studies typically finding that it is not associated with increased cancer incidence and two finding decreased cancer incidence; one actually found it to be protective against colorectal cancer in Asian populations (Wang et al., 2014), while another saw a decreased risk for acute lymphocytic leukemia (Skibola et al., 2002). Functionally the cSHMT C1420T variant was found to lead to decreased homocysteine levels in patients both heterozygous and homozygous for the point mutation (Heil et al., 2001). In addition to altered homocysteine levels, cSHMT C1420T variant was unable to be SUMOylated by UBC9 (Woeller et al., 2007). This SUMOylation is necessary for nuclear import of cSHMT, along with TYMS and DHFR, so that they can contribute thymidylate to DNA synthesis (Woeller et al., 2007). Thus, it can be reasoned that when the C1420T polymorphism is present there is less cSHMT that can be SUMOylated and thus less cSHMT that can be brought into the nucleus and participate in thymidylate synthesis. This may

allow for more folate metabolites to be directed to the methionine synthesis pathway and allow for more efficient recycling of homocysteine. Therefore, lower levels of homocysteine may be noted. It is also possible that the C1420T mutant is unable to bind and sequester 5-methylTHF, thus it can be brought into the methionine cycle for homocysteine recycling.

mSHMT is the mitochondrial version of cSHMT. mSHMT has been found to be important not only for the production of folate metabolites but also for mitochondrial production of glycine which is necessary for heme biosynthesis and can also contribute to the one-carbon pathway (Appling, 1991, di Salvo et al., 2013). Many groups have demonstrated that mSHMT contributes to tumorigenesis (Jain et al., 2012, Lee et al., 2014) with only a few studies looking at the impact of cSHMT, but more and more are starting to investigate the role cSHMT plays in carcinogenesis. Two studies have validated the role that cSHMT plays in promoting lung tumor growth. One group demonstrated that cSHMT is overexpressed in lung cancer patient samples and that when KD in a lung cancer cell line p53 related apoptosis is induced as a result of increased uracil incorporation into the DNA (Paone et al., 2014). The other group determined that expression of cSHMT was inhibited by miR-198 in samples of lung adenocarcinoma reducing cell growth (Wu et al., 2016). Another group found that the transcription factor Wilms Tumor 1 (WT1), which increased expression WT1 of leads to decreased prognosis in ovarian cancer patients, upregulates expression of cSHMT which can be pro-tumorigenic through increased production of sialic acid increasing inflammatory cytokines IL-6 and IL-8 (Gupta et al., 2017). cSHMT expression was also investigated in different thyroid cancer subtypes and

overexpression of cSHMT correlated with thyroid cancers of the papillary thyroid, poorly differentiated, and anaplastic carcinomas, and those that were positive for the BRAFV600E mutation. In addition, expression of cSHMT was associated with a shorter overall progression free survival in the follicular variant of papillary thyroid carcinomas (Sun et al., 2016). Similarly, another group found that expression of cSHMT in lacrimal gland adenoid cystic carcinoma was associated with decreased overall survival (Koo and Yoon, 2015).

1.6.2 cSHMT's role in cancer progression

Thus, there is this juxtaposition of the impact of cSHMT expression on cancer progression. In the setting of cSHMT C1420T mutant there appears to be a protective effect against cancer, versus expression of the wild type leading to decreased overall survival or poorer prognoses in ovarian, lung, thyroid, and lacrimal gland carcinomas. This indicates that there is an important functional loss occurring with the C1420T mutation. Very few have studied the impact of this mutation on overall function but as mentioned previously it was found that the mutation impacts SUMOylation of cSHMT leading to an inability of the complex with TYMS and DHFR to move to the nucleus (Woeller et al., 2007). There is an alternative scaffolding protein SHMT2α, a splice variant of mSHMT that lacks the mitochondrial import sequence, has also been found to be able to act as a scaffold for TYMS and DHFR (Anderson and Stover, 2009). SHMT2α was demonstrated to be able to make up for this missing functionality when cSHMT is mutated in cancers but it cannot completely bring the thymidylate synthesis pathway back to baseline similar to cSHMT wild type. It is only able to preserve 25% of thymidylate synthesis production (Anderson and Stover, 2009). Lastly, there may be an additional function that cSHMT

participates in that is affected by the C1420T mutation that has yet to be described, but nuclear import appears to be key in the pro-oncogenic effect of cSHMT.

With the wild type cSHMT, since there is an acknowledge role for cSHMT in cancer progression investigations are being done to determine how to target cSHMT as a new cancer therapeutic. Since both cSHMT and mSHMT require vitamin B6 to be bound to become active one group looked at using vitamin B6 as a targeting moiety for nanoparticles carrying siRNA targeting cSHMT. What they found was that these particles through regulation of cSHMT expression could induce apoptosis and senescence leading to a decrease in tumor growth *in vivo* (Pandey et al., 2014). Another group found a selective inhibitor for cSHMT, a pyrazolopyran, and demonstrated lung cancer cell line susceptibility to the drug, again demonstrating induced apoptosis and senescence (Marani et al., 2016). These studies further confirmed the pro-oncogenic capabilities of cSHMT.

In the future it would be interesting to combine these selective therapies for cSHMT with other anti-folates, like methotrexate as described previously, to see if a more dramatic therapeutic response can be induced, or if inhibiting cSHMT alone is just as effective. This would further highlight the key place that cSHMT has in the one-carbon metabolism pathway, regulating the flow of folate metabolites between the methionine cycle and the thymidylate cycle. Also, it would be of value to determine if the specific inhibitor, pyrazolopyran, not only affects cSHMT enzymatic function but also if it inhibits the ability of cSHMT to bind and sequester 5-

methylTHF. If it does affect cSHMT and 5-methlyTHF binding then there would be more 5-methylTHF to recycle homocysteine for the production of methionine. If it doesn't then by inhibiting cSHMT from participating in thymidylate synthesis there may be more to bind 5-methylTHF inducing a folate trap. Since homocysteine has been repeatedly shown to be detrimental to endothelial cell function, and thus increased risk for cardiovascular disease, an induced increase in homocysteine levels may cause dysfunction in the vascularization of the tumor and tumor microenvironment (Lai and Kan, 2015). Additional next steps would be to use the pyrazolopyran inhibitor with a genetically engineered mouse model for lung cancer and see if with the inhibitor there is decreased vascularization of the tumor or if the vascularization is less defined or leakier compared to a control treatment. This would be valuable since leaky vasculature may allow for more chemotherapeutics to gain access to the site, through passive uptake, impacting overall tumor growth and progression.

1.7 Conclusion

In this study, we investigated whether IDH3 activity is regulated in GBM, and whether such regulation, through mitochondrial and extra-mitochondrial metabolic rewiring of cancer cells, affects the tumor biologic properties of GBM. Using tissue microarray, gain- and loss-of-function studies, *in vivo* tumor models, immunoprecipitation-mass spectrometry and metabolomic studies, we demonstrate that IDH3α is overexpressed in GBM compared to normal brain tissue and promotes orthotopic xenograft progression. In addition to IDH3's canonical function in regulating TCA cycle turnover and controlling mitochondrial energy metabolism, we discovered that IDH3α by co-localizing and interacting with cSHMT at the nuclear lamina,

regulates one-carbon metabolism, a central metabolic pathway, which via activation and transfer of one-carbon units modulates purine and thymidine synthesis, as well as DNA and protein methylation. We demonstrate that IDH3α through effect on cSHMT, regulates nucleotide availability and DNA methylation. Loss of IDH3α function results in an increase in the methyl group donor SAM and DNA methylation, while decreasing nucleotide availability and cellular growth. These studies point to IDH3α-induced metabolic adaption as a novel therapeutic point of intervention to halt GBM progression.

CHAPTER 2: MATERIALS AND METHODS

2.1 Experimental design

The objective of this study was to determine the role of IDH3α in GBM progression. We investigated mRNA and protein expression of IDH3 subunits in GBM tumor specimens by analysis of RNA-Seq datasets together with IHC-TMAs. Gain- and loss-of-function explant models aimed to establish oncogenic function of IDH3α *in vivo*, and mechanistic studies, using unbiased IP-MS, metabolic flux, and subsequent functional validation studies, evaluated the role of IDH3α on mitochondrial and extra-mitochondrial metabolic pathways.

2.2 Cell culture

Patient-derived glioma-initiating cells (GIC)-20 (gift from Dr. Kenneth Aldape, University of Toronto) and #387 (gift from Dr. Jeremy Rich, UCSD) were grown using DMEM/F-12 50:50 media, containing L-glutamine (Corning) N2 and B27 supplements (Invitrogen), human Epidermal Growth Factor (Shenandoah Biotech), human Fibroblast Growth Factor (Shenandoah Biotech), human Leukemia Inhibitor Factor (Shenandoah Biotech), Glutamax (Life Technologies), and 1% pen/strep antibiotics (Life Technologies). NHAs (gift from Dr. Russell Pieper, UCSF), U87MGs, and LNZ308s were grown in DMEM 1X with 4.5 g/L glucose, L-glutamine and sodium pyruvate (Corning) media containing 10% fetal bovine serum (FBS) (Life Technologies) and 1% pen/strep antibiotics (Life Technologies).

2.3 Generation of cells modified for IDH3α knockdown, KO and overexpression

The *IDH3*α cDNA was cloned into the CSII-CMV-MCS-IRES2-Venus vector using unique NheI and AgeI restriction sites. For virus production, HEK293T cells were plated in T75 flasks.

At 70% confluency, cells were transfected with 20 μg of IDH3α or empty vector control construct, 10 μg of pMD2.G (envelope) and 15 μg psPAX2 (HIV-Gag-Pol-Rev), using Lipofectamine 2000 (ThemoFisher) according to the manufacturer's instructions. For virus concentration, the cell supernatant was spun at 114 g for 5 minutes to pellet debris. The supernatant was filtered using a 45 μm low protein binding filter (Millipore), and centrifuged at 120,000 g for 2 hours at 4°C. The virus pellet was resuspended in DMEM, aliquotted and stored at -80°C. Mission shRNA lentiviral particles (pLKO.1-puro-CMV-tGFP) targeted to IDH3α were purchased from Sigma Aldrich (sequences: sh2, TGTCTCTATCGAAGGCTATAA; sh5, TTAAGTGTCTACCTGGTAAAT), including control particles (SHC003V). Viruses to generate CRISPR/Cas9 KO clones were purchased from Sigma Aldrich. The viral plasmid contained both the gRNA and the Cas9 protein along with GFP, puromycin, and ampicillin; control virus (Sigma, CRISPR12V-1EA), sequences for gRNAs: 318: CCTTTGAAGACCCCAATAGCAG and 329: CCCAATAGCAGCCGGTCACCCA and control gRNA Ctrl: CGCGATAGCGCGAATATATTNGG. For lentiviral infection, cells were trypsinized and seeded at 50% confluency. The next day, cells were washed with PBS, resuspended in Optimem containing 0.8 μg/mL Polybrene, and virus (1:1000 or 3:1000 dilution of virus stocks). Cells were incubated at 37°C and 5% CO_2 for 4 – 6 hours, before adding fresh full growth media. After 3 – 6 days, the cells were trypsinized, washed with PBS, and resuspended in PBS for flow cytometry cell sorting by GFP signal. Sorted cells then underwent limited dilution cloning. Single cell clones were grown up and screened for IDH3α KO via WB. Those clones that showed lack of IDH3α expression were further subcloned to obtain clonal populations.

2.4 Cell growth curves

Cells were seeded into 6 wells plates at 50,000 cells/well (day 0). Every 3 days, up to day 9, cells were trypsinized, stained with trypan blue for assessment of cell viability, and counted twice using an automated cell counter.

2.5 Transwell invasion assay

Fisher/Corning Biocoat invasion chamber 24 wells (Cat#8774122) were used for this assay, and the experiments outlined below were carried out according to the manufacturer's protocol. Briefly, plates/transwells were removed from -20°C and left at room temperature for 1 hr. Bicarbonate-containing medium was added to each transwell, and wells were incubated for 2 hours in a humidified tissue culture incubator. After the media was removed, a cell suspension of 500,000 cells/0.5mL in media without any growth supplements was added to each transwell, and 0.5mL of full media was placed in the bottom well. The plate was then incubated in a humidified tissue culture incubator for 22 – 24 hours. Subsequently, the non-migratory cells were washed off with a cotton tip, and wells were fixed and stained with the Richard-Allan Scientific™ Three-Step Stain. The wells were then dried overnight before mounting on microscope slides for imaging.

2.6 Generating IDH3α deletion mutants

Mutagenesis primers were designed to delete the mitochondrial translocation sequence (MTS) of the *IDH3α* gene; F primer: ACTTTAATTCCAGGAGATGGTATTGGCCCA, R primer: CATGCTAGCGGATCTGACGGTTCACTAAAC). These primers were then added at 0.5 μM

concentration to 100 ng of IDH3α vector DNA along with 200 μM of dNTP, 1.25 units of PrimeStar HS (Takera Cat #R010A), and PrimeStar 5x Buffer to obtain a 1X final concentration. Reaction mixtures were supplemented with nuclease-free water up to a volume of 50 μL. A PCR reaction was carried out on a thermocycler using the following parameters: 95°C for 2 min, then 30 cycles of 97°C for 10 sec, 68°C for 1 min, 72°C for 10 min, and then 4°C to hold. Subsequently, 20 units of DpnI (New England BioLabs Cat# R0176) were added directly to the PCR reaction tube for 1 hour. The PCR reaction was then run on a gel, excised, and the product extracted. The resulting product was treated with 10 units of T4 PNK (New England BioLabs Cat#M0201) in 1X of T4 PNK Buffer (New England BioLabs Cat#B0201), 1 mM ATP (New England BioLabs Cat#P0756), and nuclease-free water (total volume = 50 μL. The samples were then incubated at 37°C for 30 min and heat inactivated at 65°C for 20 min. 1 μL T4 DNA ligase (Promega Cat#M1804) was added to the reaction tube. After 3 hrs incubation at RT, the plasmids were then transformed in bacteria and deletion of MTS was confirmed by sequencing.

2.7 Immunoprecipitation and mass spectroscopy

Cells were lysed in IP buffer (50 mM Tris-HCl pH 7.5, 150 mM NaCl, 5 mM EDTA, 1% Lauryl Maltose Neopentyl Glycol (Anatrace), 1x protease inhibitor cocktail, 1x phosphatase inhibitor). 5 μg of IDH3α antibody (Abcam, ab58641) or control rabbit IgG antibody (Santa Cruz, sc-2030) was added to 500 mg of cell lysate. The samples were then left to rotate at 4°C overnight. 50 μL Dynabeads ® (Life Technologies, 10004D) per sample were added. Upon placement on a magnet, beads were washed three times with 500μL/wash of IP buffer. To elute immunoprecipitated proteins, beads were resuspended in 2x30 μL of glycine buffer (100 mM

glycine pH 2.5, adjusted with HCl). Peptides were analyzed by LC-MS/MS using a Dionex UltiMate 3000 Rapid Separation nanoLC coupled to a linear ion trap – Orbitrap hybrid mass spectrometer (LTQ Velos Orbitrap, Thermo Fisher, San Jose, CA, USA). Proteins were identified from the MS raw files using the Mascot search engine (Matrix science). MS/MS spectra were searched against the SwissProt human database. All searches included carbamidomethyl cysteine as a fixed modification and oxidized Met, deamidated Asn and Gln, and acetylated *N*-terminus as variable modifications. Three missed tryptic cleavages were allowed. The MS^1 precursor mass tolerance was set to 20 ppm, and the MS^2 tolerance was set to 0.6 Da. A 1% false discovery rate cutoff was applied at the protein level.

2.8 Co-immunoprecipitation

Cells were grown in 10 or 15 cm dishes. At 80-90% confluency, plates were washed with cold PBS and collected in lysis buffer (50 mM Tris-HCl pH 7.5, 150 mM NaCl, 5 mM EDTA, 1% Lauryl Maltose Neopentyl Glycol, 1x protease inhibitor cocktail, 1x phosphatase inhibitor). The cell lysis solution was vortexed every 5 minutes for 30 minutes while kept on ice. The samples were spun down at 4°C for 15 min at 16,100 g. The supernatant was then collected and protein concentration was determined by Bradford assay. 500-1000 μg of total protein was used for IPs with IgG control and specific antibodies (*i.e.*, anti-IDH3α antibody (5 μg; Abcam, ab58641); anti-cSHMT antibody (5 μg; Abcam, ab186130). 5-20 μg of total protein was used as input. Samples were incubated at 4°C overnight while rotating. 50 μL per sample of Dynabeads® (Life Technologies, 10004D) were added, and after 30 min incubation at RT, beads were washed three times with 500μL/wash with phosphate-buffered saline (PBS) + 1xprotease inhibitor, and

resuspended in 25 μL of NuPage LDS Sample Buffer (Life Technologies) + 5% β-mercaptoethanol. The samples were then heated at 95°C for 10 minutes and analyzed via WB.

2.9 Western blot analysis

Samples were run on NuPage 4-12% Bis-Tris gels (Life Technologies), and transferred to Hybond P PVDF membranes (Genesee Scientific, GE). Membranes were washed for 5 minutes in PBS + 0.05% Tween 20 (PBS-T), blocked with 5% milk in PBS-Tween (PBS-T) for 1 hr, incubated with primary antibodies overnight, washed three times with PBS-T for 10 minutes per wash and developed with secondary goat anti-rabbit, goat anti-mouse, or donkey anti-goat IgG antibodies (Santa Cruz) in 5% milk PBS-T. After three more washes at 10 minutes each with PBS-T, membranes were developed with SuperSignal ECL (ThermoScientific) following the manufacturer's protocol. Primary antibodies: anti-cleaved caspase-3 (Cell Signaling, 9664), anti-cleaved caspase-7 (Cell Signaling, 9491), anti-IDH3α (Sigma Aldrich, SAB100035), anti-HSP70 (BD Biosciences, 610607), anti-cSHMT (Abcam, ab186130), anti-H3 (Cell Signaling, 4499S), and anti-COXIV (Cell Signaling, 4850S)

2.10 NADP+/NADPH Quantification

Quantification of NADP+ and NADPH was achieved with Biovision's colorimetric assay (Cat#K347-100). Cells were washed with cold PBS and pelleted at 2000 rpm for 5 min. They were then lysed with 800 μL of the provided NADP/NADPH Extraction Buffer and kept on ice for 10 min. Then the samples were spun at 10,000 x g for 10 min. The collected supernatant was then loaded onto a clear bottom black walled 384 well plate at 5 μL per well. For NADPH

detection half of the supernatant was heated to 60°C for 30 min and then cooled on ice before loading onto the plate. To sample wells and kit provided standard curve wells a reaction mix was added containing a cycling buffer and cycling enzyme. The plate was incubated at RT for 5 min followed by the addition of 10 μL of NADPH developer. The reaction was then incubated for 1 hr at RT and read at OD450 nm.

2.11 SAM/SAH ELISA

Samples were processed using the SAM and SAH ELISA kit from Cell Biolabs (Cat#STA-671-C). Cells were collected by centrifuging at 2000 x g for 10 min at 4°C. The supernatant was removed and the cells were resuspended in 1 mL of cold PBS followed by homogenization using 25 G syringes, passing the sample ten times. Then the samples were centrifuged at 10,000 x g for 15 mins at 4°C. The supernatant was collected and stored at -80°C. To prep the plate SAM or SAH conjugate was loaded onto the plate using 100 μL/well of either conjugate and the plate was incubated for 2 hrs at 37°C. The conjugate was then removed and the wells were washed three times with 200 μL of PBS followed by blotting. Then 200 μL of Assay diluent was added to block for 1 hr at RT. The diluent was then removed and 50 μL of samples or standards were added and the plate incubated on an orbital shaker at RT for 10 min. Then 50 μL/well of SAM or SAH antibody, with their respective conjugate well, was incubated on the plate for 1 hr at RT. The plate was then washed three times with 250 μL of wash buffer with thorough aspiration between washes before the addition of 100 μL of secondary antibody HRP conjugate to each well. The plate was then incubated for 1 hr on an orbital shaker at RT during which time the

substrate solution was warmed to RT. Following the HRP incubation, the above wash step was repeated before the addition of 100 μL of substrate solution per well and placed again on an orbital shaker at RT. At this point the plate was carefully watched for a color change at which point the reaction was stopped with 100 μL of stop solution and then the plate was read at OD 450 nm.

2.12 Homocysteine ELISA

Homocysteine was measured using the Cell Biolabs ELISA kit (Cat#STA-670). Samples were prepared similar to the SAM/SAH assay above (collect cells with spinning, homogenize, centrifuge, and collect and store the supernatant). The samples and plate were also handled similarly to the SAM/SAH assay above just using a homocysteine conjugate and an anti-homocysteine antibody.

2.13 α-Ketoglutarate Colorimetric Assay

αKG was measured using Biovision's colorimetric assay (Cat#K677-100). The cells were washed with PBS and collected by spinning at 5000 rpm for 5 min. The supernatant was removed and 50 μL of assay buffer was added to each sample. The samples were then left on ice for 30 min, vortexing at full speed every 5 min. The samples were then deproteinized with perchloric acid followed by a neutralizing solution (Biovision, Cat#K808-200). 5 μL of each sample was then loaded on to a clear bottom black wall 384 well plate. To sample and standard curve wells 5 μL of reaction mix was added, containing assay buffer, converting enzyme,

enzyme mix, and a probe. The plate was then incubated at 37°C for 30 min and then fluorescence measured with Ex/Em = 535/587 nm.

2.14 IDH activity assay

To measure IDH activity the Biovision IDH Activity Colorimetric Assay Kit was used (Cat#K756-100). Cells were washed with PBS and then assay buffer was added and the cells which were homogenized with a 25 G syringe 10 times. The samples were then spun at 13,000 x g for 10 min and 5 μL of supernatant was added to each well of a clear bottom black walled 384 well plate. To each sample and standard curve well 5 μL of reaction mix was added containing, assay buffer, developer, IDH substrate (isocitrate), and NAD+ (to evaluate IDH3 activity specifically). The plate was then placed into a plate reader set to 37°C and read at 3 min and then after a 30 min incubation read every 5 min up to 2 hrs at OD450 nm.

2.15 NAD+/NADH quantification

Abcam's colorimetric kit (Cat#ab65348) was used for quantification of NAD+ and NADH levels. Cells were harvested, washed with cold PBS and then pelleted at 2000 rpm for 5 min. The supernatant was removed and then 400 μL of extraction buffer was added to each sample. The samples then underwent two freeze thaw cycles on dry ice for 20 min and then at RT for 10 min. After vortexing for 10 seconds the samples were centrifuged for 5 min at 4°C at top speed. The supernatant was then applied to a 10 kD spin column (Cat#ab93349) and spun at 10,000 x g for 10 min to collect the enzyme free filtrate. Half of each filtrate was heated at 60°C for 30 min to degrade NAD+. Then 5 μL per well of NAD/NADH containing samples and NADH only containing samples were loaded onto a clear bottom black walled 384 well plate and to these and

standard wells 10 μL of the reaction mix containing cycling buffer and an enzyme mix was added. The plate was then incubated at RT for 5 min followed by the addition of 10 μL of NADH developer. After incubation at RT for 1 hr the plate was read at OD450 nm.

2.16 TET activity assay

TET activity was measured using the Epigenase™ 5mC Hydroxylase TET Activity/Inhibition Assay Kit (Cat#P-3087, Epigentek). Wells were prepped with 80 μL of binding solution followed by 2 μL of 0.5X TET substrate solution. The wells were then parafilmed and incubated at 37°C for 90 min. The binding solution was removed and the wells were washed three times with 150 μL of wash buffer. Samples, blank solution, or standard solution was then added to their respective wells along with assay buffer up to 50 μL. With parafilm the wells were incubated for 90 min at 37°C. Afterwards the wells were emptied and washed three times with 150 μL per well of wash buffer. Then 50 μL of capture antibody, detection antibody, and enhancer solutions were added to each well in that order and incubated for 60 min, 30 min, and 30 min respectively. Between each solution the wells were washed three, four, and five times respectively with 150 μL of wash buffer. Finally, 50 μL of the fluorescence development solution was added to each well and incubated at RT while monitoring for color change. Afterwards the wells were read at Ex/Em = 530/590 nm.

2.17 ROS quantification

Cells were seeded at 500,000 cells/well into 6 well plates, treated with 5 μM of CellROX® Deep Red reagent (ThermoFisher, C10422), and incubated for 30 min in a humidified tissue culture

incubator. The media was then removed and cells were washed 3 times with PBS followed by fixation with 3.7% formaldehyde for 15 min. Cells were then analyzed by flow cytometry.

2.18 DEVDase assay

Caspase 3/7 activation was measured by spectrophotometric detection using the BioVision kit (Cat#K106-25). After treating the cells with MTX the media was removed the cells were trypsinized, counted, and pelleted after a PBS wash. Then the cells were lysed with 50 μL of lysis buffer and a 10 min incubation on ice. The samples were spun for 1 min at 10,000 x g and the supernatant transferred to a fresh tube on ice. After measuring the protein concentration by Bradford 10 μg of protein was added to each replicate well, of a clear bottom black walled 384 well plate, followed by lysis buffer up to 5 μL. Then 5 μL of reaction buffer + 10 mM DTT was added to each sample well followed by 5 μL of 4 mM DEVD-*p*NA substrate. The plate was then incubated at 37°C for 2 hours followed by a reading at OD400 nm.

2.19 Cell fractionation

Cells were collected by centrifugation at 1500 g for 5 min. The pellet was resuspended in 200 μL hypotonic buffer pH 8 (10 mM Hepes pH 8, 10 mM KCl, 1 mM EDTA, 1xprotease inhibitor, 1.5 mM, $MgCl_2$ 0.1 mM DTT, 10 μM cytochalasin B), and incubated on ice for 30 minutes, followed by centrifugation for 5 minutes at 1500 g. The supernatant was discarded and the pellet was resuspended in 200 μL of hypotonic buffer. Next, the samples were homogenized with a 25G needle, and centrifuged at 400 g for 10 min. The supernatant representing the cytosolic and mitochondrial fraction was retained. The pellet was washed with 500 μL of hypotonic buffer

followed by centrifugation at 400 g for 10 min. The resulting pellet was washed twice with 500 µL/wash PBS containing 1 mM EDTA, 1.5 mM $MgCl_2$, 0.1 mM DTT and 10 µM cytochalasin B. The pellet was resuspended in 3 mL of S1 (0.25 mM Sucrose, 10 mM $MgCl_2$ + 1xprotease inhibitor). The S1/sample solution was layered over 3 mL of S2 (0.35 mM Sucrose, 0.5 mM $MgCl_2$ + protease inhibitor) by slowly pipetting S1 onto S2. Samples were centrifuged for 10 minutes at 4°C at 2,178 g. The supernatant was removed and the pellet was resuspended in 3 mL of S2. The S2/sample solution was layered over a 3 mL layer of S3 (0.88 mM Sucrose, 0.5 mM $MgCl_2$ + 1xprotease inhibitor) by slowly pipetting S2 onto S3 and the final sample was centrifuged for 10 minutes at 4°C at 2,178 g. The supernatant was removed and the pellet was resuspended in Thermo Fisher NER reagent + 1xprotease inhibitor. The samples were vortexed for 15 seconds followed by an incubation period of 40 min on ice. Every 10 min the samples were vortexed for 15 seconds. Samples were centrifuged at maximum speed (~16,000 x g) for 10 minutes. The resulting supernatant represented the nuclear fraction.

2.20 Cell cycle syncing

Cells were grown to 20 – 30% confluency, washed twice with DPBS and then treated with 2mM thymidine in full media for 18 hours. Cells were washed once with DPBS, resuspended in full media for 9 hours, and treated again with 2mM thymidine in full media for 17 hours. Cells were stained with propidium iodide and cell cycle distribution was analyzed by flow cytometry.

2.21 Tumor xenograft model

All animals used in the study were under an approved protocol of the Institutional Animal Care and Use Committee of Northwestern University. All cells were modified for luciferase expression as described in previous publications (Calvert et al., 2017). GIC-387 expressing shIDH3α or shScr ($2x10^3$ cells/2μL), IDH3α KO and control wild-type NHAs ($5x10^4$ cells/2μL), and GIC-20 overexpressing IDH3α and vector only ($5x10^4$ cells/2μL), were resuspended in Hank's Balanced Salt Solution. Anesthetized 6 – 8 week old female CB17 SCID mice (Taconic Farms) were placed in stereotactic frames and the surgical area was cleaned with betadine followed by 70% ethanol. Following a scalp incision, a 0.7 mm Burr hole was created in the skull with a microsurgical drill, 2 mm lateral right of the sagittal suture and 0.5 mm posterior to the bregma. Cells were injected through a Hamilton syringe after it was inserted 3 mm into the brain. Cells were injected at a rate of 1 μL per minute. Once surgery was completed the skin was closed with sutures. Mice were sacrificed at ethical endpoints based on observations of neurological impairment or severe changes in body weight. 8 – 10 animals were used in each group, and mice were randomized based on body weight. The Kaplan-Meier method was used to plot survival, and significance was determined by the log rank (Mantel-Cox) test.

2.22 In vivo bioluminescence imaging

10 minutes after IV injection with 200 μL of luciferin potassium salt (Perkin Elmer) suspended in PBS, mice were anesthetized and imaged using the IVIS Spectrum (Perkins Elmer). Bioluminescence was quantified using Living Imaging Software (Caliper Life Sciences).

2.23 Immunohistochemistry

Tissue samples were collected with patient consent at the University of Kentucky and prepped as a tissue microarray. Slides were heated at 60°C for 1 hr followed by deparaffinization and hydration, washed with water and placed into 1x Dako Target Retrieval Solution (Agilent, S1699) and subsequently incubated in a Biocare Medical Decloaking Chamber at 110°C for 10 min. Slides were washed twice with PBS for 3 min 200 μL of peroxidase block (Agilent, Dako K4011) was added and incubated for 10 min at room temperature (RT) followed by a PBS rinse. Next 2 – 5 drops of protein block background with background sniper (Biocare Medical, BS966H) was added and slides were incubated for 10 min at RT followed by 1 – 2 min PBS rinse. IDH3α antibody (Sigma Aldrich, HPA041465) was added at a 1:400 dilution to the slides and incubated for 1 hr. Slides were then rinsed three times with TBS/Tween (TBST) for 1 min each. Secondary antibody (Agilent, Dako 4011) was added and incubated for 35 min followed by three PBS washes. DAB chromogen was added and incubated up to 3 min followed by counter staining with hematoxylin and then washed with water. The slides were then dehydrated and coverslips mounted with Permount. A licensed and practicing neuropathologist then scored the tissues as concerns IDH3a staining intensity. For endothelial cell staining, tissue was deparaffinized followed by incubation with IDH3α antibody (Sigma Aldrich, HPA041465) overnight and then with CD31 antibody (Santa Cruz, sc-1506) for 1 hr. Samples were then blocked with 3% hydrogen peroxide in water for 10 min and then Avidin/Biotin Blocking for 15 minutes each. Blocking of non-specific proteins was achieved by incubating in 5% normal donkey serum for 30 min. The slides were then incubated with secondary Cy3- anti-rabbit for one hour and then secondary biotinylated anti-goat for 30 minutes, followed by an ABC kit

(Vector Labs, PK-4000) treatment for 30 min. The slides were then incubated with a working solution of biotinyl tyramide for 5 minutes and then with Alexa Fluor 488-Streptavidin for 30 min. Hoechst nuclear staining was done for 10 min.

2.24 Metabolomics steady state study

7.5×10^6 cells (NHAs with CRISPR-mediated IDH3α KO, or NHAs overexpressing IDH3α) were washed twice with Dulbecco's Phosphate Buffered Saline with calcium and magnesium 1x(DPBS) (Corning, 21-030-CV) and then snap frozen in liquid nitrogen. At Metabolon, samples were then processed by the automated MicroLab Star® system (Hamilton). Recovery standards were added to all samples for quality control measures. Methanol was added to all samples. Each sample was shaken for 2 min followed by centrifugation to release metabolites. All samples had aliquots that underwent Ultrahigh Performance Liquid Chromatography-Tandem Mass Spectroscopy (UPLC-MS/MS) (Thermo Scientific) with either Reverse Phase (RP) plus positive ion mode electrospray ionization (ESI), RP plus negative ion mode ESI, or following HILIC column (Waters UPLC BEH Amide 2.1x150 mm, 1.7 μm) elution with negative ion mode ESI. Samples were reconstituted with solvents appropriate for each method and run along-side standards. Data were analyzed using Metabolon hardware and software. Compounds were identified based on a narrow retention index that was then compared to a library of purified standards and MS/MS scores comparing the experimental spectrum to the library spectrum.

2.25 ^{13}C-labeled glucose tracer studies

6 well plates were seeded with ~50,000 cells per well and allowed to attach overnight. The next day, all wells were washed with nutrient free media (DMEM, Fischer, Cat#A144300) and then given media supplemented with 4 mM glutamine (Sigma, Cat#G8540), 10% dialyzed FBS (ThermoFischer, Cat#A3382001), 1 mM sodium pyruvate (Sigma, Cat#P5280), and 25 mM uniformly labeled ^{13}C glucose (Cambridge cat # 110187-42-3) for all time point samples excluding the 0 hr time point, which was labeled with 25 mM ^{12}C-labeled glucose (Sigma G7021). At designated time points, the media was removed, and the cells were washed with a cold 0.9% NaCl solution. Subsequently, 1 mL of ice-cold 80% methanol/water solution was added to each well and the plate was placed at -80°C. After 15 min, the plates were removed from -80°C and placed on dry ice while the sample wells were scraped and the cell/80% methanol solution was placed in collection tubes. The tubes were spun at 20,000 rcf for 10 min at 4°C. The supernatant was taken and split between two tubes per sample. The amount of supernatant taken was based off cell counting to normalize the amount of cells per tube. Finally, samples were dried in a speed vacuum set at room temperature for 2 – 3 hours. This dry pellet was then stored at -80°C until analysis by LC-MS as previously published (Liberti et al., 2017).

2.26 Seahorse assay

The day before the assay, the Seahorse cartridge was placed in the XF calibrant and incubated overnight at 37°C. On the day of the assay, cells were seeded into the Seahorse 96 well plate at 15,000 cells per 80 μL per well. The plates were incubated at room temperature for 1 hr to allow for even distribution of cells across the well floor, before going into the incubator. Before

placing the sample plates in the Seahorse XF96 Analyzer, media volume was adjusted to 175µL in each well. Oligomycin at 2 µM, CCCP at 10 µM, and Antimycin A and Rotenone at 2 µM each, diluted in DMEM media, were injected sequentially following the standard Seahorse protocol into each well including control wells, containing only media.

2.27 Immunocytochemistry

Cells were seeded either in 10 cm dishes or 24 well plates containing synthetic Poly-D-Lysine/Mouse Laminin coated 12 mm round coverslips (Corning) and allowed to attach. Cell media was removed and cells were washed with PBS before fixation with 4% paraformaldehyde (PFA) in deionized water for 5 min. The coverslips were washed with PBS and cells were permeabilized with PBS/Triton X-100 (EMD) 0.2% for 5 min. The coverslips were washed with PBS, followed by PBS/1% FBS, and then blocked for 30 min in PBS/1% FBS. The blocking solution was removed and primary antibodies diluted in PBS/1% FBS (*i.e.*, anti-IDH3α 5µg/mL (Abcam, ab58641), anti-cSHMT 1:50 (Santa Cruz, sc-514410), anti-Lamin A 1:500 (Santa Cruz sc-6214), anti-cytochrome c 1:500 (BD Biosciences, 556432), together with Hoechst 33342 1:10,000 (Invitrogen)) were added, and incubated with cells overnight at 4°C. Coverslips were washed twice with PBS/1% FBS and the secondary antibody was added (Alexa Fluor 488 anti-goat or anti-rabbit, Alexa Fluor 648 anti-rabbit, or Alexa Fluor 568 anti-mouse 1:300 (Invitrogen/Life Technologies)) for 1 hr at RT in the dark. The coverslips were washed once with PBS/1%FBS, twice with PBS, and once with water before being mounted on microscope slides. Slides were imaged using a Nikon A1R Spectral Microscope with an LED power source. To quantify IDH3α and cSHMT co-localization using Image J, a macro was designed that created a

mask for cSHMT intracellular distribution, based on the Alexa 568 staining; appropriate thresholds were used to decrease background signal. The percentage of IDH3a staining (Alexa 488) covered by the cSHMT mask, and thus colocalizing with SHMT1 was determined.

2.28 Histone methylation

NHA Controls and NHA IDH3α KO cells were grown in 10 cm dishes. At confluency, 1 million cells were collected for every biological replicate, 3 per group, washed with PBS, and flash frozen in liquid nitrogen. The samples were analyzed on the TSQ Quantum Ultra MS. To prepare the samples for MS, histones were acid-extracted, washed and then subjected propionylation and tryptic digestion (Garcia et al., 2007). Samples were then resuspended in 50 μL of 0.1% TFA/mH_2O. For each sample, we prepared 3 technical replicates. We used 3 μL per injection. HeLa cells were used as quality controls and for data comparison. Targeted analysis of unmodified and various modified histone peptides was performed. Samples were analyzed by the Proteomics core facility at Northwestern University.

2.29 RNA-seq

RNA was extracted from the Control or KO NHAs using RNeasy kit (Qiagen) according to manufacturer's protocol. RNA QC was performed using an Agilent bio-analyzer (Agilent). RNA-SEQ libraries were generated using Illumina TruSEQ mRNA stranded kits using the Illumina provided protocol. Libraries were quantitated using an Agilent bio-analyzer and the pooled libraries were sequenced using an Illumina HiSEQ4000 using Illumina reagents and protocols.

2.30 DNA global methylation array

DNA global methylation was measured in 4 biological replicates. Methylation levels were measured using the Infinium Human MethylationEPIC Beadchip array (Illumina, Inc. CA, USA), which targets over 850, 000 methylation sites. Samples were randomly plated on each chip. A 500 ng DNA sample was used to perform bisulfite conversion followed by methylation profiling according to Illumina's protocol. BeadChips were scanned with an Illumina iScan and analyzed using the Illumina GenomeStudio software. All experiments were conducted following the manufacturer's protocols in the NUSeq Core Facility at Northwestern University.

RNA-seq - RNA was extracted from control or IDH3a KO NHAs using the RNeasy kit (Qiagen) according to the manufacturer's protocol. RNA quality control was performed using an Agilent bio-analyzer (Agilent). RNA-SEQ libraries were generated using Illumina TruSEQ mRNA stranded kits following Illumina protocols. Libraries were quantitated using an Agilent bio-analyzer and the pooled libraries were sequenced using an Illumina HiSEQ4000 using Illumina reagents and protocols.

2.31 Preprocessing of RNA-Seq expression data

RNA sequencing data was preprocessed using RSEM software package with in-built STAR alignment tool (Li and Dewey, 2011, Dobin et al., 2013). Raw sequence reads were aligned to human reference genome (GRCh37/hg19 assembly).

2.32 Differential expression analysis using DESeq2

Abundance quantifications were imported into R software and gene expression matrix was constructed using R Bioconductor package *tximport* (Soneson et al., 2015). Count values summarized by *tximport* were analyzed using the *DESeq2* algorithm. Differential expression was defined at a threshold of FDR = 0.05 and absolute log fold-change > 1.

2.33 Preprocessing of methylation microarray data

Methylation microarray data from Illumina Infinium Human MethylationEPIC BeadChip platform were analyzed using R Bioconductor package *minfi* (Aryee et al., 2014). Raw IDAT files were loaded into R software and raw intensity signals were preprocessed and normalized using functional normalization algorithm optimized for multi-condition studies (Fortin et al., 2014). The resulting normalized β-values were further converted to M-values ($M = \log_2(\beta/(1-\beta))$) for downstream statistical analyses. Quality control was performed by manually checking QC density plots. Probes with SNPs were dropped as they are prone to affect methylation measurements. All probes were annotated using human reference genome GRCh37/hg19 assembly. Quality as well as sample-wise pattern of the preprocessed data were preliminarily visualized by PCA.

2.34 Differentially methylated position analysis using Limma

In order to identify which individual CpG loci were differentially methylated between KO and control conditions, we performed differentially methylated positions (DMP) analysis using *Limma* algorithm (Ritchie et al., 2015). The M-value matrix was subjected to lmfit to compute the mean difference between conditions. Differentially methylated CpG loci was defined as

Benjamini-Hochberg adjusted p-value < 0.05 and absolute M-value difference greater than 1 (|ΔM-value| > 1).

2.35 Differentially methylated region analysis using DMRcate

In order to identify and visualize consistent methylation patterns within continuous genomic regions (e.g. CpG islands) we also performed differentially methylated regions (DMR) analysis using *DMRcate* package, which applies a Gaussian kernel smoothing to demarcate adjacent CpG sites within a genomic window (Peters et al., 2015). We applied the kernel bandwidth lambda = 1000 and scaling factor C = 2 following the recommended setting. We visualized the most significant DMRs in terms of minimum FDR using the DMR.plot function within the package.

2.36 Integrative analysis of expression and methylation data

To elucidate the relationship between expression level of a gene and methylation level of a CpG locus within that gene, we performed an integrative analysis combining our RNA-Seq expression and methylation array data. To associate a methylation probe with a gene, we defined the putative promoter region as -2 kb to +500 bp of the transcription start site (TSS) and linked all CpG loci with corresponding gene. Genes with low expression were removed. We used Trimmed Mean of M-values (TMM) normalization across samples to adjust the difference in library size and $\log_2$-transformed the normalized expression values (Robinson and Oshlack, 2010). We identified 209,063 CpG-gene pairs between 23,967 genes and 835,778 CpG sites. We then performed Pearson correlation analysis between gene expression and methylation data to identify statistically significant CpG-gene pairs. A positive correlation indicates methylation and

expression change in the same direction while a negative correlation implies changes in opposite direction.

2.37 DNA dot blot

gDNA extracted in water was diluted to a final concentration of 400 ng/μL in 10 μL volume for both NHA control and IDH3α KOs. Subsequently, to each dilution, 200 μL of 6xSaline Sodium Citrate (SSC) was added. Each sample was heated at 100°C for 10 min, allowed to cool on ice and 200 μL of ice cold 20xSSC was added. Meanwhile, nitrocellulose membrane and 2 filter papers were wetted with 6xSSC and then mounted on a 96 well dot blot apparatus. To the wells to be used, 500 μL of water was added and pulled through the membrane with gentle vacuum pressure. Subsequently, the diluted samples were added and pulled through. Finally, the membrane was washed with 500 μL of 2xSSC solution, and pulled through the membrane. The membrane was allowed to air dry before UV DNA crosslinking for 5 min at 100 μJ/cm^2. The membrane was incubated in 5% milk overnight. The following day, 5-methylcytosine antibody (#MABE146, Millipore) or 5'-hydroxymethylcytosine antibody (#39769, Active Motif) was applied (1:1000 dilution in 5% milk) for 1 hr, washed three times with PBS-T (5 min each), incubated with secondary mouse antibody (1:2500) for 30 min, washed three times with PBS-T again and then developed with ECL. The loading was determined by 0.02% methylene blue stain.

2.38 MTT assay

Cells were seeded at 10,000 cells per well in a 96 well plate, and treated with vehicle/Optimem, or 0.1, 1, 10, or 100 μM of methotrexate, 0.5 mM *N*-acetyl cysteine (NAC), or 1mM formate/0.4mM glycine. The MTT assay was performed following the manufacturer's protocol (ATCC). To each well containing 100 μL of median 10 μL of MTT reagent was added and the plate was incubated in the humidified culture incubator at 37°C for 2 hrs. Then 100 μL of detergent reagent was added to each well and the plate was then incubated overnight at RT. Then the plate was read at OD450 nm.

2.39 Histone methylation

NHA Controls and NHA IDH3α KO cells were grown in 10 cm dishes. At confluency, 1 million cells were collected for every biological replicate, 3 per group, washed with PBS, and flash frozen in liquid nitrogen. The samples were analyzed on the TSQ Quantum Ultra MS. To prepare the samples for MS, histones were acid-extracted, washed and then subjected propionylation and tryptic digestion (Garcia et al., 2007). Samples were then resuspended in 50 μL of 0.1% TFA/mH_2O. For each sample, we prepared 3 technical replicates. We used 3 μL per injection. HeLa cells were used as quality controls and for data comparison. Targeted analysis of unmodified and various modified histone peptides was performed. Samples were analyzed by the Proteomics core facility at Northwestern University.

2.40 Statistical analysis

All graphical and WB data are a culmination or representation of $n \geq 3$ biological replicates with technical replicates ($n \geq 3$) within each biological replicate. Data is represented by the mean ±

SD, or SEM for bioluminescence. Two-tailed Student's t-test was used to compare control to experimental groups, unless otherwise stated. *P*-values ≤ 0.05 were considered to be statistically significant.

CHAPTER 3: RESULTS

3.1 IDH3α is overexpressed in GBM

In contrast to its paralogs IDH1 and IDH2, genomic sequencing studies revealed that *IDH3α, β,* and γ subunits are not mutated in GBM (Krell et al., 2011). Analysis of the Ivy Glioblastoma Atlas Project (Ivy GAP) database, which contains RNA-seq data from 10 regionally microdissected GBM tumors (http://glioblastoma.alleninstitute.org/) (Puchalski et al., 2018), revealed enrichment of *IDH3α*, and to a lesser degree of *IDH3β* and *IDH3γ* transcript levels in cells of the leading edge and infiltrating tumor region when compared to the tumor center (Fig. 4A). Immunohistochemical (IHC) analysis of IDH3α protein on tissue microarray using a target specific antibody (Fig. 5A), confirmed by IDH3α staining in IDH3α wild-type and IDH3α KO, followed by semi-quantitative evaluation of protein expression by light microscopy (Fig. 4B) revealed that IDH3α protein is elevated two-fold within the glioma tumor core compared to glial cells within normal brain tissue (Fig. 4C). IDH3α expression was also significantly elevated in lower grade gliomas hinting that IDH3α expression may be maintained throughout secondary GBM development (Fig. 5B). In correlation with the IVY database IHC analysis also showed the most robust expression, four-fold increase, within the GBM leading edge (Fig 4B-C).

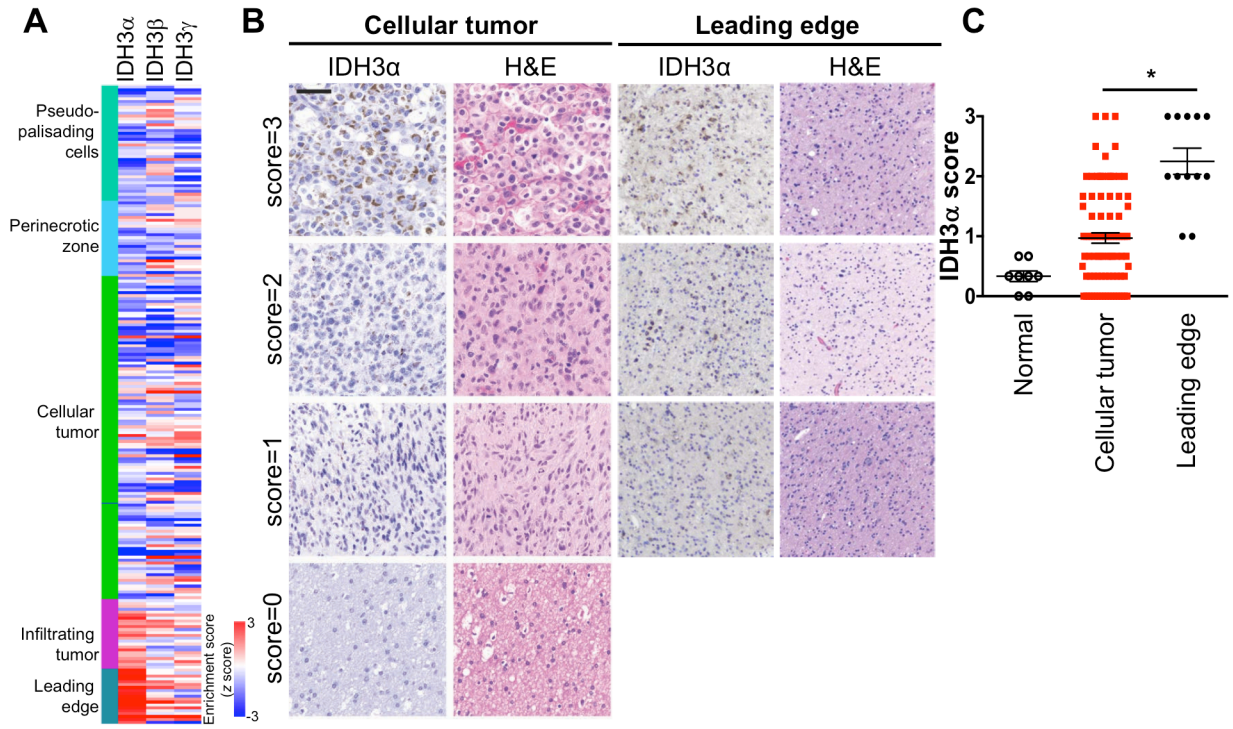

Fig. 4. IDH3α expression is elevated in human derived gliomas.
(A) *IDH3α*, *IDH3β* and *IDH3γ* mRNA expression as determined by RNAseq of 122 RNA samples from 10 regionally dissected GBM tumors (obtained from the Ivy Glioblastoma Atlas Project (Ivy GAP), http://glioblastoma.alleninstitute.org/). **(B)** Representative images of IDH3α IHC stainings with different grading scores (scale bar, 50 μM). **(C)** Tissue microarrays of GBM patient tumor samples, obtained from the University of Kentucky, and GBM tissue blocks containing tumor tissue of the leading edge were stained with IDH3α antibody and expression was quantified in glial cells of non-tumor brain vs. GBM tumor cells; *$p=0.03$, $n=8$ for non-tumor, $n=87$ for tumor samples.

Of note, *in silico* analysis of TCGA bulk tumor expression profiles (Cancer Genome Atlas Research, 2008) found reduced *IDH3α, β,* and *γ* transcripts within the tumor core when compared to normal brain elements (Calvert et al., 2017). Analysis of IDH3α protein expression profiles within normal brain tissue, however, demonstrated high expression of IDH3α in neurons (Fig. 5C), prompting the more detailed comparative analysis of IDH3α protein expression in

cells of glial origin in normal brain versus GBM tumor cells presented here. In addition to mitochondrial distribution observed, which is consistent with well-described functions of IDH3α within the mitochondrial TCA cycle (Gabriel et al., 1986), IDH3α staining was also found to be associated with the tumor cell nucleus, as determined by confocal immunofluorescence (IF) microscopy on tumor sections (Fig. 5D). Further, IDH3α was also found in the tumor-associated endothelium, but not in the endothelium of normal brain tissue, with 0/8 normal cortex samples versus 12/12 GBM samples positive for IDH3α endothelial cell staining (Fig. 5E). To confirm co-localization of IDH3α to the endothelium additional IF studies were done, staining for both IDH3α and endothelium using an endothelium specific marker CD31. Together, these observations suggest that GBM are characterized by elevated IDH3α expression, with significant IDH3α expression detectable in peripheral tumor cells and tumor-associated endothelial cells.

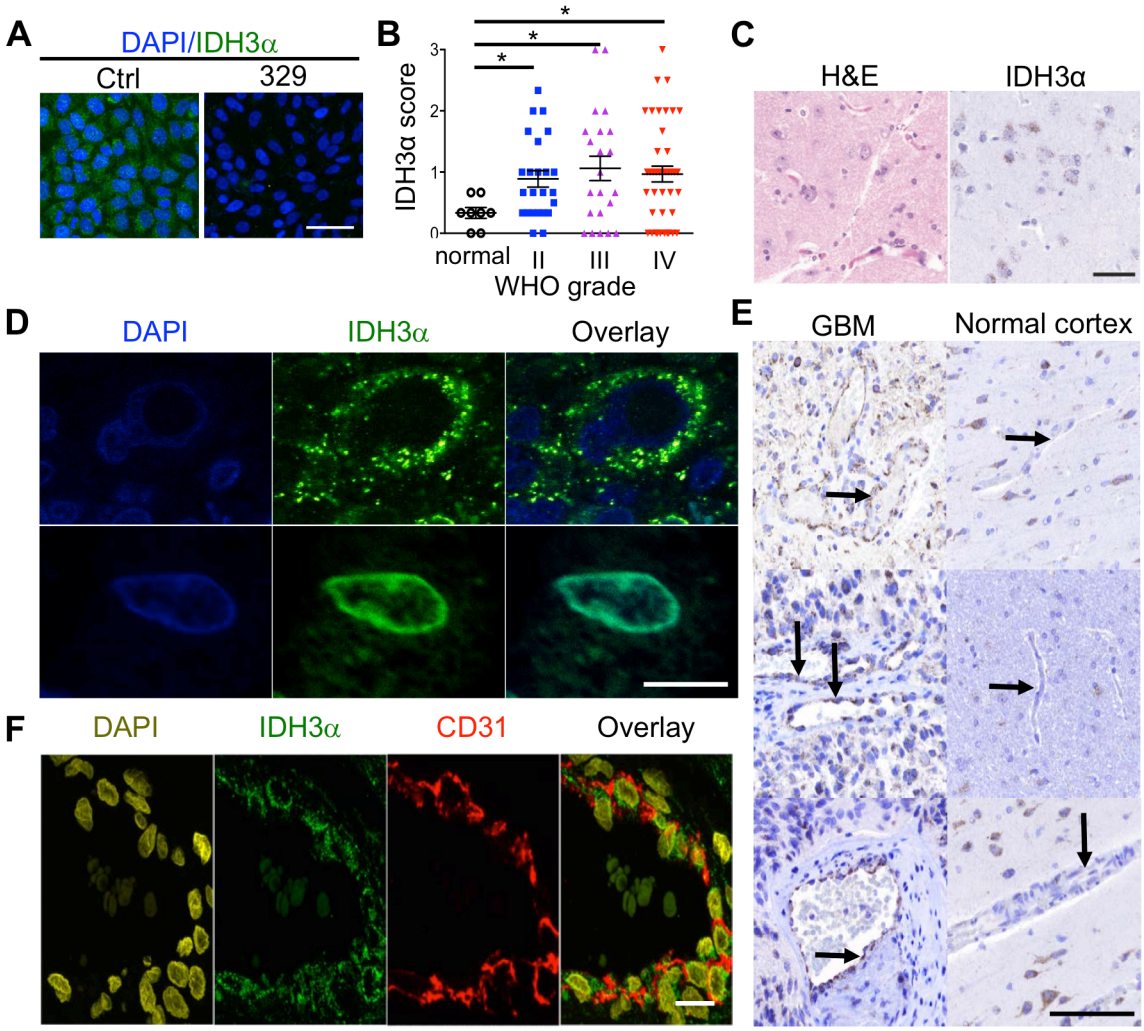

Fig. 5. IDH3α is confined to the nuclear periphery, and highly expressed in the tumor-associated vasculature.

(A) IHC staining for IDH3α in IDH3α wildtype and IDH3α-deficient NHAs, to validate antibody target specificity; bar, 50 μm **(B)** Tissue microarrays of glioma patient tumor samples of WHO grade II - IV, obtained from the University of Kentucky, were stained with IDH3α antibody and expression was quantified in glial cells of non-tumor brain vs. GBM tumor cells, **p<0.05, Normal: n = 8, Grade II: n = 24, Grade III: n = 22, Grade IV: n = 41*. **(C)** Representative image of IDH3α expression in normal neurons; bar, 50 μm **(D)** Immunofluorescence staining of IDH3α on tumor tissue reveals IDH3α association with the nucleus; bar, 10 μm. **(E)** Normal cortex and glioma tissue from patients, collected at Northwestern Memorial Hospital, were stained for IDH3α; in 0 out of 8 normal cortex samples versus 12 out of 12 glioma samples, IDH3α was found to be expressed in the vascular endothelium; *p<0.0001;* bar, 150 μm **(F)** Co-staining of IDH3α (green), CD31 (red) and DAPI (yellow) in tumor sections; bar, 20 μm.

3.2 IDH3α promotes GBM progression

To determine whether IDH3α can regulate *in vivo* GBM tumor progression, we generated a series of IDH3α gain- and loss-of-function cell culture and derivative orthotopic xenograft model systems using minimally transformed cortical astrocytes (normal human astrocytes, NHAs) and patient-derived glioma initiating cells (GICs). Suppression of IDH3α expression in luciferase-labeled NHAs via CRISPR/Cas9 genome editing (Fig. 6A) using two different sgRNA constructs robustly decreased cellular growth by about half (Fig. 6B). Animal subjects engrafted with IDH3α-deficient NHAs showed reduced intracranial GBM tumor progression as measured by luciferin signal (Fig. 6C, D), and increased survival when compared to control explants (Fig. 6E). This reduction in tumor size and increase in overall survival correlate with IDH3α expression. Histopathological analysis of sections from resected mouse brains revealed that IDH3α knockout was associated with a phenotypic shift from grade IV to grade III malignancy (Fig. 6F), reduced intratumoral proliferation as evidenced by diminished intratumoral mitoses (Fig. 6G), and reduced tumor cell invasion (Fig. 7A).

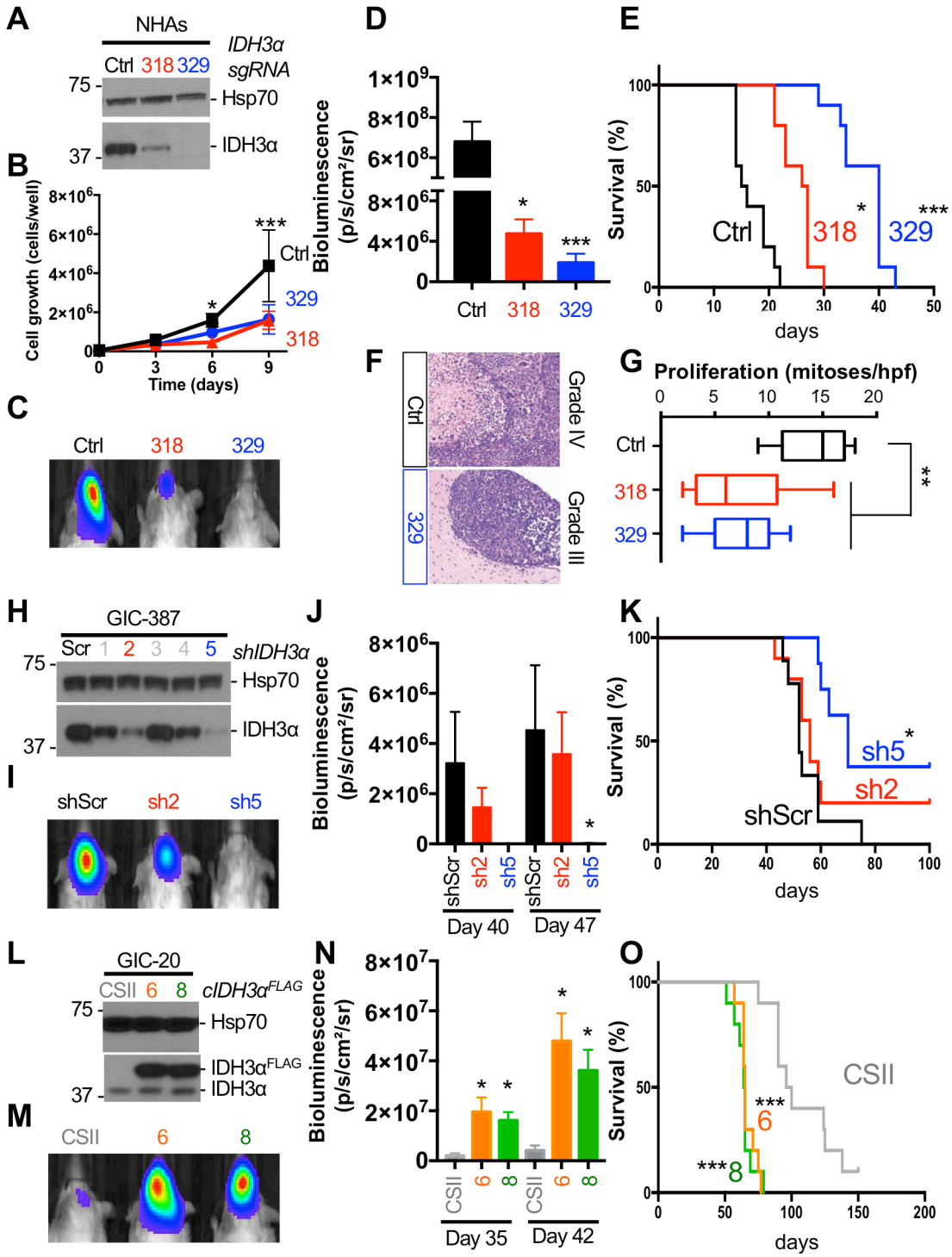

Fig. 6. IDH3α regulates GBM progression *in vivo*.

Fig. 6. IDH3α regulates GBM progression *in vivo. (cont)*
(A-G) IDH3α ablation reduces glioma tumor progression. **(A)** Western blot showing IDH3α expression in CRISPR/Cas9-modified normal human astrocytes; NHAs were transduced with a scrambled sgRNA (ctrl) and two different IDH3α-targeting sgRNAs, *i.e.*, sgRNA-318 and -329). Hsp70 is shown as a control. **(B)** *In vitro* cell growth curves of IDH3α wild-type and IDH3α KO NHAs. Cells were counted every 3 days using trypan blue and an automated cell counter. Shown is the mean +/- SD; *n = 3*, *$p<0.05$, **$p<0.005$. **(C)** Representative *In vivo* imaging system (IVIS) images of brain tumor-bearing mice, demonstrating reduced bioluminescence in IDH3α KO cells compared to the wild-type control. **(D)** Quantification of bioluminescence signal at day 13 post intracranial cell inoculation. Shown is the mean +/- SEM, *$p<0.05$, *** $p<0.0005$, *n=10 per group*. **(E)** Kaplan-Meier survival curves of mice orthotopically implanted with IDH3α wild-type or KO NHAs. *$p<0.05$, ***$p<0.0005$, *n=10* per group. **(F)** Representative H&E stainings of tumor sections from IDH3α wild-type and KO tumors. **(G)** Number of mitoses in tumors per high power field; 2 tumors per group, 8 slices per tumor; **$p<0.005$. **(H-K)** RNAi-mediated IDH3α knockdown reduces tumor progression in PDX mice. **(H)** Western blot analysis for IDH3α in different GIC clones modified for stable IDH3α knockdown. Hsp70 is shown as a loading control. **(I)** Representative IVIS images of PDX-bearing mice. **(J)** Quantification of bioluminescence signal 40 and 47 days post tumor implantation; *$p<0.05$, *n=8 per group*. **(K)** Kaplan-Meyer survival curves of mice intracranially injected with GICs modified for IDH3α stable knockdown in comparison to PDX tumors expressing a scrambled control shRNA; *$p<0.05$, *n=8 per group*. **(L-O)** IDH3α overexpression in GICs promotes GBM tumor progression. **(L)** Western blot analysis for endogenous and FLAG epitope-tagged IDH3α. Hsp70 is shown as a loading control. **(M)** Representative IVIS images of mice harboring vector (CSII) control, and $IDH3\alpha^{FLAG}$-expressing brain tumors. **(N)** Quantification of bioluminescence signal in mice 35 and 42 days post cell inoculation; *$p<0.05$, *n=10 per group*. **(O)** Kaplan-Meyer survival curves of mice intracranially injected with CSII vector control and IDH3α-overexpressing GICs; ***$p<0.0005$, *n=10 per group.*

Control NHAs showed robust *in vivo* growth within the mouse cerebrum, including extensive invasion through the parenchyma into the leptomeningeal space (Fig. 7A-a, b), while isogenic NHAs tumors with *IDH3A* knockout were characterized by greatly attenuated growth in the cerebrum, but were still capable of growth within the leptomeninges (Fig. 7A-c-f). Enhanced migratory and invasive properties of IDH3α expression was confirmed in primary human

cerebral microvascular endothelial cells ectopically expressing IDH3α protein (Fig. 7B, C). Using a transwell migration assay with chemoattractive media those endothelial cells with increased IDH3α expression had fix to six times higher cell migration than the control.

Similar to CRISPR/Cas-9 mediated gene knockout in NHAs, shRNA-mediated silencing of IDH3α expression in patient-derived GICs (Fig. 6H) resulted in reduced GBM progression (Fig. 6I-J) and improved animal subject survival (Fig. 6K) although these decreases were not as robust as in the CRISPR/Cas-9 system. Correspondingly, in a gain-of-function approach, animal subjects engrafted with IDH3α-overexpressing GICs (Fig. 6L) showed accelerated intracranial tumor progression (Fig. 6M, N) and reduced survival when compared to vector controls (Fig. 6O). These data support GBM tumor-promoting activities of IDH3α in physiologically relevant gain- and loss-of-function mouse models *in vivo* and suggest that IDH3α inactivation reduces GBM progression and grade.

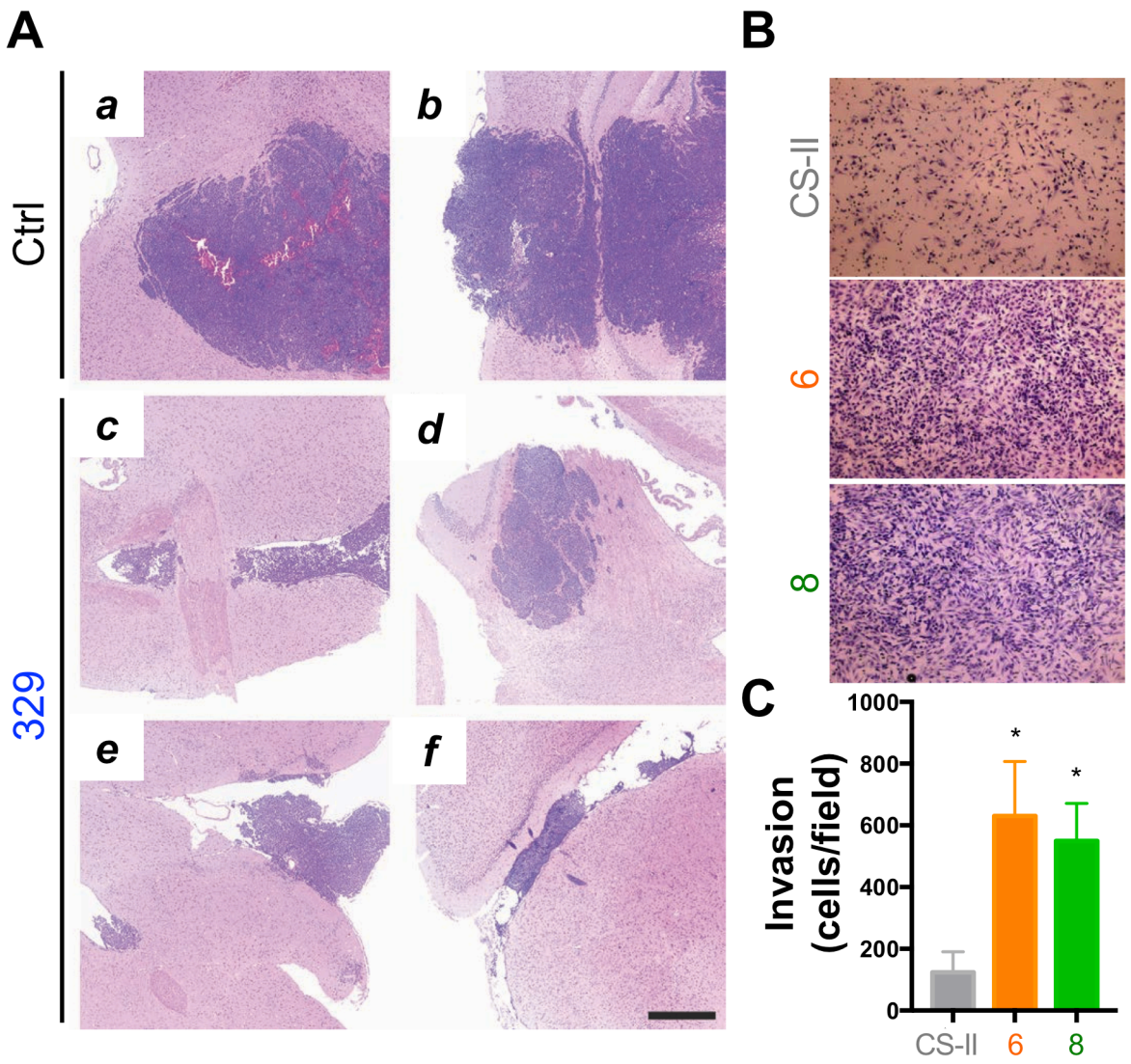

Fig. 7. IDH3α regulates cellular invasiveness.
(A) Representative H&E images of tumor explants derived from control and IDH3α-KO NHAs; bar, 500 μm. (B) IDH3α promotes endothelial cell invasion as determined by transwell invasion assay. Representative images of transwell membranes for IDH3α-expressing and empty vector-expressing human primary cerebral microvascular endothelial cells (hCMECs). (C) Quantification of the number of cells that migrated through the transwell membrane after 24 hrs. Representative of *n=3* biological replicates with *n=5* representative images.

3.3 IDH3α regulates TCA cycle turnover and glycolytic rates

IDH3α catalyzes a rate-limiting, tightly controlled enzymatic reaction of the TCA cycle, the conversion of ICT to αKG, which represents one of the most central metabolic pathways controlling cellular energy metabolism (Cohen and Colman, 1972). To molecularly define IDH3α pro-tumor effect, we determined the metabolic alterations provoked by gain or loss of IDH3α through mass spectrometry-based metabolomic profiling (see Table 1 for global metabolic changes comparing IDH3α wild-type versus KO NHAs, and NHAs expressing vector control versus NHAs engineered to ectopically express IDH3α. For all studies described below, logarithmically growing cells were harvested and subjected to Ultrahigh Performance Liquid Chromatography-Tandem Mass Spectroscopy. To account for the different growth rates of control versus IDH3α-modified NHAs, we confirmed identical numbers of viable cells by trypan blue exclusion and hemocytometer counting. Consistent with a central role of IDH3 governing TCA cycle turnover, TCA cycle intermediates upstream of the IDH3-catalyzed reaction, *i.e.,* citrate, aconitate, and ICT, were increased up to 50-fold in IDH3α-deficient NHAs compared to control cells, and correspondingly, were decreased in NHAs engineered to stably express an IDH3α transgene (Fig. 8A). A smaller yet significant accumulation of the later intermediates (*i.e.,* succinate, fumarate, and malate) downstream of IDH3 further suggests that overall TCA cycle activity is low in IDH3α-deficient NHAs (Fig. 8A). Targeted metabolomic studies using uniformly ^{13}C-labeled glucose and liquid chromatography-mass spectrometry (LC-MS) confirmed decreased TCA flux in IDH3α-deficient cells (Fig. 8B), resulting in a decreased αKG to succinate and fumarate ratio (Fig. 8C). As a consequence of reduced TCA cycle turnover in

IDH3α-deficient NHAs, oxygen consumption rates are diminished (Fig. 8D), and aerobic glycolysis increased (Fig. 8E) as evidenced by lower levels of glycolysis intermediates, including glucose, glucose 6-phosphate, pyruvate, coenzyme A, phosphoenolpyruvic acid, 3-phosphoglycerate, and 2-phosphoglycerate (see also table 1), and increased glycolytic carbon flux (Fig. 8F). Together, these metabolomic and functional studies demonstrate that ablation of IDH3α is associated with a metabolic switch from oxidative phosphorylation to glycolysis.

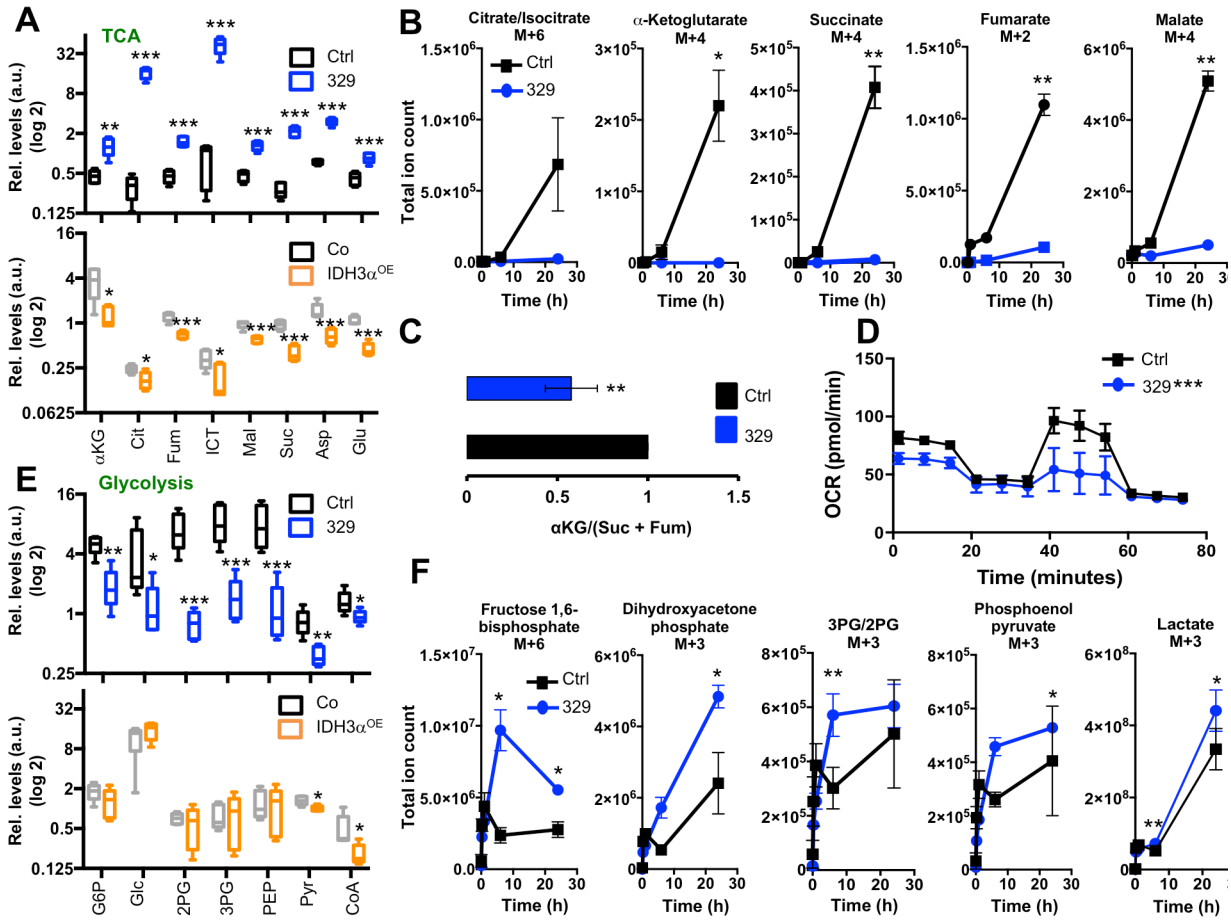

Fig. 8. IDH3α modulates TCA cycle and glycolysis.

Fig. 8. IDH3α modulates TCA cycle and glycolysis. ***(cont)***
(A) Levels of TCA cycle intermediates as determined by liquid chromatography-mass spectrometry; significance was determined by Welch's two-sample t-test; **p<0.05, **p<0.005 ***p<0.0005; n=5*. **(B)** Total ion counts of ^{13}C-labeled TCA metabolites. Samples were analyzed at 0 hr, 15 min, 1 hr, 6 hr, and 24 hr after addition of ^{13}C uniformly labeled glucose. Plotted is the mean +/- SD; **p<0.05; n = 3* per time point. **(C)** Ratio of αKG to succinate and fumarate. Shown is the mean +/- SD. **(D)** Changes in the oxygen consumption rate in IDH3α wild-type versus IDH3α KO cells. The concentrations of Oligomycin, CCCP, Antimycin A, and Rotenone were 2 μM, 10 μM, 2 μM, and 2 μM respectively. Each data point represents mean +/- SD and is representative of 18 technical replicates; ****p=0.0048, n=3*. **(E)** Levels of glycolysis intermediates as determined by liquid chromatography-mass spectrometry, significance determined by Welch's two-sample t-test; **p<0.05, **p<0.005 ***p<0.0005; n=5*. **(F)** Total ion counts of ^{13}C-labeled glycolysis metabolites. Samples were analyzed at 0 hr, 15 min, 1 hr, 6 hrs, and 24 hrs after addition of ^{13}C uniformly labeled glucose. Plotted is the mean +/- SD; **p<0.05; n = 3* per time point.

3.4 IDH3α interacts with cSHMT at the nuclear lamina during S phase

Consistent with an evolutionary conserved monopartite nuclear localization signal (NLS) at amino acid position of 124 of the IDH3α polypeptide (GASKRIAEFAF), our IF studies on tumor sections (Fig. 5D), together with previous studies (Qattan et al., 2012) demonstrate nuclear distribution of the IDH3α subunit and suggest IDH3α extra-mitochondrial activity. To assess subcellular localization of IDH3α in GBM tumor cells, and to determine whether IDH3α intracellular distribution is controlled by the cell cycle, cell fractionation into nuclear and extranuclear fractions, the latter containing cytoplasmic and heavy membrane components, revealed predominant extranuclear localization of IDH3α, with nuclear localization of IDH3α evident in S phase-arrested glioma cells, as determined by propidium iodide staining (Fig. 9A-B). Confocal IF microscopy confirmed predominant mitochondrial localization of IDH3α in unsynchronized cells (Fig. 9C-a), with few cells showing association of IDH3α with the cell nucleus (Fig. 9C-b; Fig. 10A-a), and a more diffuse cytosolic distribution and enhanced nuclear

association of IDH3α in S phase-arrested cells (Fig. 9C-c; Fig. 10A-b). To determine the molecular function of cell cycle-induced extra-mitochondrial IDH3α, we defined the IDH3α interactome using immunoprecipitation-mass spectroscopy (IP-MS) studies in patient-derived GICs, expressing a scrambled or an IDH3α-targeting shRNA. Peptides derived from 4 proteins were reproducibly detected in shScr-expressing GICs upon IDH3α-specific pull-down, but not in IgG isotype-matched control precipitates or in GICs stably expressing shRNA targeted to IDH3α (Fig. 9D, E). Among the four candidates, cSHMT was the only IDH3α interactor that co-precipitated with IDH3α in all transformed GBM cell lines, patient-derived GICs and NHAs. cSHMT, an integral enzyme involved in one-carbon metabolism, is part of a multi-enzyme complex, which consists of cSHMT, thymidylate synthase (TYMS), and dihydrofolate reductase (DHFR). The complex, which regulates thymidylate biosynthesis, localizes to the cytosol, with suggestions that it can translocate to the cell nucleus during S phase (Anderson et al., 2012). cSHMT catalyzes the rate-limiting step and serves as a scaffold essential for complex formation. Within the cell nucleus, the complex can associate with the nuclear lamina, for which cSHMT is necessary, localize at sites of DNA replication and is associated with components of the DNA replication machinery (Anderson et al., 2012, Woeller et al., 2007). Reciprocal IPs following western blot analysis using both IDH3α and cSHMT precipitating antibodies validated the IDH3α-cSHMT interaction again using IgG as a control (Fig. 9F).

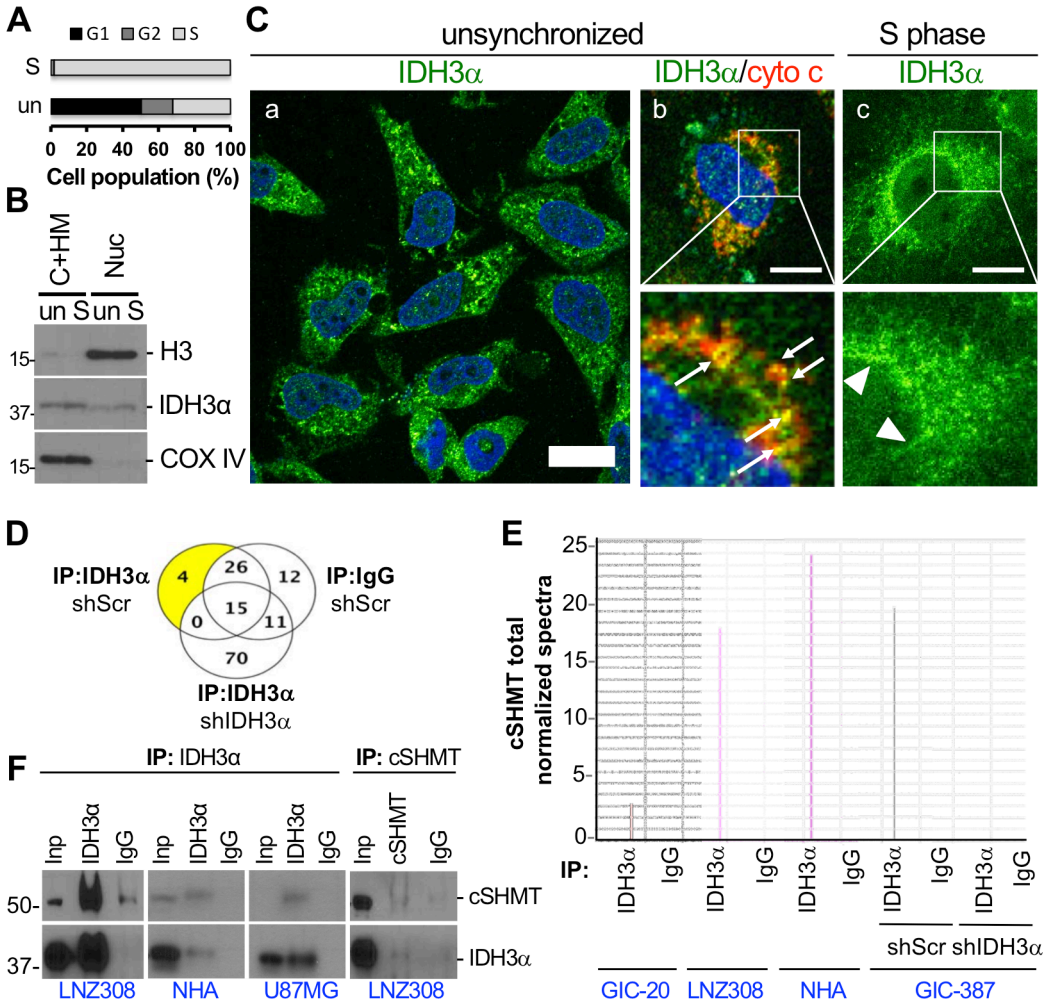

Fig. 9. IDH3α interacts with cSHMT during S phase at the nuclear lamina.
(A) Cell cycle distribution in unsynchronized and S phase arrested NHA cells as indicated by propidium iodide staining and flow cytometry-based quantification of G1, G2/M and S phase content; U, unsynchronized; S, synchronized. **(B)** Western Blot analysis of IDH3α in heavy membrane (HM) and cytosolic (C), compared to nuclear (N) fractions. Histone H3 and cytochrome c oxidase Subunit IV (COXIV) are shown as nuclear and mitochondrial markers, respectively. **(C)** Confocal immunofluorescence (IF) images of unsynchronized *(a-b)* and S phase arrested NHAs *(c)* stained for IDH3α (green), cytochrome *c* (cyto *c*, red), and DNA (Hoechst, blue). *(a)* bar, 20 µm; *(b)* bar, 14 µm; *(c)* bar, 22 µm. Arrows point to IDH3α co-localizing with cyto *c*, arrow heads to IDH3α associated with the nuclear lamina. **(D)** Venn diagram illustrating IDH3α co-immunoprecipitated (IP) proteins using IgG control or IDH3α specific antibodies in shScr and shIDH3α expressing GICs. **(E)** Bar graph illustrating total normalized cSHMT spectra in IgG and IDH3α-immunoprecipitates in the indicated cell lines. **(F)** IP-western blot analysis of IDH3α and cSHMT validates the IDH3α-cSHMT complex.

While cell cycle distribution did not affect total protein levels of IDH3α and cSHMT as evidenced by western blot analysis of whole cell lysate derived from unsynchronized and S phase arrested NHAs (Fig. 10B), confocal IF microscopy analysis confirmed co-localization of IDH3α and cSHMT in cytosol (Fig. 10A-b) and nuclear envelope (Fig. 10A-a; C), selectively in S phase arrested cells. The co-localization of IDH3α and cSHMT was quantified using an Image J macro. This quantification of the extent of IHD3α/cSHMT co-localization demonstrated approximately a three-fold increase in co-localization (Fig. 10D).

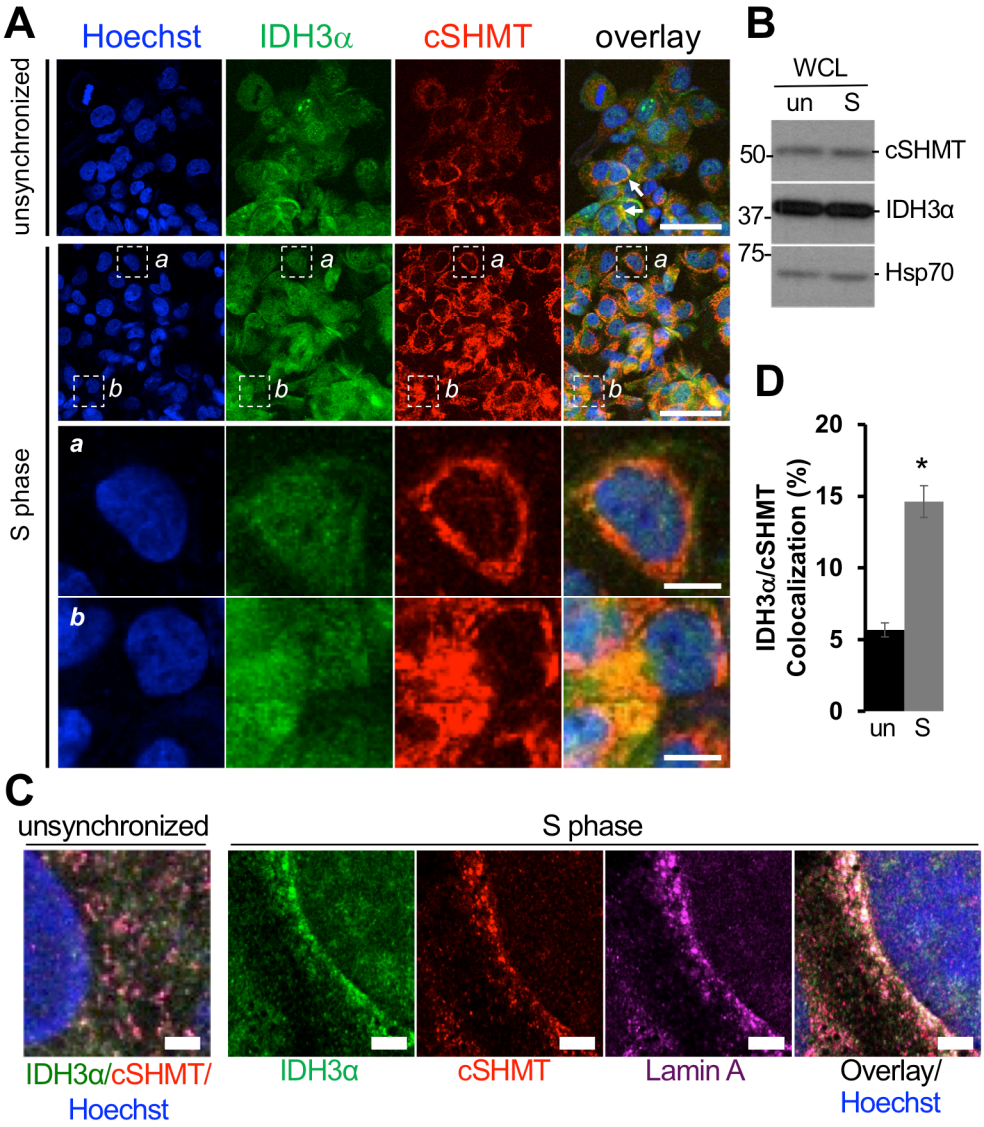

Fig. 10. Subcellular redistribution of IDH3α and co-localization with cSHMT.
(A) Confocal IF analysis of IDH3α and cSHMT in unsynchronized and S phase arrested cells. Open arrows heads point to cells with mitochondrial localization of IDH3α; closed arrow head points to cells with IDH3α and cSHMT1 nuclear association, which is more evident in S phase arrested cells (subpanel *a*). Subpanel *b* highlights cells with cytosolic co-localization of IDH3α and cSHMT in S phase arrested cells; bar 50 μm in overview images; bar 12 μm in enlarged images. **(B)** Western blot analysis of whole cell lysate (WCL) for IDH3α and cSHMT; Hsp70 is shown as a loading control. **(C)** Confocal IF analysis in unsynchronized and S phase-arrested NHAs for IDH3α (green), cSHMT (red), lamin A (purple), and nucleus (Hoechst); bar, 4 μm. **(D)** Quantification of IDH3α/cSHMT colocalization using in unsynchronized cells versus S phase-arrested cells (*n=3* biological replicate experiments).

3.5 IDH3α regulates nucleotide biosynthesis and DNA methylation

cSHMT controls one-carbon metabolism, a central metabolic pathway, which utilizes folate molecules as carriers of one-carbon units, to support nucleotide synthesis, as well as DNA and protein methylation (Ducker and Rabinowitz, 2017). THF, the biologically active form of folate, interconverts bound one-carbon units between different oxidation states, *i.e.*, N^5, N^{10}-methylene-THF, N^5-methyl-THF, and N^{10}-formyl-THF, each supporting distinct biosynthetic functions (Fig. 11).

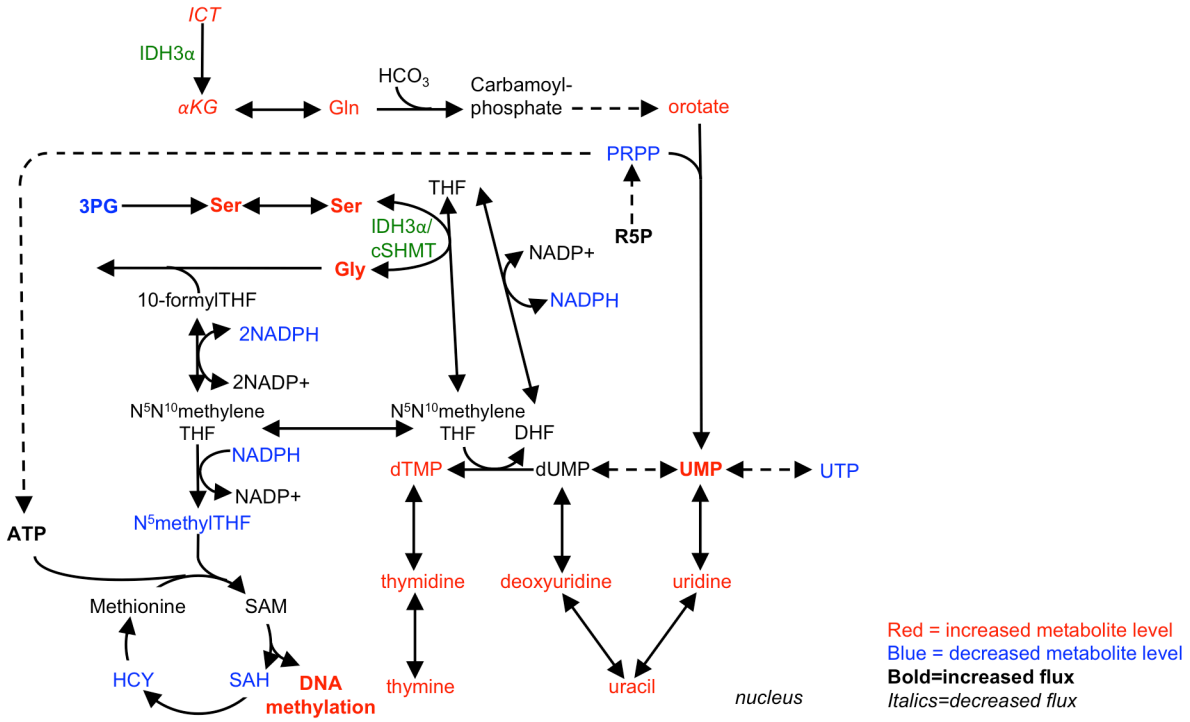

Fig. 11. Effect of IDH3α ablation on glycolysis, TCA and folate-one carbon metabolism. Schematic depicts changes in metabolite levels and flux in response to IDH3α compromise. Red = increased metabolite level; blue = decreased metabolite level; bold=increased flux; italics=decreased flux. ICT = isocitrate; α-KG=α-ketoglutarate; Gln = glutamine; HCO_3^- = bicarbonate; R5P = ribose 5-phosphate; PRPP = phosphoribosyl pyrophosphate; UMP = uridine monophosphate; UTP = uridine triphosphate; dUMP = deoxyuridine monophosphate; dTMP = deoxythymidine monophosphate; ATP = adenosine triphosphate; 3PG = 3-phosphoglyceric acid; Ser = serine; Gly = glycine; THF = tetrahydrofolate; DHF = dihydrofolate; NADP+/NADPH = Nicotinamide adenine dinucleotide phosphate; SAM = S-adenosyl methionine; SAH = S-adenosyl homocysteine; HCY = homocysteine.

N^5, N^{10}-methylene-THF drives thymidine synthesis, N^{10}-formyl-THF supports *de novo* purine synthesis, and can be fully oxidized, generating CO_2 and NADPH (Krupenko et al., 2010); N^5-methyl-THF is channeled into the methionine salvage pathway, to produce the reactive methyl donor *S*-adenosyl methionine (SAM), and to methylate DNA and protein (Fig. 11). The conversion of N^5, N^{10}-methylene-THF into N^5-methyl-THF commits THF to the methionine salvage pathway since that conversion is irreversible and uses one molecule of NADPH as a

cofactor. cSHMT appropriates N^5, N^{10}-methylene-THF between nucleotide and SAM biosynthesis, with cSHMT overexpression increasing nucleotide, and decreasing SAM availability (MacFarlane et al., 2011, MacFarlane et al., 2008). Therefore, using LC-MS metabolite profiling and targeted flux studies together with metabolite rescue and DNA methylation experiments, we assessed whether and to what extent IDH3α regulates cSHMT-controlled nucleotide biosynthesis versus methionine salvage pathway utilization. IDH3α-deficient NHAs showed increased ^{13}C label incorporation into both serine and glycine compared to wild-type cultures (Fig. 12A). This flux increase likely results from increased glycolytic activity, with the glycolytic intermediate 3-phosphoglycerate (3PG) being diverted toward the serine synthesis pathway to contribute to endogenous production of serine (Fig. 11) (Pollari et al., 2011). Similarly, IDH3α ablation resulted in increased flux into the pentose phosphate pathway (PPP, Fig. 12B), as the glycolytic intermediate glucose-6-phosphate can be channeled into the PPP to generate ribose-5-phosphate, a precursor for nucleotide biosynthesis (Fig. 11). As a result of increased PPP utilization, ^{13}C label incorporation into UMP is elevated (Fig. 12C), yet TMP levels together with other pyrimidine biosynthesis intermediates *i.e.*, uridine, uracil, thymidine, thymine and TMP accumulated in IDH3α-deficient cells, as determined by LC-MS (Fig. 12D). These results are consistent with reduced pyrimidine pathway activity that leads to an accumulation of intermediates. Mirroring the accumulation of intermediates in IDH3α-deficient cells, NHA cultures engineered to ectopically express IDH3α showed a corresponding decrease in pathway intermediates (Fig. 12D). While decreasing pyrimidine biosynthesis activity (Fig. 12D), IDH3α deficiency augmented the SAM/SAH ratio two-fold and reduced the

methionine pathway intermediates N^5-methyl-THF and homocysteine (HCY), which was seen in both the steady state and in an ELISA study, indicative of increased metabolic flux through the methionine salvage pathway (Fig. 12E-G). SAM supports methylation of lipids, DNA, RNA, metabolites and proteins (Kottakis et al., 2016) and thus SAM levels are viewed as a measure of the overall methylation potential of a cell.

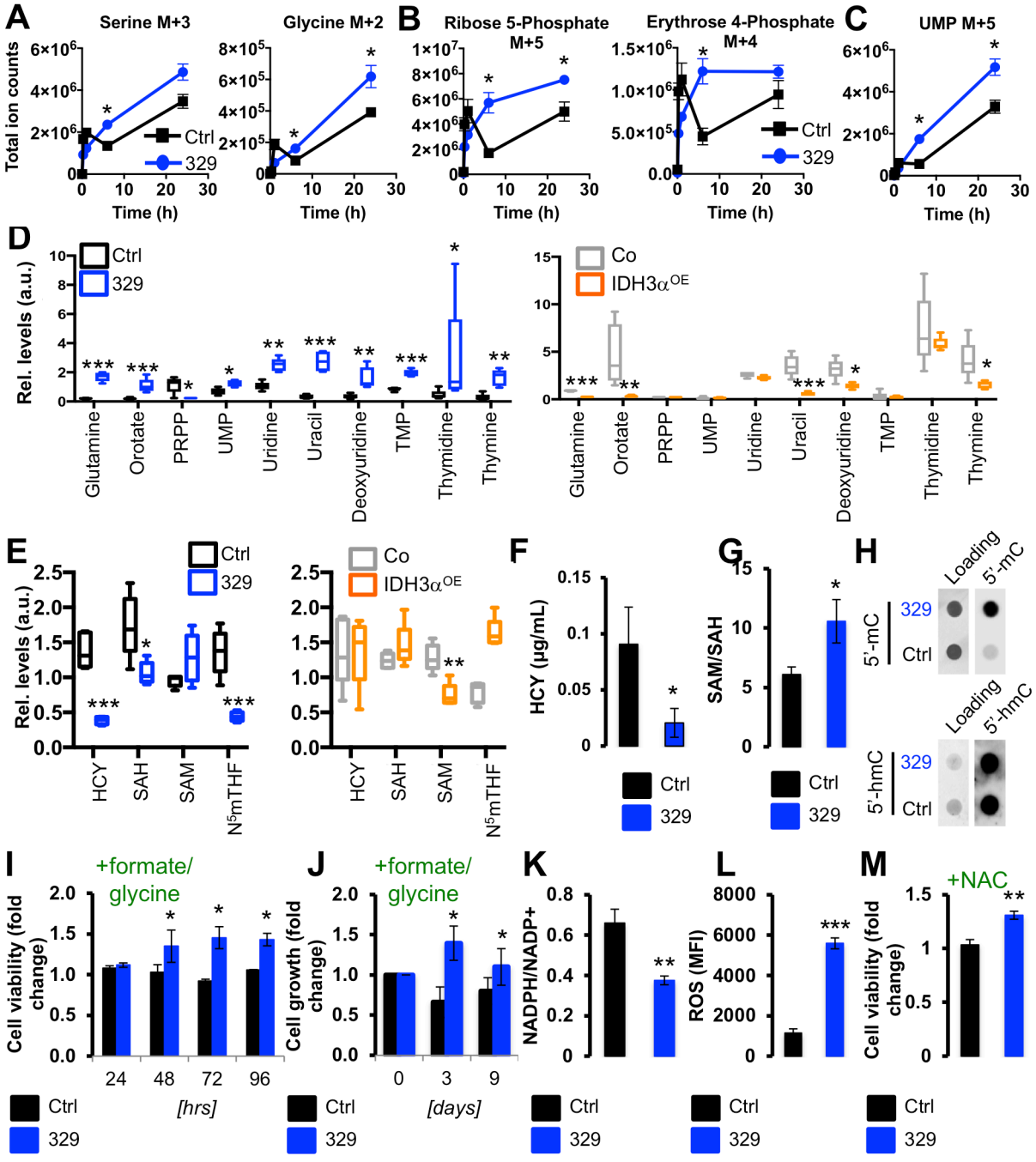

Fig. 12. IDH3α modulates one-carbon metabolism.

Fig. 12. IDH3α modulates one-carbon metabolism. (cont)
(A-C) Total ion counts of ^{13}C-labeled serine and glycine (A), PPP pathway metabolites (B) and UMP (C) in NHAs with IDH3α loss-of-function. Samples were taken at 0 hr, 15 min, 1 hr, 6 hr, and 24 hr time points. Shown is the mean +/- SD; *$p<0.05$; $n = 3$ per time point. **(D-E)** Histograms showing changes in pyrimidine (D) and methionine (E) metabolite levels in NHAs with IDH3α loss- or gain-of-function as identified by liquid chromatography–mass spectrometry; significance was determined by Welch's two-sample t-test; *$p<0.05$, **$p<0.005$, ***$p<0.0005$; $n=5$. **(F)** Homocysteine levels in control versus IDH3α KO as determined by ELISA. Shown is mean +/- SD; *$p<0.05$; $n=3$. **(G)** Ratio of intercellular SAM/SAH in control wild-type versus IDH3α KO NHAs. Shown is the mean +/- SD; *$p<0.05$; $n=3$. **(H)** Global 5'-mC and 5'-hmC levels in IDH3α wild-type and KO NHAs as determine by DNA dot blot analysis. **(I-J)** Relative viability as assessed by MTT assay (I) and growth (J) of IDH3α-wild-type versus IDH3α-KO NHAs treated with 1mM formate and 0.4 mM glycine compared to cultures treated with glycine only. Data are expressed as relative to day 0. Shown are means +/- SD; $p<0.05$; $n=3$. **(K)** Levels of intracellular NADPH/NADP+ in IDH3α wild-type versus IDH3α KO NHAs. Shown is the mean +/- SD; **$p<0.005$; $n=4$. **(L)** Relative ROS levels in IDH3α wild-type versus IDH3α KO Shown is the mean +/- SD; ***$p<0.0005$; $n=3$. **(M)** Relative cell viability of wild-type versus IDH3α KO NHAs after treatment with 0.5 mM of *N*-acetyl cysteine (NAC) or vehicle for 48 hrs. Shown in the mean +/- SD, **$p<0.005$; $n=3$.

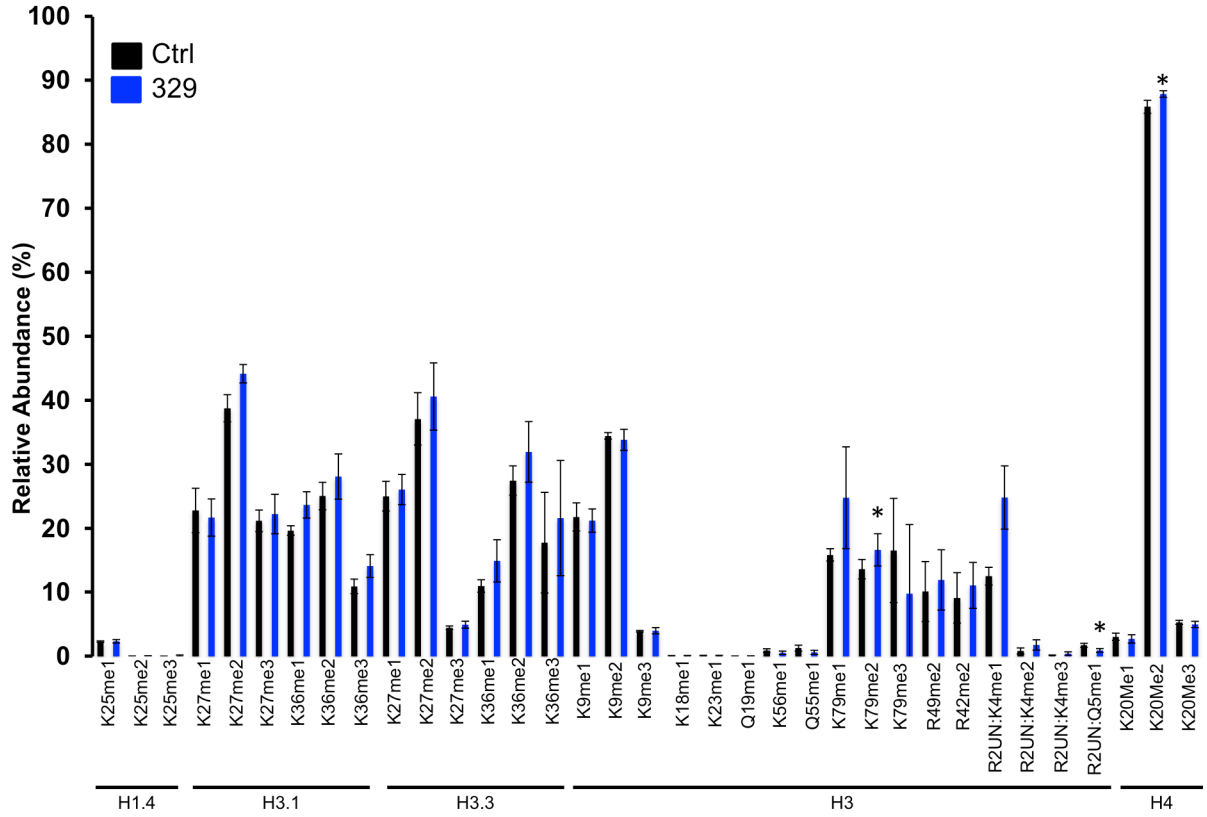

Fig. 13. IDH3α KO does not affect global histone methylation status.
Bar graph showing the relative abundance of different histone methylation markers in control versus IDH3α KO NHAs. Shown are the means +/- SDs; *$p<0.05$, $n=3$.

While mass spectrometry did not detect robust changes in global levels of histone methylation marks (fig. S5), IDH3a KO NHAs compared to IDH3a wild-type cells showed increased levels of DNA methylation as determined by quantification of global 5′-methylcytosine (5’-mC) levels, while levels of 5’hydroxymethyl-cytosine (5’-hmC) remained unchanged (Fig. 5H). To evaluate whether and to what extent differential methylation in IDH3a-deficient versus proficient NHAs controls gene expression, we performed integrative RNA-Seq and methylation profiling experiments. RNA-Seq analysis identified 8,711 differentially expressed genes, with differential

expression defined at a threshold of FDR=0.05 and an absolute log fc >1 **(**new Fig. 14A-B). Through integrative analysis of expression and methylation data, we determined that out of the 8,711 differentially expressed genes, expression of 3,084 genes correlated with their CpG methylation status (new Fig. 14C). Expectedly, correlation was primarily observed for CpG sites located within island and shores, in comparison to shelf and open sea. Pathway enrichment analysis of genes with correlation between gene expression and methylation pointed to cAMP mediated signaling and the regulation of epithelial-to-mesenchymal transition (EMT) as key pathways deregulated through methylation-driven expression changes upon IDH3a deletion (new Fig. 14D). Of note, while the higher number of hypermethylated relative to hypomethylated CpGs revealed an overall global increase in DNA methylation in IDH3a knockout cells (new Fig. 14E), confirming our 5'-mC dot blot analysis (Fig. 5H), hypermethylated CpGs in IDH3a KO cells are enriched in open sea regions (new Fig. 14F). Together with the overall modest overlap between differentially methylated genes with those showing differential expression, these data suggest that gene regulation may occur through additional mechanisms other than methylation of promoter-proximal regulatory elements (see discussion below).

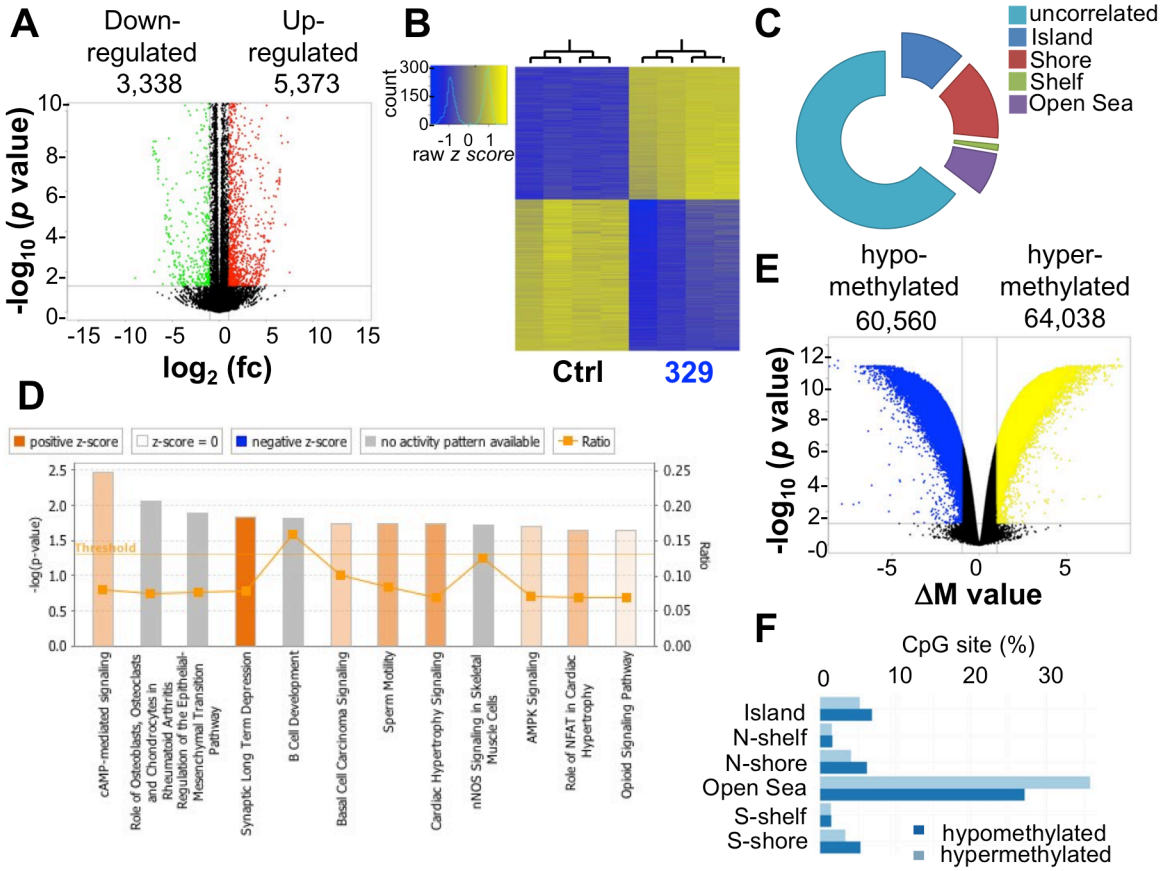

Fig. 14. IDH3α loss-of-function through impact on DNA methylation regulates gene expression.

(A) Volcano plot of genes up- and down-regulated in the IDH3α KO compared to wild-type, n = 4 **(B)** Heat map representation of genes up- and down-regulated in both wild-type and IDH3α KO in individual samples (n = 4 per group.) **(C)** Graphical representation of the number of differentially genes that correlated with CpG methylation, organized by CpG functional location. **(D)** Pathway enrichment analysis using Ingenuity pathway analysis (IPA) of the genes showing correlation between mRNA expression and methylation **(E)** Volcano plot of all CpG sites differentially methylated in IDH3α KO compared to wild-type NHAs (n = 4 per group). **(F)** Bar graph representation of hyper- and hypomethylated CpG sites by genomic regions in the IDH3α KO compared to wild-type NHAs.

In further support of an IDH3α-cSHMT signaling axis, pathway enrichment analysis of the IDH3α controlled metabolome confirmed folate one-carbon metabolism as a high priority

metabolic pathway modulated by IDH3α (enrichment scores of 5.75 in KO vs WT, and 3.2 in the OE vs WT NHAs, with a *p* value cutoff of 0.001). Correspondingly, addition of formate to replenish THF levels selectively increased viability and growth of IDH3α-KO cells, compared to wild-type NHAs (Fig. 12I, J). Furthermore, as NADPH is utilized by the folate pathway and by the conversion of serine to sphingolipids (Lewis et al., 2014, Gault et al., 2010), IDH3α-deficiency resulted in decreased NADPH levels (Fig. 12K), and increased levels of reactive oxygen species (ROS) (Fig. 12L); treatment of cells with the ROS scavenger *N*-acetyl cysteine (NAC) increased viability of IDH3α KO compared to wild-type NHAs (Fig. 12M). Furthermore, treatment of IDH3α-deficient cells with methotrexate (MTX), an inhibitor of thymidylate synthase (TYMS) and dihydrofolate reductase (DHFR) (Osborn et al., 1958, Chu et al., 1990), which promotes apoptosis through ROS generation (Phillips et al., 2003), reduced cell viability in IDH3α K.O. NHAs compared to wild-type control cells at a concentration of only 10 nM and precipitously at concentrations at 1 μM and above (Fig. 15A), while IDH3α overexpressing NHAs were protected against MTX cytotoxic effect (Fig. 15B). Analysis of effector caspase activation confirmed increased levels of apoptosis in IDH3α-deficient cells when compared to wild-type controls. Introduction of an IDH3α cDNA into IDH3α-deficient cells was able to rescue the pro-apoptotic phenotype of IDH3α compromise (Fig. 15C). These results suggest that IDH3α loss through reduced cSHMT and thymidylate synthesis cooperates with anti-folate therapy to promote apoptosis. To assess the relative contribution of mitochondrial versus extra-mitochondrial activity to IDH3α anti-apoptotic effect, we generated an IDH3α protein that lacks the mitochondrial targeting signal which has been preserved across species (ΔMTS; Fig. 15D).

ΔMTS-IDH3α failed to co-localize with the mitochondrial marker cytochrome *c* (Fig. 15E). Several factors were evaluated to determine the enzymatic activity of the ΔMTS-IDH3α enzyme. First, we measured overall cellular αKG using cell lysates. In both the full length and the ΔMTS-IDH3α, αKG levels were elevated in the IDH3α KOs compared to an empty vector plasmid (Fig. 15F). Then IDH3 specific function was measured with an IDH assay in which co-factors can be controlled. Therefore NAD+ was supplied along with ICT. By only supplying NAD+ only IDH3 will be active since IDH1 and 2 require NADP+ instead. Under such conditions and with the full and mutant IDH3α there was increased production of NADH as a marker of increased IDH3 activity (Fig. 15G). Unsurprisingly when the total cellular ratio of NAD+/NADH was measured in these cells there was a decrease in both the full and ΔMTS-IDH3α expressing cultures (Fig. 15H). Finally treating the NHA KOs with MTX was repeated but with both the full and ΔMTS-IDH3α expressed (Fig. 15I). When compared to full-length IDH3α protein, ΔMTS-IDH3α was even more active in blocking MTX induced effector caspase activation (Fig. 15I), suggesting that IDH3α mitochondrial activity is dispensable for anti-apoptotic effect. Together, these data suggest that similar to cSHMT compromise (MacFarlane et al., 2011, MacFarlane et al., 2008), IDH3α loss-of-function impairs redox homeostasis and nucleotide biosynthesis, while increasing the cellular methylation potential.

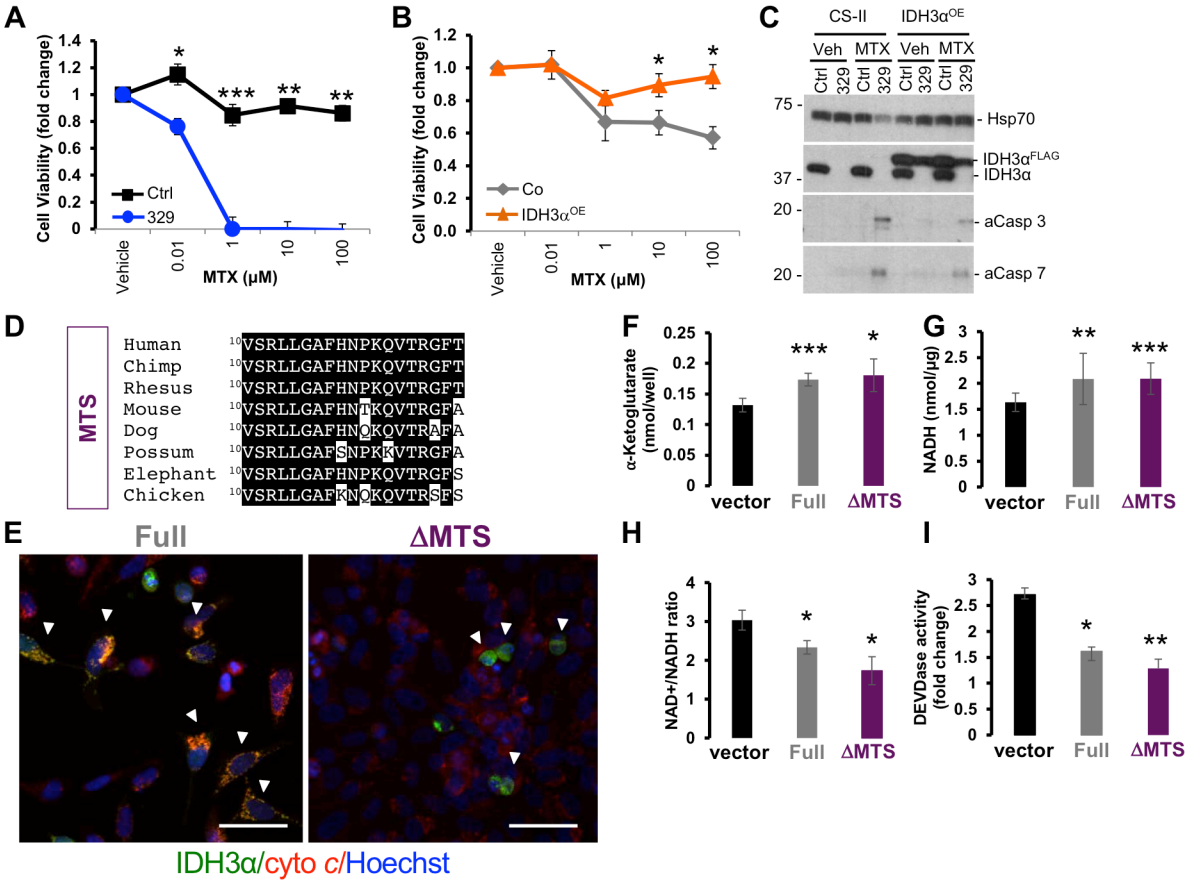

Fig. 15. IDH3α expression affects methotrexate (MTX) treatment response.
(A) Cell viability as determined by MTT assay of IDH3α KO cells vs. control; and **(B)** IDH3α OE cells versus vector control treated with increasing concentrations of MTX. Shown is the mean +/- SD; *$p<0.05$, **$p<0.005$, ***$p<0.0005$. *(n = 3)* **(C)** Western blot analysis of effector caspase activation in response to MTX treatment in IDH3α KO NHAs versus wild-type controls, in the presence or absence of transiently expressed FLAG-tagged IDH3α; *n=3*. aCasp-3/7, active caspase-3/7. Hsp70 is shown as a loading control. **(D)** Amino acid sequence of the IDH3α mitochondrial targeting signal (MTS) derived from various species. **(E)** Representative IHC images of full-length IDH3α or mutant IDH3α protein lacking the mitochondrial transport signal (green), cytochrome *c* = mitochondrial staining (red), Hoechst = nuclear staining (blue). Plasmids expressing either protein were transiently expressed in the IDH3α deficient NHAs. Arrows indicate positively transfected cells. Scale bar = 50 μm. **(F - H)** Assays evaluating enzymatic activity of mutant IDH3α versus an empty vector control and full length IDH3α transiently expressed in IDH3α-deficient NHAs, measuring total cellular αKG levels **(F)**; NADH production **(G);** total cellular NAD+/NADH ratio **(H);** DEVDase activity of IDH3α-deficient NHs transfected with vector control, full-length or ΔMTS-IDH3α, and treated with vehicle or MTX **(I)**. *$p< 0.05$, **$p<0.005$, ***$p<0.0005$.

CHAPTER 4: DISCUSSION

We demonstrated that IDH3α protein is upregulated in GBM tumor, and as shown in physiologically relevant CRISPR/Cas9 and RNAi loss-of-function, together with gain-of-function studies in orthotopic tumor models, promotes GBM progression. On molecular levels, IDH3α ablation reduces TCA cycle turnover and shunts energy metabolism. In addition, IDH3α impacts one-carbon metabolism, regulates nucleotide production and DNA methylation through effect on cSHMT.

In contrast to its paralogs IDH1 and IDH2, genomic sequencing studies revealed that glioma-associated IDH3α, β, and γ subunits are not mutated (Krell et al., 2011). As mentioned previously this may be due to the fact that a mutated version of IDH3 subunits cannot produce the oncogenic metabolite 2-HG since it can only conduct the ICT to αKG reaction in the forward direction. Additionally, the role of IDH3 in the TCA may be so critical to normal cellular physiology that loss in a cancerous state would be detrimental to cancer growth, as we see here. Therefore, cancers that may initiate with IDH3 mutations might find themselves at a disadvantage and be destroyed by the immune system or may be starved out, unable to grow to a clinically relevant size. We found that GBM tumor cells up-regulate IDH3α mRNA and protein when compared to glial cells in normal brain, with IDH3α abundance most prominent within the leading edge of GBM tumor specimens. This upregulation of IDH3 may increase TCA flux providing those metabolites and the energy needed for effective rapid cell growth. Selective association with tumor cells of the leading edge was more evident for *IHD3α* mRNA, compared

to IDH3α protein, suggesting regulation of IDH3α expression through additional mechanisms besides transcriptional control. Expectedly, due to TCA cycle and respiratory compromise, IDH3α ablation triggered a compensatory metabolic shift to aerobic glycolysis and increased PPP utilization. This was demonstrated by steady-state metabolite and metabolic flux levels. With IDH3α KO there was a massive increase in those metabolites upstream of the IDH3 reaction while a much smaller increase in metabolite levels were noted afterward. Flux studies showed almost complete inhibition of the TCA cycle in the IDH3α KOs. Combined these results confirm the key role that IDH3α plays in the TCA cycle. The small increases in downstream metabolites may be due to the fact that the overall cycle flux is decreased but there is a small compensatory action of IDH2 which parallels IDH3 in the mitochondria. These results complement and contrast with previous studies. In studying IDH3α knockdown in cancer associated fibroblasts they also saw this increase in glycolysis which they attributed to decreased αKG and increased HIF1α stabilization, which can upregulate glycolysis enzymes (Zhang et al., 2015). We also looked at glycolysis associated enzymes and saw no differences in protein expression by western blot or mRNA expression by RT-qPCR. These differences in regulation of glycolysis with the same outcome, increased glycolytic flux, could be due to the differences in cellular systems studied. Yet both our study and the fibroblast study are in opposition to the results looking at IDH3α ablation in cervical epithelial adenocarcinoma cells in which they found that decreased IDH3α expression was associated with increased αKG. Therefore, they concluded that IDH3α expression decreases αKG, increases HIF1α stability, and thus contributes to an overall more cancerous state (Zeng et al., 2014). This conclusion is also counter

to the belief that IDH3 is the key enzyme contributing to TCA cycle flux. Here our study demonstrates the opposite effect on αKG but we do agree on the point of IDH3 function supporting cancer progression. Again, these differences could be due to different cell model systems, but it highlights the important fact that the role of IDH3 in normal cellular physiology and cancer pathophysiology needs further study. More investigation needs to happen into IDH3 function in multiple different normal cell and cancer systems. Such work could shed light on why patients with mutations in IDH3α and β may develop retinitis pigmentosa but don't demonstrate disease elsewhere in the body. As discussed earlier it is possible that IDH3's role is more important than IDH2 in neurological systems.

In addition to mitochondrial distribution of IDH3α, our subcellular fractionation and IF studies revealed cell cycle-induced cytosolic and nuclear localization of IDH3α, the latter consistent with an evolutionary conserved monopartite nuclear localization signal at amino acid position of 124 of the IDH3α polypeptide (GASKRIAEFAF). This finding confirms previous proteomic analyses of isolated cancer cell nuclei and mitochondria, which demonstrated distribution of various TCA cycle enzymes, including IDH3α, to both nucleus and mitochondria (Qattan et al., 2012). Our study is the first to demonstrate IDH3α nuclear localization with both western and immunofluorescence. In glioma cells and NHAs, IDH3α extra-mitochondrial localization was cell cycle-dependent, as S phase arrested cells showed predominant accumulation of IDH3α in cytosol and at the nuclear lamina. Previously there had been no evidence as to what role IDH3α may play in the nucleus although it was hypothesized that it may be involved in genome stability

(Gemoll et al., 2013). Here, IDH3α co-localized and interacted with cSHMT, a rate-limiting enzyme of the *de novo* thymidylate synthesis pathway (Anderson et al., 2012). As mentioned previously, cSHMT is a lamin-binding protein that serves as a scaffold protein required for the recruitment of TYMS, and DHFR into a multienzyme complex in both cytosol and nucleus (Woeller et al., 2007, Anderson et al., 2012). cSHMT, TYMS, and DHFR can translocate to the nucleus via post-translational modification with the small ubiquitin-like modifier (SUMO) (Woeller et al., 2007), can accumulate at the nuclear lamina during S and G2/M phase, and through cSHMT interact with components of the DNA replication machinery to support *de novo* thymidylate synthesis at sites of DNA replication (Anderson et al., 2012). During DNA replication, cSHMT appropriates N^5N^{10}-methylene-THF between nucleotide synthesis and methionine salvage pathways (MacFarlane et al., 2008). cSHMT compromise causes elevated levels of uracil in nuclear DNA, and increased N^5N^{10}-methylene-THF flux into the salvage methionine cycle as evidenced by increased SAM levels (MacFarlane et al., 2008), predisposing mice with heterozygous loss of cSHMT to neural tube defects (Beaudin et al., 2011). Similarly, reduced *de novo* thymidylate synthesis resulting from folate deficiency or anti-folate treatment results in deoxyuridine misincorporation into mitochondrial DNA and nuclear DNA, leading to genome instability (Paone et al., 2014). Mirroring cSHMT compromise, IDH3α deficiency caused accumulation of pyrimidine pathway intermediates, and a decrease in total NADPH/NADP+ ratio. Despite increased PPP utilization in NHAs with IDH3α compromise, PPP pathway activity was unable to compensate for increased NADPH consumption through the folate-methionine salvage pathway; two NADPH molecules are generated by the PPP, while 3

NADPH molecules are consumed by the folate pathway in converting THF to 5-methylTHF for the methionine pathway, and 1 NADPH molecule is consumed by converting DHF to THF by DHFR (Fig. 11). In the steady state metabolite data we also noticed increased levels of fatty acids and sphingolipids (Table 1). In a system where TCA flux is greatly diminished excess acetyl-CoA may be shuttled into fatty acid synthesis utilizing two molecules of NADPH. Similarly, with increased glycolytic flux 3-phosphoglycerate can be shuttle into the serine synthesis pathway and then serine can be taken for the production of sphingolipids along with one molecule of NADPH. Thus, inhibited TCA flux and increased glycolytic flux can shunt metabolites into these alternative pathways that while utilizing these increased metabolites cause the decreased NADPH/NADP+ ratio noted in the IDH3α KO NHAs.

In further support of IDH3α as a cSHMT interactor and modulator of the thymidylate synthesis pathway, levels of methionine salvage pathway intermediates, such as HCY and SAH decreased, and SAM levels and associated DNA methylation increased. Addition of the THF precursor formate to IDH3α KO NHA restored cell viability, suggesting that blunted one-carbon metabolism is central to the growth deficit in response to IDH3α loss. As mentioned above the THF metabolite N^{10}-formyl-THF can be utilized by the purine synthesis pathway along with glycine to produce ATP. ATP can then contribute to dTMP production through interacting with thymidine as part of the TTP salvage pathway and the action of thymidine kinase, completely bypassing the *de novo* thymidylate synthesis pathway involved cSHMT (Nyhan). Thus, by providing additional formate and glycine blunted *de novo* thymidylate synthesis can be overcome

by increased ATP production. In the absence of such addition, while TCA compromise and resultant decrease in cell viability associated with IDH3α deficiency can be antagonized by increased glycolysis, we propose that blunted nucleotide biosynthesis together with epigenetic silencing of potent growth and multipotency factors in response to IDH3α loss-of-function creates a unique metabolic vulnerability in highly proliferative cells, such as tumor cells, that decreases cellular viability, and cooperates with anti-folate therapy, such as MTX, known to target the thymidylate pathway enzymes DHFR and TYMS, to promote programmed cell death. The extra-mitochondrial function of IDH3α was illustrated by the ΔMTS-IDH3α mutation experiments. Since we still saw reduced DEVDase or caspase 3 activity with the ΔMTS-IDH3α, even more so than the full protein, in response to MTX treatment this supports the argument that the contribution of IDH3α to thymidylate synthesis is not related to mitochondrial contributions. We made attempts to also study the effect of IDH3α with a loss of the nuclear localization signal but these experiments were not effective. Even though we could demonstrate a loss of the nuclear localization signal when using IF to study the cellular distribution these ΔNLS-IDH3α mutants were still localizing to the nucleus. It is possible that the NLS is not the only contributor to IDH3α localization to the nucleus. Similar to cSHMT post-translational modifications may occur that facilitate IDH3α nuclear localization.

cSHMT scaffold function rather than its enzymatic activity appears to be critical for *de novo* thymidylate biosynthesis (Anderson et al., 2012). Neuroblastoma cells expressing a dominant negative, enzymatically inactive cSHMT that retained lamin binding activity showed

reduced incorporation of cSHMT-derived one-carbon units into the cytoplasmic methionine salvage pathway, while *de novo* thymidylate synthesis was not impaired (Anderson et al., 2012). We propose that IDH3α binds cSHMT in the cytosol, as indicated by co-localization of IDH3α and cSHMT in the cytosol of S phase arrest cells, and aids in recruiting cSHMT to the nuclear lamina, and in doing so, enhances nucleotide biosynthesis to support unabated cancer cell growth. Genetic inactivation of IDH3α, while impairing nucleotide biosynthesis for DNA replication thereby hampering cellular growth, enhances the cellular methylation potential by increasing methionine salvage pathway utilization and the SAM to SAH ratio, resulting in DNA hypermethylation and the suppression of an oncogenic signature important for cellular growth and differentiation. What was not demonstrated in our study but could be a contributing factor to increased methionine recycling is that the enzyme responsible for the conversion of SAH to homocysteine, SAH hydrolase, uses NAD+ as a cofactor. Thus, decreased utilization of NAD+ in the mitochondria by IDH3 may inhibit NAD+ transmission into the mitochondria increasing the concentration in the cytosol and thus increasing SAH hydrolase activity pushing forward the methionine cycle.

In the presence of exogenous methionine, serine can contribute to *de novo* synthesis of ATP, which is required to convert methionine to SAM (Maddocks et al., 2016) (Fig. 11) cSHMT-generated glycine, together with PRPP and 10-formyl THF, which in the absence of functional IDH3α does not significantly contribute to thymidylate synthesis, can enter the *de novo* ATP synthesis pathway. Therefore, the IDH3α-cSHMT may not only impact folate appropriation

between nucleotide synthesis and methionine salvage pathways but may also regulate DNA methylation through effect on *de novo* ATP production (Fig. 11). Finally, due to reduced αKG to fumarate and succinate ratio, increased DNA methylation in IDH3α KO NHAs could be due to reduced activity of Ten-eleven translocation methylcytosine (TET) dioxygenases, which are inhibited by succinate and fumarate (Laukka et al., 2016). TET enzymes catalyze the conversion of the 5-mC to 5-hmC, considered to be the initial step of DNA demethylation (Laukka et al., 2016). We quantified levels of 5'hmC in IDH3α wild-type versus KO NHAs, via dot blot and using a fluorometric ELISA that measures abundance of a hydroxymethylated product; where product level is directly proportional to TET activity. We did not observe a difference in 5'hmC levels between wild-type and KO cells, as assessed by dot blot analysis for 5'hmC, and observed a trend toward lower TET activity in IDH3α-deficient cells [relative TET activity: WT (0.32+/-0.18); KO (0.24+/-0.07)], and a trend toward higher TET activity in IDH3α OE cells [relative TET activity: Co (0.12+/-0.055); IDH3α^{OE} (0.17+/-0.08)], using a colorimetric readout; these differences, however, did not reach significance, suggesting that the contribution of TET enzymes to the observed DNA hypermethylation phenotype in IDH3α-deficient cells is minor. Additionally, in previous studies looking at the effect of succinate and fumarate on αKG enzymes there is usually an effect not only on TET enzymes but also on histone demethylases (Xiao et al., 2012). Again, in our studies we saw no significant differences in histone methylation marks with a pan histone methylation screen. Both of these experiments together point to the fact that loss of IDH3α function leads to a metabolic state that is unique to IDH3 and not a mimic of IDH1 or IDH2. In the setting of IDH1 or IDH2 mutation it is the production of 2HG that inhibits

those enzymes dependent on αKG function (Xu et al., 2011). In the setting of SDH or FH silencing in cancer there is still production of αKG but there is a buildup of succinate or fumarate respectively which causes an increase in these metabolites, similar to what we saw with ICT that can be 50 times higher than normal allowing for them to out compete αKG for its enzymatic pocket (Xiao et al., 2012).

The interplay between altered cancer cell metabolism and epigenetic reprogramming has been well established. Aberrant expression or mutation of cancer-promoting genes causes alterations in metabolites that modify chromatin structure and gene expression, such as NAD^+/NADH, FAD^+, O-linked *N*-acetylglucosamine, free fatty acids, SAM and acetyl-CoA (Lu and Thompson, 2012). Aberrant expression of IDH3a through effects on one-carbon metabolism impacts the methylation potential of cells, and in so doing, regulates transcription of cancer causing genes. Through integrative analysis of methylation array and RNA-seq data, followed by pathway enrichment analysis, we found that the cAMP mediated signaling and regulation of epithelial-to-mesenchymal transition pathways were deregulated in the setting of IDH3α deletion. With limited overlap between differentially methylated and differentially expressed genes, and the enrichment of hypermethylated CpG elements in IDH3a KO NHAs within open sea regions, we anticipate that IDH3a by promoting DNA hypermethylation regulates gene expression through additional mechanisms, *e.g.*, by regulating the repetitive genome. A recent study discovered that loss of LKB1 in the setting of KRAS mutation alters serine/glycine one-carbon metabolism

metabolism in prostate cancer, and affects DNA methylation of retrotransposon elements, which upon methylation were transcriptionally silenced (Kottakis et al., 2016).

Together, the identification of a non-canonical extra-mitochondrial function of IDH3α suggests a previously unrecognized functional interplay between mitochondrial energy and one-carbon metabolism. Our study points to cancer-associated IDH3α expression and IDH3α controlled one-carbon metabolism as novel metabolic vulnerabilities in GBM and suggests that reducing IDH3α expression or targeting the IDH3α-cSHMT signaling axis via small molecules to disrupt their interaction might represent a novel therapeutic strategy for the treatment of GBM. As cancer cells depend upon DNA synthesis to support unabated growth, multiple enzymes implicated in one-carbon metabolism are upregulated in cancer, including TYMS, DHFR and SHMT2, but not cSHMT (Mehrmohamadi et al., 2014). Our data point to IDH3α over-expression as a means to regulate cSHMT function and underscores the importance of therapeutic strategies to target components of the thymidylate pathway to halt GBM tumor progression.

4.1 Summary and Future Directions

Together, the identification of a non-canonical nuclear function of IDH3α suggests a previously unrecognized functional interplay between mitochondrial energy and nuclear one-carbon metabolism. Our study points to cancer-associated IDH3α expression and IDH3α controlled one-carbon metabolism as novel metabolic vulnerabilities in GBM and suggests that reducing IDH3α

expression or targeting the IDH3α-cSHMT signaling axis via small molecules to disrupt their interaction might represent a novel therapeutic strategy for the treatment of GBM. As cancer cells depend upon DNA synthesis to support unabated growth, multiple enzymes implicated in one-carbon metabolism are upregulated in cancer, including TYMS, DHFR and SHMT2, but not cSHMT (Mehrmohamadi et al., 2014). Our data point to IDH3α over-expression as a means to regulate cSHMT function and underscores the importance of therapeutic strategies to target components of the thymidylate pathway to halt GBM tumor progression. This study also starts to explain how one-carbon metabolism may integrate with signals from other nutrient inputs to properly regulate downstream carbon partitioning.

There are several questions that are left unanswered and can be built from this research. First, the role that IDH3α may play in cellular invasion. Since IDH3α was so heavily expressed at the leading edge and in endothelial cells only associated with the tumor microenvironment indicates that IDH3α is involved in invasion since both groups need to migrate to carry out their function. Going back to the methylation array many of the genes involved in both the axonal guidance signaling pathway and the WNT pathway are involved in invasion including metalloproteases and invasion promoting cadherins. It would be interesting to determine if tumor microenvironment signals promote IDH3α expression as a way to regulate its own invasion and tumor vascularization. In this study we did not evaluate the impact of mitochondrial localization of IDH3α on invasion capacity. Currently we are working on creating cell lines using the IDH3α KO NHAs that stably express the full or ΔMTS-IDH3α. These could be used *in vivo* to see if

invasive capacity is restored with addback of IDH3α and if both mitochondrial and nuclear function are necessary for this invasive nature. In addition to invasion the WNT pathway can contribute to angiogenesis in both normal cellular physiology and in cancer (Olsen et al., 2017). Thus expression of IDH3α may promote WNT signaling, supporting angiogenesis in addition to invasion. Similar to our studies CRISPR/Cas9 mediated KO of IDH3α in hCMEC could elucidate the functional role of IDH3α in endothelial function and invasion and could study the interplay of blood brain barrier endothelium with cancer in the absence of IDH3α. Lastly, since the difference in staining was so stark with regards to IDH3α staining of the tumor associated endothelium future studies could examine the extent to which the IDH3α staining says with the tumor associated endothelium back to the originating blood vessel branch point. From a surgical stand point there is a benefit in being able to determine if a vessel is important for normal brain function or if it is exclusively serving the tumor. If staining could be done that is specific for tumor vasculature cutting off those connections would be a way to save normal brain function while targeting the tumor. Such studies may be carried out in GBM genetically engineered mouse models (GEMMs). After initiating tumor growth brains with tumors could be collected, serial sectioned and stained in an attempt to trace a tumor vessel back to its origin.

Another question is whether or not the IDH3α that regulates cSHMT is derived from a mitochondrial or a nuclear pool. IDH3α is a nuclear encoded protein so it is possible that after translation it stays near the nucleus and nuclear lamina since IF data demonstrated both cytosolic and mitochondrial localization in unsynchronized cells. It is also possible that in response to

ATP, an inhibitor of IDH3, the heterotetrameric enzyme breaks apart. This division of the enzyme would then allow IDH3α to engage with cSHMT indicating to the cell that there is enough energy to carry out cellular division and thus stimulates thymidylate synthesis. Along with these studies the precise mechanism of IDH3α subcellular redistribution could be elucidated in the future. Discussed earlier was the failure of a nuclear localization sequence IDH3α mutant to prevent IDH3α being present in the nucleus. The alternative means of bring IDH3α to the nucleus should be investigated. It is possible that IDH3α along with cSHMT can be SUMOylated as an additional mechanism of driving IDH3α to the nucleus.

Next, would be to determine if IDH3α binding to cSHMT alters cSHMT enzymatic orientation. Previously it has been described that excess cSHMT can sequester 5-methylTHF (Herbig et al., 2002). It would be valuable to assess whether this sequestration ability changes with regard to IDH3α binding. Based off our data I would hypothesize that when IDH3α is present cSHMT may have an increased binding affinity for N^5-methyl-THF so in the absence of IDH3α there is an alteration in cSHMT's enzymatic structure decreasing its binding affinity for N^5-methyl-THF. Therefore, more N^5-methyl-THF can progress into the methionine cycle boosting homocysteine recycling and increased SAM production.

Also, what was not determined with this work is where IDH3α binds to cSHMT. If the binding interface between the two can be determined, then small molecule inhibitors could be designed to fit within that binding space. Such an inhibitor may re-capitulate the KO studies carried here

and cause increased sensitivity to anti-folates, like MTX, in GBM. At the same time, such an inhibitor would not need to eliminate IDH3's mitochondrial function thereby avoiding the detrimental side effects of reduced TCA cycle activity in normal cells. Such an inhibitor could then be administered systemically instead of locally increasing the likelihood of clinical usage, especially if a tumor is deemed unresectable due to location or poor pre-surgical evaluation.

If a small molecule cannot be designed to interrupt the IDH3α-cSHMT binding interface it is possible that genetic silencing of IDH3α would not be a lethal form of therapy. Since familial studies have now demonstrated only retinitis pigmentosa as an outcome of homozygous loss of function of *IDH3B* or variants of *IDH3A* (Hartong et al., 2008, Pierrache et al., 2017) there may be very few side effects associated with gene silencing of *IDH3A*, again making it an attractive target for sensitizing GBM to anti-folate therapy. It would be important to develop animal models, those lacking IDH3α expression all together along with animals that have altered IDH3α protein, like our ΔMTS-IDH3α. Such systems would aid in determining the potential side effects of IDH3α inhibitors, may validate the clinical observations of familial *IDH3A* variants leading to disease, and could be combined with GBM GEMMs to further elucidate the impact of IDH3α function on GBM pathogenesis, particularly focusing on disease initiation.

References

AHMED, A. U., AUFFINGER, B. & LESNIAK, M. S. 2013. Understanding glioma stem cells: rationale, clinical relevance and therapeutic strategies. *Expert Rev Neurother,* 13**,** 545-55.

AMARY, M. F., BACSI, K., MAGGIANI, F., DAMATO, S., HALAI, D., BERISHA, F., POLLOCK, R., O'DONNELL, P., GRIGORIADIS, A., DISS, T., ESKANDARPOUR, M., PRESNEAU, N., HOGENDOORN, P. C., FUTREAL, A., TIRABOSCO, R. & FLANAGAN, A. M. 2011. IDH1 and IDH2 mutations are frequent events in central chondrosarcoma and central and periosteal chondromas but not in other mesenchymal tumours. *J Pathol,* 224**,** 334-43.

ANDERSON, D. D. & STOVER, P. J. 2009. SHMT1 and SHMT2 are functionally redundant in nuclear de novo thymidylate biosynthesis. *PLoS One,* 4**,** e5839.

ANDERSON, D. D., WOELLER, C. F., CHIANG, E. P., SHANE, B. & STOVER, P. J. 2012. Serine hydroxymethyltransferase anchors de novo thymidylate synthesis pathway to nuclear lamina for DNA synthesis. *J Biol Chem,* 287**,** 7051-62.

APPLING, D. R. 1991. Compartmentation of folate-mediated one-carbon metabolism in eukaryotes. *FASEB J,* 5**,** 2645-51.

ARYEE, M. J., JAFFE, A. E., CORRADA-BRAVO, H., LADD-ACOSTA, C., FEINBERG, A. P., HANSEN, K. D. & IRIZARRY, R. A. 2014. Minfi: a flexible and comprehensive Bioconductor package for the analysis of Infinium DNA methylation microarrays. *Bioinformatics,* 30**,** 1363-9.

AUDET-WALSH, E., PAPADOPOLI, D. J., GRAVEL, S. P., YEE, T., BRIDON, G., CARON, M., BOURQUE, G., GIGUERE, V. & ST-PIERRE, J. 2016. The PGC-1alpha/ERRalpha Axis Represses One-Carbon Metabolism and Promotes Sensitivity to Anti-folate Therapy in Breast Cancer. *Cell Rep,* 14**,** 920-931.

AUFFINGER, B., TOBIAS, A. L., HAN, Y., LEE, G., GUO, D., DEY, M., LESNIAK, M. S. & AHMED, A. U. 2014. Conversion of differentiated cancer cells into cancer stem-like cells in a glioblastoma model after primary chemotherapy. *Cell Death Differ,* 21**,** 1119-31.

AVELDANO, M. I. & BAZAN, N. G. 1983. Molecular species of phosphatidylcholine, -ethanolamine, -serine, and -inositol in microsomal and photoreceptor membranes of bovine retina. *J Lipid Res,* 24**,** 620-7.

BALSS, J., MEYER, J., MUELLER, W., KORSHUNOV, A., HARTMANN, C. & VON DEIMLING, A. 2008. Analysis of the IDH1 codon 132 mutation in brain tumors. *Acta Neuropathol,* 116**,** 597-602.

BAO, S., WU, Q., SATHORNSUMETEE, S., HAO, Y., LI, Z., HJELMELAND, A. B., SHI, Q., MCLENDON, R. E., BIGNER, D. D. & RICH, J. N. 2006. Stem cell-like glioma cells promote tumor angiogenesis through vascular endothelial growth factor. *Cancer Res,* 66**,** 7843-8.

BEAUDIN, A. E., ABARINOV, E. V., NODEN, D. M., PERRY, C. A., CHU, S., STABLER, S. P., ALLEN, R. H. & STOVER, P. J. 2011. Shmt1 and de novo thymidylate biosynthesis underlie folate-responsive neural tube defects in mice. *The American Journal of Clinical Nutrition,* 93**,** 789-798.

BEHIN, A., HOANG-XUAN, K., CARPENTIER, A. F. & DELATTRE, J. Y. 2003. Primary brain tumours in adults. *Lancet,* 361**,** 323-31.

BERGSTROM, M., ERICSON, K., HAGENFELDT, L., MOSSKIN, M., VON HOLST, H., NOREN, G., ERIKSSON, L., EHRIN, E. & JOHNSTROM, P. 1987. PET study of methionine accumulation in glioma and normal brain tissue: competition with branched chain amino acids. *J Comput Assist Tomogr,* 11**,** 208-13.

BORGER, D. R., GOYAL, L., YAU, T., POON, R. T., ANCUKIEWICZ, M., DESHPANDE, V., CHRISTIANI, D. C., LIEBMAN, H. M., YANG, H., KIM, H., YEN, K., FARIS, J. E., IAFRATE, A. J., KWAK, E. L., CLARK, J. W., ALLEN, J. N., BLASZKOWSKY, L. S., MURPHY, J. E., SAHA, S. K., HONG, T. S., WO, J. Y., FERRONE, C. R., TANABE, K. K., BARDEESY, N., STRALEY, K. S., AGRESTA, S., SCHENKEIN, D. P., ELLISEN, L. W., RYAN, D. P. & ZHU, A. X. 2014. Circulating

oncometabolite 2-hydroxyglutarate is a potential surrogate biomarker in patients with isocitrate dehydrogenase-mutant intrahepatic cholangiocarcinoma. *Clin Cancer Res,* 20**,** 1884-90.

BORGER, D. R., TANABE, K. K., FAN, K. C., LOPEZ, H. U., FANTIN, V. R., STRALEY, K. S., SCHENKEIN, D. P., HEZEL, A. F., ANCUKIEWICZ, M., LIEBMAN, H. M., KWAK, E. L., CLARK, J. W., RYAN, D. P., DESHPANDE, V., DIAS-SANTAGATA, D., ELLISEN, L. W., ZHU, A. X. & IAFRATE, A. J. 2012. Frequent mutation of isocitrate dehydrogenase (IDH)1 and IDH2 in cholangiocarcinoma identified through broad-based tumor genotyping. *Oncologist,* 17**,** 72-9.

BRASCHI, E., GOYON, V., ZUNINO, R., MOHANTY, A., XU, L. & MCBRIDE, H. M. 2010. Vps35 mediates vesicle transport between the mitochondria and peroxisomes. *Curr Biol,* 20**,** 1310-5.

BZYMEK, K. P. & COLMAN, R. F. 2007. Role of alpha-Asp181, beta-Asp192, and gamma-Asp190 in the distinctive subunits of human NAD-specific isocitrate dehydrogenase. *Biochemistry,* 46**,** 5391-7.

CAHILL, D. P., LEVINE, K. K., BETENSKY, R. A., CODD, P. J., ROMANY, C. A., REAVIE, L. B., BATCHELOR, T. T., FUTREAL, P. A., STRATTON, M. R., CURRY, W. T., IAFRATE, A. J. & LOUIS, D. N. 2007. Loss of the mismatch repair protein MSH6 in human glioblastomas is associated with tumor progression during temozolomide treatment. *Clin Cancer Res,* 13**,** 2038-45.

CALVERT, A. E., CHALASTANIS, A., WU, Y., HURLEY, L. A., KOURI, F. M., BI, Y., KACHMAN, M., MAY, J. L., BARTOM, E., HUA, Y., MISHRA, R. K., SCHILTZ, G. E., DUBROVSKYI, O., MAZAR, A. P., PETER, M. E., ZHENG, H., JAMES, C. D., BURANT, C. F., CHANDEL, N. S., DAVULURI, R. V., HORBINSKI, C. & STEGH, A. H. 2017. Cancer-Associated IDH1 Promotes Growth and Resistance to Targeted Therapies in the Absence of Mutation. *Cell Reports,* 19**,** 1858-1873.

CANCER GENOME ATLAS RESEARCH, N. 2008. Comprehensive genomic characterization defines human glioblastoma genes and core pathways. *Nature,* 455**,** 1061-8.

CHANETON, B., HILLMANN, P., ZHENG, L., MARTIN, A. C. L., MADDOCKS, O. D. K., CHOKKATHUKALAM, A., COYLE, J. E., JANKEVICS, A., HOLDING, F. P., VOUSDEN, K. H., FREZZA, C., O'REILLY, M. & GOTTLIEB, E. 2012. Serine is a natural ligand and allosteric activator of pyruvate kinase M2. *Nature,* 491**,** 458-462.

CHEN, J. Q., CAMMARATA, P. R., BAINES, C. P. & YAGER, J. D. 2009. Regulation of mitochondrial respiratory chain biogenesis by estrogens/estrogen receptors and physiological, pathological and pharmacological implications. *Biochim Biophys Acta,* 1793**,** 1540-70.

CHU, E., DRAKE, J. C., BOARMAN, D., BARAM, J. & ALLEGRA, C. J. 1990. Mechanism of thymidylate synthase inhibition by methotrexate in human neoplastic cell lines and normal human myeloid progenitor cells. *J Biol Chem,* 265**,** 8470-8.

COHEN, P. F. & COLMAN, R. F. 1972. Diphosphopyridine nucleotide dependent isocitrate dehydrogenase from pig heart. Characterization of the active substrate and modes of regulation. *Biochemistry,* 11**,** 1501-8.

COMBS, S. E., RIEKEN, S., WICK, W., ABDOLLAHI, A., VON DEIMLING, A., DEBUS, J. & HARTMANN, C. 2011. Prognostic significance of IDH-1 and MGMT in patients with glioblastoma: one step forward, and one step back? *Radiat Oncol,* 6**,** 115.

COMMISSO, C., DAVIDSON, S. M., SOYDANER-AZELOGLU, R. G., PARKER, S. J., KAMPHORST, J. J., HACKETT, S., GRABOCKA, E., NOFAL, M., DREBIN, J. A., THOMPSON, C. B., RABINOWITZ, J. D., METALLO, C. M., VANDER HEIDEN, M. G. & BAR-SAGI, D. 2013. Macropinocytosis of protein is an amino acid supply route in Ras-transformed cells. *Nature,* 497**,** 633-7.

DAHAN, P., MARTINEZ GALA, J., DELMAS, C., MONFERRAN, S., MALRIC, L., ZENTKOWSKI, D., LUBRANO, V., TOULAS, C., COHEN-JONATHAN MOYAL, E. & LEMARIE, A. 2014. Ionizing radiations sustain glioblastoma cell dedifferentiation to a stem-like phenotype through survivin: possible involvement in radioresistance. *Cell Death Dis,* 5**,** e1543.

DANG, L., JIN, S. & SU, S. M. 2010. IDH mutations in glioma and acute myeloid leukemia. *Trends Mol Med,* 16**,** 387-97.

DANG, L., WHITE, D. W., GROSS, S., BENNETT, B. D., BITTINGER, M. A., DRIGGERS, E. M., FANTIN, V. R., JANG, H. G., JIN, S., KEENAN, M. C., MARKS, K. M., PRINS, R. M., WARD, P. S., YEN, K. E., LIAU, L. M., RABINOWITZ, J. D., CANTLEY, L. C., THOMPSON, C. B., VANDER HEIDEN, M. G. & SU, S. M. 2009. Cancer-associated IDH1 mutations produce 2-hydroxyglutarate. *Nature,* 462**,** 739-44.

DANG, L., YEN, K. & ATTAR, E. C. 2016. IDH mutations in cancer and progress toward development of targeted therapeutics. *Ann Oncol,* 27**,** 599-608.

DAY, B. W., STRINGER, B. W., AL-EJEH, F., TING, M. J., WILSON, J., ENSBEY, K. S., JAMIESON, P. R., BRUCE, Z. C., LIM, Y. C., OFFENHAUSER, C., CHARMSAZ, S., COOPER, L. T., ELLACOTT, J. K., HARDING, A., LEVEQUE, L., INGLIS, P., ALLAN, S., WALKER, D. G., LACKMANN, M., OSBORNE, G., KHANNA, K. K., REYNOLDS, B. A., LICKLITER, J. D. & BOYD, A. W. 2013. EphA3 maintains tumorigenicity and is a therapeutic target in glioblastoma multiforme. *Cancer Cell,* 23**,** 238-48.

DE FARIA, G. P., DE OLIVEIRA, J. A., DE OLIVEIRA, J. G., ROMANO SDE, O., NETO, V. M. & MAIA, R. C. 2008. Differences in the expression pattern of P-glycoprotein and MRP1 in low-grade and high-grade gliomas. *Cancer Invest,* 26**,** 883-9.

DE KONING, T. J. & KLOMP, L. W. 2004. Serine-deficiency syndromes. *Curr Opin Neurol,* 17**,** 197-204.

DEAN, M., FOJO, T. & BATES, S. 2005. Tumour stem cells and drug resistance. *Nat Rev Cancer,* 5**,** 275-84.

DI SALVO, M. L., CONTESTABILE, R., PAIARDINI, A. & MARAS, B. 2013. Glycine consumption and mitochondrial serine hydroxymethyltransferase in cancer cells: the heme connection. *Med Hypotheses,* 80**,** 633-6.

DOBIN, A., DAVIS, C. A., SCHLESINGER, F., DRENKOW, J., ZALESKI, C., JHA, S., BATUT, P., CHAISSON, M. & GINGERAS, T. R. 2013. STAR: ultrafast universal RNA-seq aligner. *Bioinformatics,* 29**,** 15-21.

DU, Y. & DREYFUS, C. F. 2002. Oligodendrocytes as providers of growth factors. *J Neurosci Res,* 68**,** 647-54.

DUCKER, G. S. & RABINOWITZ, J. D. 2017. One-Carbon Metabolism in Health and Disease. *Cell Metab,* 25**,** 27-42.

DUNCAN, C. G., BARWICK, B. G., JIN, G., RAGO, C., KAPOOR-VAZIRANI, P., POWELL, D. R., CHI, J. T., BIGNER, D. D., VERTINO, P. M. & YAN, H. 2012. A heterozygous IDH1R132H/WT mutation induces genome-wide alterations in DNA methylation. *Genome Res,* 22**,** 2339-55.

ELSTROM, R. L., BAUER, D. E., BUZZAI, M., KARNAUSKAS, R., HARRIS, M. H., PLAS, D. R., ZHUANG, H., CINALLI, R. M., ALAVI, A., RUDIN, C. M. & THOMPSON, C. B. 2004. Akt stimulates aerobic glycolysis in cancer cells. *Cancer Res,* 64**,** 3892-9.

FARBER, S. & DIAMOND, L. K. 1948. Temporary remissions in acute leukemia in children produced by folic acid antagonist, 4-aminopteroyl-glutamic acid. *N Engl J Med,* 238**,** 787-93.

FARRELL, C. J. & PLOTKIN, S. R. 2007. Genetic causes of brain tumors: neurofibromatosis, tuberous sclerosis, von Hippel-Lindau, and other syndromes. *Neurol Clin,* 25**,** 925-46, viii.

FATTAL-VALEVSKI, A., ELIYAHU, H., FRAENKEL, N. D., ELMALIACH, G., HAUSMAN-KEDEM, M., SHAAG, A., MANDEL, D., PINES, O. & ELPELEG, O. 2017. Homozygous mutation, p.Pro304His, in IDH3A, encoding isocitrate dehydrogenase subunit is associated with severe encephalopathy in infancy. *Neurogenetics,* 18**,** 57-61.

FIDLER, I. J. & KRIPKE, M. L. 1977. Metastasis results from preexisting variant cells within a malignant tumor. *Science,* 197**,** 893-5.

FIGUEROA, M. E., ABDEL-WAHAB, O., LU, C., WARD, P. S., PATEL, J., SHIH, A., LI, Y., BHAGWAT, N., VASANTHAKUMAR, A., FERNANDEZ, H. F., TALLMAN, M. S., SUN, Z., WOLNIAK, K., PEETERS, J. K., LIU, W., CHOE, S. E., FANTIN, V. R., PAIETTA, E., LOWENBERG, B., LICHT, J. D., GODLEY, L. A., DELWEL, R., VALK, P. J., THOMPSON, C. B., LEVINE, R. L. & MELNICK, A. 2010. Leukemic IDH1 and IDH2 mutations result in a hypermethylation phenotype, disrupt TET2 function, and impair hematopoietic differentiation. *Cancer Cell,* 18**,** 553-67.

FORTIN, J. P., LABBE, A., LEMIRE, M., ZANKE, B. W., HUDSON, T. J., FERTIG, E. J., GREENWOOD, C. M. & HANSEN, K. D. 2014. Functional normalization of 450k methylation array data improves replication in large cancer studies. *Genome Biol,* 15**,** 503.

FRANCESCHI, S., LESSI, F., ARETINI, P., MAZZANTI, C. M., MENICAGLI, M., LA FERLA, M., DE GREGORIO, V., CARAMELLA, D., NACCARATO, A. G., BEVILACQUA, G., BONADIO, A. G. & PASQUALETTI, F. 2016. Molecular portrait of a rare case of metastatic glioblastoma: somatic and germline mutations using whole-exome sequencing. *Neuro Oncol,* 18**,** 298-300.

FRANCO, M., ROSWALL, P., CORTEZ, E., HANAHAN, D. & PIETRAS, K. 2011. Pericytes promote endothelial cell survival through induction of autocrine VEGF-A signaling and Bcl-w expression. *Blood,* 118**,** 2906-17.

FRIEDMAN, H. S., PRADOS, M. D., WEN, P. Y., MIKKELSEN, T., SCHIFF, D., ABREY, L. E., YUNG, W. K., PALEOLOGOS, N., NICHOLAS, M. K., JENSEN, R., VREDENBURGH, J., HUANG, J., ZHENG, M. & CLOUGHESY, T. 2009. Bevacizumab alone and in combination with irinotecan in recurrent glioblastoma. *J Clin Oncol,* 27**,** 4733-40.

GABRIEL, J. L., ZERVOS, P. R. & PLAUT, G. W. 1986. Activity of purified NAD-specific isocitrate dehydrogenase at modulator and substrate concentrations approximating conditions in mitochondria. *Metabolism,* 35**,** 661-7.

GARCIA, B. A., MOLLAH, S., UEBERHEIDE, B. M., BUSBY, S. A., MURATORE, T. L., SHABANOWITZ, J. & HUNT, D. F. 2007. Chemical derivatization of histones for facilitated analysis by mass spectrometry. *Nat Protoc,* 2**,** 933-8.

GAULT, C. R., OBEID, L. M. & HANNUN, Y. A. 2010. An overview of sphingolipid metabolism: from synthesis to breakdown. *Adv Exp Med Biol,* 688**,** 1-23.

GEMOLL, T., HABERMANN, J. K., BECKER, S., SZYMCZAK, S., UPENDER, M. B., BRUCH, H. P., HELLMAN, U., RIED, T., AUER, G., JORNVALL, H. & ROBLICK, U. J. 2013. Chromosomal aneuploidy affects the global proteome equilibrium of colorectal cancer cells. *Anal Cell Pathol (Amst),* 36**,** 149-61.

GNYSZKA, A., JASTRZEBSKI, Z. & FLIS, S. 2013. DNA methyltransferase inhibitors and their emerging role in epigenetic therapy of cancer. *Anticancer Res,* 33**,** 2989-96.

GREAVES, M. & MALEY, C. C. 2012. Clonal evolution in cancer. *Nature,* 481**,** 306-13.

GROSS, S., CAIRNS, R. A., MINDEN, M. D., DRIGGERS, E. M., BITTINGER, M. A., JANG, H. G., SASAKI, M., JIN, S., SCHENKEIN, D. P., SU, S. M., DANG, L., FANTIN, V. R. & MAK, T. W. 2010. Cancer-associated metabolite 2-hydroxyglutarate accumulates in acute myelogenous leukemia with isocitrate dehydrogenase 1 and 2 mutations. *J Exp Med,* 207**,** 339-44.

GUO, D., BELL, E. H., MISCHEL, P. & CHAKRAVARTI, A. 2014. Targeting SREBP-1-driven lipid metabolism to treat cancer. *Curr Pharm Des,* 20**,** 2619-26.

GUPTA, R., YANG, Q., DOGRA, S. K. & WAJAPEYEE, N. 2017. Serine hydroxymethyl transferase 1 stimulates pro-oncogenic cytokine expression through sialic acid to promote ovarian cancer tumor growth and progression. *Oncogene,* 36**,** 4014-4024.

HAMMOUDI, N., AHMED, K. B., GARCIA-PRIETO, C. & HUANG, P. 2011. Metabolic alterations in cancer cells and therapeutic implications. *Chin J Cancer,* 30**,** 508-25.

HANAHAN, D. & WEINBERG, R. A. 2011. Hallmarks of cancer: the next generation. *Cell,* 144**,** 646-74.

HARTONG, D. T., DANGE, M., MCGEE, T. L., BERSON, E. L., DRYJA, T. P. & COLMAN, R. F. 2008. Insights from retinitis pigmentosa into the roles of isocitrate dehydrogenases in the Krebs cycle. *Nat Genet,* 40**,** 1230-4.

HEBY, O. & PERSSON, L. 1990. Molecular genetics of polyamine synthesis in eukaryotic cells. *Trends Biochem Sci,* 15**,** 153-8.

HEGI, M. E., DISERENS, A. C., GODARD, S., DIETRICH, P. Y., REGLI, L., OSTERMANN, S., OTTEN, P., VAN MELLE, G., DE TRIBOLET, N. & STUPP, R. 2004. Clinical trial substantiates the predictive value of O-6-methylguanine-DNA methyltransferase promoter methylation in glioblastoma patients treated with temozolomide. *Clin Cancer Res,* 10**,** 1871-4.

HEGI, M. E., DISERENS, A. C., GORLIA, T., HAMOU, M. F., DE TRIBOLET, N., WELLER, M., KROS, J. M., HAINFELLNER, J. A., MASON, W., MARIANI, L., BROMBERG, J. E., HAU, P., MIRIMANOFF, R. O., CAIRNCROSS, J. G., JANZER, R. C. & STUPP, R. 2005. MGMT gene silencing and benefit from temozolomide in glioblastoma. *N Engl J Med,* 352**,** 997-1003.

HEIL, S. G., VAN DER PUT, N. M., WAAS, E. T., DEN HEIJER, M., TRIJBELS, F. J. & BLOM, H. J. 2001. Is mutated serine hydroxymethyltransferase (SHMT) involved in the etiology of neural tube defects? *Mol Genet Metab,* 73**,** 164-72.

HERBIG, K., CHIANG, E. P., LEE, L. R., HILLS, J., SHANE, B. & STOVER, P. J. 2002. Cytoplasmic serine hydroxymethyltransferase mediates competition between folate-dependent deoxyribonucleotide and S-adenosylmethionine biosyntheses. *J Biol Chem,* 277**,** 38381-9.

HERRERO-MENDEZ, A., ALMEIDA, A., FERNANDEZ, E., MAESTRE, C., MONCADA, S. & BOLANOS, J. P. 2009. The bioenergetic and antioxidant status of neurons is controlled by continuous degradation of a key glycolytic enzyme by APC/C-Cdh1. *Nat Cell Biol,* 11**,** 747-52.

HICKMAN, M. J., PETTI, A. A., HO-SHING, O., SILVERMAN, S. J., MCISAAC, R. S., LEE, T. A. & BOTSTEIN, D. 2011. Coordinated regulation of sulfur and phospholipid metabolism reflects the importance of methylation in the growth of yeast. *Mol Biol Cell,* 22**,** 4192-204.

HJELMELAND, A. B., WU, Q., HEDDLESTON, J. M., CHOUDHARY, G. S., MACSWORDS, J., LATHIA, J. D., MCLENDON, R., LINDNER, D., SLOAN, A. & RICH, J. N. 2011. Acidic stress promotes a glioma stem cell phenotype. *Cell Death Differ,* 18**,** 829-40.

HORBINSKI, C. 2013. What do we know about IDH1/2 mutations so far, and how do we use it? *Acta Neuropathol,* 125**,** 621-36.

HOUILLIER, C., WANG, X., KALOSHI, G., MOKHTARI, K., GUILLEVIN, R., LAFFAIRE, J., PARIS, S., BOISSELIER, B., IDBAIH, A., LAIGLE-DONADEY, F., HOANG-XUAN, K., SANSON, M. & DELATTRE, J. Y. 2010. IDH1 or IDH2 mutations predict longer survival and response to temozolomide in low-grade gliomas. *Neurology,* 75**,** 1560-6.

HUANG, Z., CHENG, L., GURYANOVA, O. A., WU, Q. & BAO, S. 2010. Cancer stem cells in glioblastoma--molecular signaling and therapeutic targeting. *Protein Cell,* 1**,** 638-55.

HUNTER, C., SMITH, R., CAHILL, D. P., STEPHENS, P., STEVENS, C., TEAGUE, J., GREENMAN, C., EDKINS, S., BIGNELL, G., DAVIES, H., O'MEARA, S., PARKER, A., AVIS, T., BARTHORPE, S., BRACKENBURY, L., BUCK, G., BUTLER, A., CLEMENTS, J., COLE, J., DICKS, E., FORBES, S., GORTON, M., GRAY, K., HALLIDAY, K., HARRISON, R., HILLS, K., HINTON, J., JENKINSON, A., JONES, D., KOSMIDOU, V., LAMAN, R., LUGG, R., MENZIES, A., PERRY, J., PETTY, R., RAINE, K., RICHARDSON, D., SHEPHERD, R., SMALL, A., SOLOMON, H., TOFTS, C., VARIAN, J., WEST, S., WIDAA, S., YATES, A., EASTON, D. F., RIGGINS, G., ROY, J. E., LEVINE, K. K., MUELLER, W., BATCHELOR, T. T., LOUIS, D. N., STRATTON, M. R., FUTREAL, P. A. & WOOSTER, R. 2006. A hypermutation phenotype and somatic MSH6 mutations in recurrent human malignant gliomas after alkylator chemotherapy. *Cancer Res,* 66**,** 3987-91.

JAIN, M., NILSSON, R., SHARMA, S., MADHUSUDHAN, N., KITAMI, T., SOUZA, A. L., KAFRI, R., KIRSCHNER, M. W., CLISH, C. B. & MOOTHA, V. K. 2012. Metabolite profiling identifies a key role for glycine in rapid cancer cell proliferation. *Science,* 336**,** 1040-4.

JURATLI, T. A., KIRSCH, M., GEIGER, K., KLINK, B., LEIPNITZ, E., PINZER, T., SOUCEK, S., SCHROCK, E., SCHACKERT, G. & KREX, D. 2012a. The prognostic value of IDH mutations and MGMT promoter status in secondary high-grade gliomas. *J Neurooncol,* 110**,** 325-33.

JURATLI, T. A., KIRSCH, M., ROBEL, K., SOUCEK, S., GEIGER, K., VON KUMMER, R., SCHACKERT, G. & KREX, D. 2012b. IDH mutations as an early and consistent marker in low-grade astrocytomas WHO grade II and their consecutive secondary high-grade gliomas. *J Neurooncol,* 108**,** 403-10.

KEUM, Y. S. & CHOI, B. Y. 2015. Isocitrate dehydrogenase mutations: new opportunities for translational research. *BMB Rep,* 48**,** 266-70.

KIEFMANN, M., TANK, S., KELLER, P., BORNCHEN, C., RINNENTHAL, J. L., TRITT, M. O., SCHULTE-UENTROP, L., OLOTU, C., GOETZ, A. E. & KIEFMANN, R. 2017. IDH3 mediates apoptosis of alveolar epithelial cells type 2 due to mitochondrial Ca2+ uptake during hypocapnia. *Cell Death Dis,* 8**,** e3005.

KING, A., SELAK, M. A. & GOTTLIEB, E. 2006. Succinate dehydrogenase and fumarate hydratase: linking mitochondrial dysfunction and cancer. *Oncogene,* 25**,** 4675-82.

KINNAIRD, A., ZHAO, S., WELLEN, K. E. & MICHELAKIS, E. D. 2016. Metabolic control of epigenetics in cancer. *Nat Rev Cancer,* 16**,** 694-707.

KINNEY, A. J. & MOORE, T. S. 1987. Phosphatidylcholine Synthesis in Castor Bean Endosperm : I. Metabolism of l-Serine. *Plant Physiol,* 84**,** 78-81.

KIRSON, E. D., DBALY, V., TOVARYS, F., VYMAZAL, J., SOUSTIEL, J. F., ITZHAKI, A., MORDECHOVICH, D., STEINBERG-SHAPIRA, S., GURVICH, Z., SCHNEIDERMAN, R., WASSERMAN, Y., SALZBERG, M., RYFFEL, B., GOLDSHER, D., DEKEL, E. & PALTI, Y. 2007. Alternating electric fields arrest cell proliferation in animal tumor models and human brain tumors. *Proc Natl Acad Sci U S A,* 104**,** 10152-7.

KLEIHUES, P. & OHGAKI, H. 2000. Phenotype vs genotype in the evolution of astrocytic brain tumors. *Toxicol Pathol,* 28**,** 164-70.

KOO, J. S. & YOON, J. S. 2015. Expression of metabolism-related proteins in lacrimal gland adenoid cystic carcinoma. *Am J Clin Pathol,* 143**,** 584-92.

KOTTAKIS, F., NICOLAY, B. N., ROUMANE, A., KARNIK, R., GU, H., NAGLE, J. M., BOUKHALI, M., HAYWARD, M. C., LI, Y. Y., CHEN, T., LIESA, M., HAMMERMAN, P. S., WONG, K. K., HAYES, D. N., SHIRIHAI, O. S., DYSON, N. J., HAAS, W., MEISSNER, A. & BARDEESY, N. 2016. LKB1 loss links serine metabolism to DNA methylation and tumorigenesis. *Nature,* 539**,** 390-395.

KRANENDIJK, M., STRUYS, E. A., VAN SCHAFTINGEN, E., GIBSON, K. M., KANHAI, W. A., VAN DER KNAAP, M. S., AMIEL, J., BUIST, N. R., DAS, A. M., DE KLERK, J. B., FEIGENBAUM, A. S., GRANGE, D. K., HOFSTEDE, F. C., HOLME, E., KIRK, E. P., KORMAN, S. H., MORAVA, E., MORRIS, A., SMEITINK, J., SUKHAI, R. N., VALLANCE, H., JAKOBS, C. & SALOMONS, G. S. 2010. IDH2 mutations in patients with D-2-hydroxyglutaric aciduria. *Science,* 330**,** 336.

KRELL, D., ASSOKU, M., GALLOWAY, M., MULHOLLAND, P., TOMLINSON, I. & BARDELLA, C. 2011. Screen for IDH1, IDH2, IDH3, D2HGDH and L2HGDH mutations in glioblastoma. *PLoS One,* 6**,** e19868.

KROEMER, G. & POUYSSEGUR, J. 2008. Tumor cell metabolism: cancer's Achilles' heel. *Cancer Cell,* 13**,** 472-82.

KRUPENKO, N. I., DUBARD, M. E., STRICKLAND, K. C., MOXLEY, K. M., OLEINIK, N. V. & KRUPENKO, S. A. 2010. ALDH1L2 is the mitochondrial homolog of 10-formyltetrahydrofolate dehydrogenase. *J Biol Chem,* 285**,** 23056-63.

LACROIX, M., ABI-SAID, D., FOURNEY, D. R., GOKASLAN, Z. L., SHI, W., DEMONTE, F., LANG, F. F., MCCUTCHEON, I. E., HASSENBUSCH, S. J., HOLLAND, E., HESS, K., MICHAEL, C., MILLER, D. & SAWAYA, R. 2001. A multivariate analysis of 416 patients with glioblastoma multiforme: prognosis, extent of resection, and survival. *J Neurosurg,* 95**,** 190-8.

LAI, W. K. & KAN, M. Y. 2015. Homocysteine-Induced Endothelial Dysfunction. *Ann Nutr Metab,* 67**,** 1-12.

LAUKKA, T., MARIANI, C. J., IHANTOLA, T., CAO, J. Z., HOKKANEN, J., KAELIN, W. G., JR., GODLEY, L. A. & KOIVUNEN, P. 2016. Fumarate and Succinate Regulate Expression of Hypoxia-inducible Genes via TET Enzymes. *J Biol Chem,* 291**,** 4256-65.

LE, D. M., BESSON, A., FOGG, D. K., CHOI, K. S., WAISMAN, D. M., GOODYER, C. G., REWCASTLE, B. & YONG, V. W. 2003. Exploitation of astrocytes by glioma cells to facilitate invasiveness: a mechanism involving matrix metalloproteinase-2 and the urokinase-type plasminogen activator-plasmin cascade. *J Neurosci,* 23**,** 4034-43.

LEE, G. Y., HAVERTY, P. M., LI, L., KLJAVIN, N. M., BOURGON, R., LEE, J., STERN, H., MODRUSAN, Z., SESHAGIRI, S., ZHANG, Z., DAVIS, D., STOKOE, D., SETTLEMAN, J., DE SAUVAGE, F. J.

& NEVE, R. M. 2014. Comparative oncogenomics identifies PSMB4 and SHMT2 as potential cancer driver genes. *Cancer Res,* 74**,** 3114-26.

LEE, J., SHARMA, S., KIM, J., FERRANTE, R. J. & RYU, H. 2008. Mitochondrial nuclear receptors and transcription factors: who's minding the cell? *J Neurosci Res,* 86**,** 961-71.

LEE, N. & KIM, D. 2016. Cancer Metabolism: Fueling More than Just Growth. *Mol Cells,* 39**,** 847-854.

LEIGH-BROWN, S., ENRIQUEZ, J. A. & ODOM, D. T. 2010. Nuclear transcription factors in mammalian mitochondria. *Genome Biol,* 11**,** 215.

LEWIS, C. A., PARKER, S. J., FISKE, B. P., MCCLOSKEY, D., GUI, D. Y., GREEN, C. R., VOKES, N. I., FEIST, A. M., VANDER HEIDEN, M. G. & METALLO, C. M. 2014. Tracing compartmentalized NADPH metabolism in the cytosol and mitochondria of mammalian cells. *Mol Cell,* 55**,** 253-63.

LI, B. & DEWEY, C. N. 2011. RSEM: accurate transcript quantification from RNA-Seq data with or without a reference genome. *BMC Bioinformatics,* 12**,** 323.

LIBERTI, M. V., DAI, Z., WARDELL, S. E., BACCILE, J. A., LIU, X., GAO, X., BALDI, R., MEHRMOHAMADI, M., JOHNSON, M. O., MADHUKAR, N. S., SHESTOV, A. A., CHIO, I. I. C., ELEMENTO, O., RATHMELL, J. C., SCHROEDER, F. C., MCDONNELL, D. P. & LOCASALE, J. W. 2017. A Predictive Model for Selective Targeting of the Warburg Effect through GAPDH Inhibition with a Natural Product. *Cell Metab,* 26**,** 648-659 e8.

LINNET, K. & EJSING, T. B. 2008. A review on the impact of P-glycoprotein on the penetration of drugs into the brain. Focus on psychotropic drugs. *Eur Neuropsychopharmacol,* 18**,** 157-69.

LIU, J., GUO, S., LI, Q., YANG, L., XIA, Z., ZHANG, L., HUANG, Z. & ZHANG, N. 2013. Phosphoglycerate dehydrogenase induces glioma cells proliferation and invasion by stabilizing forkhead box M1. *J Neurooncol,* 111**,** 245-55.

LOSMAN, J. A. & KAELIN, W. G., JR. 2013. What a difference a hydroxyl makes: mutant IDH, (R)-2-hydroxyglutarate, and cancer. *Genes Dev,* 27**,** 836-52.

LOUIS, D. N. 2006. Molecular pathology of malignant gliomas. *Annu Rev Pathol,* 1**,** 97-117.

LOUIS, D. N., OHGAKI, H., WIESTLER, O. D., CAVENEE, W. K., BURGER, P. C., JOUVET, A., SCHEITHAUER, B. W. & KLEIHUES, P. 2007. The 2007 WHO classification of tumours of the central nervous system. *Acta Neuropathol,* 114**,** 97-109.

LOUIS, D. N., PERRY, A., REIFENBERGER, G., VON DEIMLING, A., FIGARELLA-BRANGER, D., CAVENEE, W. K., OHGAKI, H., WIESTLER, O. D., KLEIHUES, P. & ELLISON, D. W. 2016. The 2016 World Health Organization Classification of Tumors of the Central Nervous System: a summary. *Acta Neuropathol,* 131**,** 803-20.

LU, C. & THOMPSON, C. B. 2012. Metabolic regulation of epigenetics. *Cell Metabolism,* 16**,** 9-17.

LUBANSKA, D., MARKET-VELKER, B. A., DECARVALHO, A. C., MIKKELSEN, T., FIDALGO DA SILVA, E. & PORTER, L. A. 2014. The cyclin-like protein Spy1 regulates growth and division characteristics of the CD133+ population in human glioma. *Cancer Cell,* 25**,** 64-76.

LUCAS, E. K., REID, C. S., MCMEEKIN, L. J., DOUGHERTY, S. E., FLOYD, C. L. & COWELL, R. M. 2014. Cerebellar transcriptional alterations with Purkinje cell dysfunction and loss in mice lacking PGC-1alpha. *Front Cell Neurosci,* 8**,** 441.

LUN, M., LOK, E., GAUTAM, S., WU, E. & WONG, E. T. 2011. The natural history of extracranial metastasis from glioblastoma multiforme. *J Neurooncol,* 105**,** 261-73.

MACDONALD, M. J., BROWN, L. J., LONGACRE, M. J., STOKER, S. W., KENDRICK, M. A. & HASAN, N. M. 2013. Knockdown of both mitochondrial isocitrate dehydrogenase enzymes in pancreatic beta cells inhibits insulin secretion. *Biochim Biophys Acta,* 1830**,** 5104-11.

MACFARLANE, A. J., ANDERSON, D. D., FLODBY, P., PERRY, C. A., ALLEN, R. H., STABLER, S. P. & STOVER, P. J. 2011. Nuclear localization of de novo thymidylate biosynthesis pathway is required to prevent uracil accumulation in DNA. *J Biol Chem,* 286**,** 44015-22.

MACFARLANE, A. J., LIU, X., PERRY, C. A., FLODBY, P., ALLEN, R. H., STABLER, S. P. & STOVER, P. J. 2008. Cytoplasmic Serine Hydroxymethyltransferase Regulates the Metabolic Partitioning of Methylenetetrahydrofolate but Is Not Essential in Mice. *Journal of Biological Chemistry,* 283**,** 25846-25853.

MADDOCKS, O. D., BERKERS, C. R., MASON, S. M., ZHENG, L., BLYTH, K., GOTTLIEB, E. & VOUSDEN, K. H. 2013. Serine starvation induces stress and p53-dependent metabolic remodelling in cancer cells. *Nature,* 493**,** 542-6.

MADDOCKS, O. D., LABUSCHAGNE, C. F., ADAMS, P. D. & VOUSDEN, K. H. 2016. Serine Metabolism Supports the Methionine Cycle and DNA/RNA Methylation through De Novo ATP Synthesis in Cancer Cells. *Mol Cell,* 61**,** 210-21.

MALMSTROM, A., GRONBERG, B. H., MAROSI, C., STUPP, R., FRAPPAZ, D., SCHULTZ, H., ABACIOGLU, U., TAVELIN, B., LHERMITTE, B., HEGI, M. E., ROSELL, J., HENRIKSSON, R. & NORDIC CLINICAL BRAIN TUMOUR STUDY, G. 2012. Temozolomide versus standard 6-week radiotherapy versus hypofractionated radiotherapy in patients older than 60 years with glioblastoma: the Nordic randomised, phase 3 trial. *Lancet Oncol,* 13**,** 916-26.

MAO, P., JOSHI, K., LI, J., KIM, S. H., LI, P., SANTANA-SANTOS, L., LUTHRA, S., CHANDRAN, U. R., BENOS, P. V., SMITH, L., WANG, M., HU, B., CHENG, S. Y., SOBOL, R. W. & NAKANO, I. 2013. Mesenchymal glioma stem cells are maintained by activated glycolytic metabolism involving aldehyde dehydrogenase 1A3. *Proc Natl Acad Sci U S A,* 110**,** 8644-9.

MARANI, M., PAONE, A., FIASCARELLI, A., MACONE, A., GARGANO, M., RINALDO, S., GIARDINA, G., PONTECORVI, V., KOES, D., MCDERMOTT, L., YANG, T., PAIARDINI, A., CONTESTABILE, R. & CUTRUZZOLA, F. 2016. A pyrazolopyran derivative preferentially inhibits the activity of human cytosolic serine hydroxymethyltransferase and induces cell death in lung cancer cells. *Oncotarget,* 7**,** 4570-83.

MASHIMO, T., PICHUMANI, K., VEMIREDDY, V., HATANPAA, K. J., SINGH, D. K., SIRASANAGANDLA, S., NANNEPAGA, S., PICCIRILLO, S. G., KOVACS, Z., FOONG, C., HUANG, Z., BARNETT, S., MICKEY, B. E., DEBERARDINIS, R. J., TU, B. P., MAHER, E. A. & BACHOO, R. M. 2014. Acetate is a bioenergetic substrate for human glioblastoma and brain metastases. *Cell,* 159**,** 1603-14.

MEHRMOHAMADI, M., LIU, X., SHESTOV, A. A. & LOCASALE, J. W. 2014. Characterization of the usage of the serine metabolic network in human cancer. *Cell Rep,* 9**,** 1507-19.

MELLAI, M., MONZEGLIO, O., PIAZZI, A., CALDERA, V., ANNOVAZZI, L., CASSONI, P., VALENTE, G., CORDERA, S., MOCELLINI, C. & SCHIFFER, D. 2012. MGMT promoter hypermethylation and its associations with genetic alterations in a series of 350 brain tumors. *J Neurooncol,* 107**,** 617-31.

MINARD, K. I. & MCALISTER-HENN, L. 1999. Dependence of peroxisomal beta-oxidation on cytosolic sources of NADPH. *J Biol Chem,* 274**,** 3402-6.

MULLARKY, E., LUCKI, N. C., BEHESHTI ZAVAREH, R., ANGLIN, J. L., GOMES, A. P., NICOLAY, B. N., WONG, J. C., CHRISTEN, S., TAKAHASHI, H., SINGH, P. K., BLENIS, J., WARREN, J. D., FENDT, S. M., ASARA, J. M., DENICOLA, G. M., LYSSIOTIS, C. A., LAIRSON, L. L. & CANTLEY, L. C. 2016. Identification of a small molecule inhibitor of 3-phosphoglycerate dehydrogenase to target serine biosynthesis in cancers. *Proc Natl Acad Sci U S A,* 113**,** 1778-83.

MULLARKY, E., MATTAINI, K. R., VANDER HEIDEN, M. G., CANTLEY, L. C. & LOCASALE, J. W. 2011. PHGDH amplification and altered glucose metabolism in human melanoma. *Pigment Cell Melanoma Res,* 24**,** 1112-5.

MUNOZ, J. L., RODRIGUEZ-CRUZ, V., GRECO, S. J., NAGULA, V., SCOTTO, K. W. & RAMESHWAR, P. 2014. Temozolomide induces the production of epidermal growth factor to regulate MDR1 expression in glioblastoma cells. *Mol Cancer Ther,* 13**,** 2399-411.

NAKAGAWACHI, T., SOEJIMA, H., URANO, T., ZHAO, W., HIGASHIMOTO, K., SATOH, Y., MATSUKURA, S., KUDO, S., KITAJIMA, Y., HARADA, H., FURUKAWA, K., MATSUZAKI, H., EMI, M., NAKABEPPU, Y., MIYAZAKI, K., SEKIGUCHI, M. & MUKAI, T. 2003. Silencing effect of CpG island hypermethylation and histone modifications on O6-methylguanine-DNA methyltransferase (MGMT) gene expression in human cancer. *Oncogene,* 22**,** 8835-44.

NAKAZAWA, M. S., KEITH, B. & SIMON, M. C. 2016. Oxygen availability and metabolic adaptations. *Nat Rev Cancer,* 16**,** 663-73.

NAMIKI, T. 1981. [Pathology of brain tumours (1). With special reference to WHO's histological typing of tumours of the central nervous system (author's transl)]. *Rinsho Byori,* 29**,** 1119-22.

NAVIN, N., KENDALL, J., TROGE, J., ANDREWS, P., RODGERS, L., MCINDOO, J., COOK, K., STEPANSKY, A., LEVY, D., ESPOSITO, D., MUTHUSWAMY, L., KRASNITZ, A., MCCOMBIE, W. R., HICKS, J. & WIGLER, M. 2011. Tumour evolution inferred by single-cell sequencing. *Nature,* 472**,** 90-4.

NICHOLAS, M. K., LUKAS, R. V., CHMURA, S., YAMINI, B., LESNIAK, M. & PYTEL, P. 2011. Molecular heterogeneity in glioblastoma: therapeutic opportunities and challenges. *Semin Oncol,* 38**,** 243-53.

NYHAN, W. L. Nucleotide Synthesis via Salvage Pathway. *eLS.*

OHGAKI, H. 2009. Epidemiology of brain tumors. *Methods Mol Biol,* 472**,** 323-42.

OHGAKI, H., DESSEN, P., JOURDE, B., HORSTMANN, S., NISHIKAWA, T., DI PATRE, P. L., BURKHARD, C., SCHULER, D., PROBST-HENSCH, N. M., MAIORKA, P. C., BAEZA, N., PISANI, P., YONEKAWA, Y., YASARGIL, M. G., LUTOLF, U. M. & KLEIHUES, P. 2004. Genetic pathways to glioblastoma: a population-based study. *Cancer Res,* 64**,** 6892-9.

OHGAKI, H. & KLEIHUES, P. 2007. Genetic pathways to primary and secondary glioblastoma. *Am J Pathol,* 170**,** 1445-53.

OLAR, A. & ALDAPE, K. D. 2014. Using the molecular classification of glioblastoma to inform personalized treatment. *J Pathol,* 232**,** 165-77.

OLSEN, J. J., POHL, S. O., DESHMUKH, A., VISWESWARAN, M., WARD, N. C., ARFUSO, F., AGOSTINO, M. & DHARMARAJAN, A. 2017. The Role of Wnt Signalling in Angiogenesis. *Clin Biochem Rev,* 38**,** 131-142.

OSBORN, M. J., FREEMAN, M. & HUENNEKENS, F. M. 1958. Inhibition of dihydrofolic reductase by aminopterin and amethopterin. *Proc Soc Exp Biol Med,* 97**,** 429-31.

OSTROM, Q. T., GITTLEMAN, H., FARAH, P., ONDRACEK, A., CHEN, Y., WOLINSKY, Y., STROUP, N. E., KRUCHKO, C. & BARNHOLTZ-SLOAN, J. S. 2013. CBTRUS statistical report: Primary brain and central nervous system tumors diagnosed in the United States in 2006-2010. *Neuro Oncol,* 15 Suppl 2**,** ii1-56.

OSTROM, Q. T., GITTLEMAN, H., XU, J., KROMER, C., WOLINSKY, Y., KRUCHKO, C. & BARNHOLTZ-SLOAN, J. S. 2016. CBTRUS Statistical Report: Primary Brain and Other Central Nervous System Tumors Diagnosed in the United States in 2009-2013. *Neuro Oncol,* 18**,** v1-v75.

OUDARD, S., ARVELO, F., MICCOLI, L., APIOU, F., DUTRILLAUX, A. M., POISSON, M., DUTRILLAUX, B. & POUPON, M. F. 1996. High glycolysis in gliomas despite low hexokinase transcription and activity correlated to chromosome 10 loss. *Br J Cancer,* 74**,** 839-45.

PACOLD, M. E., BRIMACOMBE, K. R., CHAN, S. H., ROHDE, J. M., LEWIS, C. A., SWIER, L. J., POSSEMATO, R., CHEN, W. W., SULLIVAN, L. B., FISKE, B. P., CHO, S., FREINKMAN, E., BIRSOY, K., ABU-REMAILEH, M., SHAUL, Y. D., LIU, C. M., ZHOU, M., KOH, M. J., CHUNG, H., DAVIDSON, S. M., LUENGO, A., WANG, A. Q., XU, X., YASGAR, A., LIU, L., RAI, G., WESTOVER, K. D., VANDER HEIDEN, M. G., SHEN, M., GRAY, N. S., BOXER, M. B. & SABATINI, D. M. 2016. A PHGDH inhibitor reveals coordination of serine synthesis and one-carbon unit fate. *Nat Chem Biol,* 12**,** 452-8.

PALANICHAMY, K. & CHAKRAVARTI, A. 2017. Diagnostic and Prognostic Significance of Methionine Uptake and Methionine Positron Emission Tomography Imaging in Gliomas. *Front Oncol,* 7**,** 257.

PALANICHAMY, K., THIRUMOORTHY, K., KANJI, S., GORDON, N., SINGH, R., JACOB, J. R., SEBASTIAN, N., LITZENBERG, K. T., PATEL, D., BASSETT, E., RAMASUBRAMANIAN, B., LAUTENSCHLAEGER, T., FISCHER, S. M., RAY-CHAUDHURY, A. & CHAKRAVARTI, A. 2016. Methionine and Kynurenine Activate Oncogenic Kinases in Glioblastoma, and Methionine Deprivation Compromises Proliferation. *Clin Cancer Res,* 22**,** 3513-23.

PANDEY, S., GARG, P., LEE, S., CHOUNG, H. W., CHOUNG, Y. H., CHOUNG, P. H. & CHUNG, J. H. 2014. Nucleotide biosynthesis arrest by silencing SHMT1 function via vitamin B6-coupled vector and effects on tumor growth inhibition. *Biomaterials,* 35**,** 9332-42.

PAONE, A., MARANI, M., FIASCARELLI, A., RINALDO, S., GIARDINA, G., CONTESTABILE, R., PAIARDINI, A. & CUTRUZZOLA, F. 2014. SHMT1 knockdown induces apoptosis in lung cancer cells by causing uracil misincorporation. *Cell Death Dis,* 5**,** e1525.

PATEL, J. P., GONEN, M., FIGUEROA, M. E., FERNANDEZ, H., SUN, Z., RACEVSKIS, J., VAN VLIERBERGHE, P., DOLGALEV, I., THOMAS, S., AMINOVA, O., HUBERMAN, K., CHENG, J., VIALE, A., SOCCI, N. D., HEGUY, A., CHERRY, A., VANCE, G., HIGGINS, R. R., KETTERLING, R. P., GALLAGHER, R. E., LITZOW, M., VAN DEN BRINK, M. R., LAZARUS, H. M., ROWE, J. M., LUGER, S., FERRANDO, A., PAIETTA, E., TALLMAN, M. S., MELNICK, A., ABDEL-WAHAB, O. & LEVINE, R. L. 2012. Prognostic relevance of integrated genetic profiling in acute myeloid leukemia. *N Engl J Med,* 366**,** 1079-89.

PETERS, T. J., BUCKLEY, M. J., STATHAM, A. L., PIDSLEY, R., SAMARAS, K., R, V. L., CLARK, S. J. & MOLLOY, P. L. 2015. De novo identification of differentially methylated regions in the human genome. *Epigenetics Chromatin,* 8**,** 6.

PHILLIPS, D. C., WOOLLARD, K. J. & GRIFFITHS, H. R. 2003. The anti-inflammatory actions of methotrexate are critically dependent upon the production of reactive oxygen species. *Br J Pharmacol,* 138**,** 501-11.

PIERRACHE, L. H. M., KIMCHI, A., RATNAPRIYA, R., ROBERTS, L., ASTUTI, G. D. N., OBOLENSKY, A., BERYOZKIN, A., TJON-FO-SANG, M. J. H., SCHUIL, J., KLAVER, C. C. W., BONGERS, E., HAER-WIGMAN, L., SCHALIJ, N., BREUNING, M. H., FISCHER, G. M., BANIN, E., RAMESAR, R. S., SWAROOP, A., VAN DEN BORN, L. I., SHARON, D. & CREMERS, F. P. M. 2017. Whole-Exome Sequencing Identifies Biallelic IDH3A Variants as a Cause of Retinitis Pigmentosa Accompanied by Pseudocoloboma. *Ophthalmology,* 124**,** 992-1003.

PIETRAK, B., ZHAO, H., QI, H., QUINN, C., GAO, E., BOYER, J. G., CONCHA, N., BROWN, K., DURAISWAMI, C., WOOSTER, R., SWEITZER, S. & SCHWARTZ, B. 2011. A tale of two subunits: how the neomorphic R132H IDH1 mutation enhances production of alphaHG. *Biochemistry,* 50**,** 4804-12.

PISTOLLATO, F., ABBADI, S., RAMPAZZO, E., PERSANO, L., DELLA PUPPA, A., FRASSON, C., SARTO, E., SCIENZA, R., D'AVELLA, D. & BASSO, G. 2010. Intratumoral hypoxic gradient drives stem cells distribution and MGMT expression in glioblastoma. *Stem Cells,* 28**,** 851-62.

POLLARI, S., KAKONEN, S. M., EDGREN, H., WOLF, M., KOHONEN, P., SARA, H., GUISE, T., NEES, M. & KALLIONIEMI, O. 2011. Enhanced serine production by bone metastatic breast cancer cells stimulates osteoclastogenesis. *Breast Cancer Res Treat,* 125**,** 421-30.

POSSEMATO, R., MARKS, K. M., SHAUL, Y. D., PACOLD, M. E., KIM, D., BIRSOY, K., SETHUMADHAVAN, S., WOO, H. K., JANG, H. G., JHA, A. K., CHEN, W. W., BARRETT, F. G., STRANSKY, N., TSUN, Z. Y., COWLEY, G. S., BARRETINA, J., KALAANY, N. Y., HSU, P. P., OTTINA, K., CHAN, A. M., YUAN, B., GARRAWAY, L. A., ROOT, D. E., MINO-KENUDSON, M., BRACHTEL, E. F., DRIGGERS, E. M. & SABATINI, D. M. 2011. Functional genomics reveal that the serine synthesis pathway is essential in breast cancer. *Nature,* 476**,** 346-50.

PUCHALSKI, R. B., SHAH, N., MILLER, J., DALLEY, R., NOMURA, S. R., YOON, J. G., SMITH, K. A., LANKEROVICH, M., BERTAGNOLLI, D., BICKLEY, K., BOE, A. F., BROUNER, K., BUTLER, S., CALDEJON, S., CHAPIN, M., DATTA, S., DEE, N., DESTA, T., DOLBEARE, T., DOTSON, N., EBBERT, A., FENG, D., FENG, X., FISHER, M., GEE, G., GOLDY, J., GOURLEY, L., GREGOR, B. W., GU, G., HEJAZINIA, N., HOHMANN, J., HOTHI, P., HOWARD, R., JOINES, K., KRIEDBERG, A., KUAN, L., LAU, C., LEE, F., LEE, H., LEMON, T., LONG, F., MASTAN, N., MOTT, E., MURTHY, C., NGO, K., OLSON, E., REDING, M., RILEY, Z., ROSEN, D., SANDMAN, D., SHAPOVALOVA, N., SLAUGHTERBECK, C. R., SODT, A., STOCKDALE, G., SZAFER, A., WAKEMAN, W., WOHNOUTKA, P. E., WHITE, S. J., MARSH, D., ROSTOMILY, R. C., NG, L., DANG, C., JONES, A., KEOGH, B., GITTLEMAN, H. R., BARNHOLTZ-SLOAN, J. S., CIMINO, P. J., UPPIN, M. S., KEENE, C. D., FARROKHI, F. R., LATHIA, J. D., BERENS, M. E., IAVARONE, A., BERNARD, A., LEIN, E., PHILLIPS, J. W., ROSTAD, S. W., COBBS, C., HAWRYLYCZ, M. J.

& FOLTZ, G. D. 2018. An anatomic transcriptional atlas of human glioblastoma. *Science,* 360**,** 660-663.

QATTAN, A. T., RADULOVIC, M., CRAWFORD, M. & GODOVAC-ZIMMERMANN, J. 2012. Spatial distribution of cellular function: the partitioning of proteins between mitochondria and the nucleus in MCF7 breast cancer cells. *J Proteome Res,* 11**,** 6080-101.

QI, F., CHEN, X. & BEARD, D. A. 2008. Detailed kinetics and regulation of mammalian NAD-linked isocitrate dehydrogenase. *Biochimica et Biophysica Acta (BBA) - Proteins and Proteomics,* 1784**,** 1641-1651.

RAHMAN, L., VOELLER, D., RAHMAN, M., LIPKOWITZ, S., ALLEGRA, C., BARRETT, J. C., KAYE, F. J. & ZAJAC-KAYE, M. 2004. Thymidylate synthase as an oncogene: a novel role for an essential DNA synthesis enzyme. *Cancer Cell,* 5**,** 341-51.

RAMNARAIN, D. B., PARK, S., LEE, D. Y., HATANPAA, K. J., SCOGGIN, S. O., OTU, H., LIBERMANN, T. A., RAISANEN, J. M., ASHFAQ, R., WONG, E. T., WU, J., ELLIOTT, R. & HABIB, A. A. 2006. Differential gene expression analysis reveals generation of an autocrine loop by a mutant epidermal growth factor receptor in glioma cells. *Cancer Res,* 66**,** 867-74.

RAO, J. S. 2003. Molecular mechanisms of glioma invasiveness: the role of proteases. *Nat Rev Cancer,* 3**,** 489-501.

REITMAN, Z. J. & YAN, H. 2010. Isocitrate dehydrogenase 1 and 2 mutations in cancer: alterations at a crossroads of cellular metabolism. *J Natl Cancer Inst,* 102**,** 932-41.

RHEINBAY, E., SUVA, M. L., GILLESPIE, S. M., WAKIMOTO, H., PATEL, A. P., SHAHID, M., OKSUZ, O., RABKIN, S. D., MARTUZA, R. L., RIVERA, M. N., LOUIS, D. N., KASIF, S., CHI, A. S. & BERNSTEIN, B. E. 2013. An aberrant transcription factor network essential for Wnt signaling and stem cell maintenance in glioblastoma. *Cell Rep,* 3**,** 1567-79.

RITCHIE, M. E., PHIPSON, B., WU, D., HU, Y., LAW, C. W., SHI, W. & SMYTH, G. K. 2015. limma powers differential expression analyses for RNA-sequencing and microarray studies. *Nucleic Acids Res,* 43**,** e47.

RIVERA, A. L., PELLOSKI, C. E., GILBERT, M. R., COLMAN, H., DE LA CRUZ, C., SULMAN, E. P., BEKELE, B. N. & ALDAPE, K. D. 2010. MGMT promoter methylation is predictive of response to radiotherapy and prognostic in the absence of adjuvant alkylating chemotherapy for glioblastoma. *Neuro Oncol,* 12**,** 116-21.

ROBINSON, M. D. & OSHLACK, A. 2010. A scaling normalization method for differential expression analysis of RNA-seq data. *Genome Biol,* 11**,** R25.

ROHLE, D., POPOVICI-MULLER, J., PALASKAS, N., TURCAN, S., GROMMES, C., CAMPOS, C., TSOI, J., CLARK, O., OLDRINI, B., KOMISOPOULOU, E., KUNII, K., PEDRAZA, A., SCHALM, S., SILVERMAN, L., MILLER, A., WANG, F., YANG, H., CHEN, Y., KERNYTSKY, A., ROSENBLUM, M. K., LIU, W., BILLER, S. A., SU, S. M., BRENNAN, C. W., CHAN, T. A., GRAEBER, T. G., YEN, K. E. & MELLINGHOFF, I. K. 2013. An inhibitor of mutant IDH1 delays growth and promotes differentiation of glioma cells. *Science,* 340**,** 626-30.

SASAKI, M., KNOBBE, C. B., ITSUMI, M., ELIA, A. J., HARRIS, I. S., CHIO, II, CAIRNS, R. A., MCCRACKEN, S., WAKEHAM, A., HAIGHT, J., TEN, A. Y., SNOW, B., UEDA, T., INOUE, S., YAMAMOTO, K., KO, M., RAO, A., YEN, K. E., SU, S. M. & MAK, T. W. 2012a. D-2-hydroxyglutarate produced by mutant IDH1 perturbs collagen maturation and basement membrane function. *Genes Dev,* 26**,** 2038-49.

SASAKI, M., KNOBBE, C. B., MUNGER, J. C., LIND, E. F., BRENNER, D., BRUSTLE, A., HARRIS, I. S., HOLMES, R., WAKEHAM, A., HAIGHT, J., YOU-TEN, A., LI, W. Y., SCHALM, S., SU, S. M., VIRTANEN, C., REIFENBERGER, G., OHASHI, P. S., BARBER, D. L., FIGUEROA, M. E., MELNICK, A., ZUNIGA-PFLUCKER, J. C. & MAK, T. W. 2012b. IDH1(R132H) mutation increases murine haematopoietic progenitors and alters epigenetics. *Nature,* 488**,** 656-9.

SEIDEL, S., GARVALOV, B. K., WIRTA, V., VON STECHOW, L., SCHANZER, A., MELETIS, K., WOLTER, M., SOMMERLAD, D., HENZE, A. T., NISTER, M., REIFENBERGER, G.,

LUNDEBERG, J., FRISEN, J. & ACKER, T. 2010. A hypoxic niche regulates glioblastoma stem cells through hypoxia inducible factor 2 alpha. *Brain,* 133**,** 983-95.

SHAPIRO, J. R., YUNG, W. K. & SHAPIRO, W. R. 1981. Isolation, karyotype, and clonal growth of heterogeneous subpopulations of human malignant gliomas. *Cancer Res,* 41**,** 2349-59.

SHEN, L., SUN, X., FU, Z., YANG, G., LI, J. & YAO, L. 2012. The fundamental role of the p53 pathway in tumor metabolism and its implication in tumor therapy. *Clin Cancer Res,* 18**,** 1561-7.

SHLOMI, T., FAN, J., TANG, B., KRUGER, W. D. & RABINOWITZ, J. D. 2014. Quantitation of cellular metabolic fluxes of methionine. *Anal Chem,* 86**,** 1583-91.

SICA, A., ALLAVENA, P. & MANTOVANI, A. 2008. Cancer related inflammation: the macrophage connection. *Cancer Lett,* 267**,** 204-15.

SINGH, S. K., CLARKE, I. D., TERASAKI, M., BONN, V. E., HAWKINS, C., SQUIRE, J. & DIRKS, P. B. 2003. Identification of a cancer stem cell in human brain tumors. *Cancer Res,* 63**,** 5821-8.

SINGH, S. K., HAWKINS, C., CLARKE, I. D., SQUIRE, J. A., BAYANI, J., HIDE, T., HENKELMAN, R. M., CUSIMANO, M. D. & DIRKS, P. B. 2004. Identification of human brain tumour initiating cells. *Nature,* 432**,** 396-401.

SKIBOLA, C. F., SMITH, M. T., HUBBARD, A., SHANE, B., ROBERTS, A. C., LAW, G. R., ROLLINSON, S., ROMAN, E., CARTWRIGHT, R. A. & MORGAN, G. J. 2002. Polymorphisms in the thymidylate synthase and serine hydroxymethyltransferase genes and risk of adult acute lymphocytic leukemia. *Blood,* 99**,** 3786-91.

SNELL, K. 1985. Enzymes of serine metabolism in normal and neoplastic rat tissues. *Biochim Biophys Acta,* 843**,** 276-81.

SONESON, C., LOVE, M. I. & ROBINSON, M. D. 2015. Differential analyses for RNA-seq: transcript-level estimates improve gene-level inferences. *F1000Res,* 4**,** 1521.

SONG, H. & MOON, A. 2006. Glial cell-derived neurotrophic factor (GDNF) promotes low-grade Hs683 glioma cell migration through JNK, ERK-1/2 and p38 MAPK signaling pathways. *Neurosci Res,* 56**,** 29-38.

SONGTAO, Q., LEI, Y., SI, G., YANQING, D., HUIXIA, H., XUELIN, Z., LANXIAO, W. & FEI, Y. 2012. IDH mutations predict longer survival and response to temozolomide in secondary glioblastoma. *Cancer Sci,* 103**,** 269-73.

SOUNDAR, S., O'HAGAN, M., FOMULU, K. S. & COLMAN, R. F. 2006. Identification of Mn2+-binding aspartates from alpha, beta, and gamma subunits of human NAD-dependent isocitrate dehydrogenase. *J Biol Chem,* 281**,** 21073-81.

SREEKUMAR, A., POISSON, L. M., RAJENDIRAN, T. M., KHAN, A. P., CAO, Q., YU, J., LAXMAN, B., MEHRA, R., LONIGRO, R. J., LI, Y., NYATI, M. K., AHSAN, A., KALYANA-SUNDARAM, S., HAN, B., CAO, X., BYUN, J., OMENN, G. S., GHOSH, D., PENNATHUR, S., ALEXANDER, D. C., BERGER, A., SHUSTER, J. R., WEI, J. T., VARAMBALLY, S., BEECHER, C. & CHINNAIYAN, A. M. 2009. Metabolomic profiles delineate potential role for sarcosine in prostate cancer progression. *Nature,* 457**,** 910-4.

STUMMER, W., PICHLMEIER, U., MEINEL, T., WIESTLER, O. D., ZANELLA, F., REULEN, H. J. & GROUP, A. L.-G. S. 2006. Fluorescence-guided surgery with 5-aminolevulinic acid for resection of malignant glioma: a randomised controlled multicentre phase III trial. *Lancet Oncol,* 7**,** 392-401.

STUPP, R., HEGI, M. E., MASON, W. P., VAN DEN BENT, M. J., TAPHOORN, M. J., JANZER, R. C., LUDWIN, S. K., ALLGEIER, A., FISHER, B., BELANGER, K., HAU, P., BRANDES, A. A., GIJTENBEEK, J., MAROSI, C., VECHT, C. J., MOKHTARI, K., WESSELING, P., VILLA, S., EISENHAUER, E., GORLIA, T., WELLER, M., LACOMBE, D., CAIRNCROSS, J. G., MIRIMANOFF, R. O., EUROPEAN ORGANISATION FOR, R., TREATMENT OF CANCER BRAIN, T., RADIATION ONCOLOGY, G. & NATIONAL CANCER INSTITUTE OF CANADA CLINICAL TRIALS, G. 2009. Effects of radiotherapy with concomitant and adjuvant temozolomide versus radiotherapy alone on survival in glioblastoma in a randomised phase III study: 5-year analysis of the EORTC-NCIC trial. *Lancet Oncol,* 10**,** 459-66.

STUPP, R., MASON, W. P., VAN DEN BENT, M. J., WELLER, M., FISHER, B., TAPHOORN, M. J., BELANGER, K., BRANDES, A. A., MAROSI, C., BOGDAHN, U., CURSCHMANN, J., JANZER, R. C., LUDWIN, S. K., GORLIA, T., ALLGEIER, A., LACOMBE, D., CAIRNCROSS, J. G., EISENHAUER, E., MIRIMANOFF, R. O., EUROPEAN ORGANISATION FOR, R., TREATMENT OF CANCER BRAIN, T., RADIOTHERAPY, G. & NATIONAL CANCER INSTITUTE OF CANADA CLINICAL TRIALS, G. 2005. Radiotherapy plus concomitant and adjuvant temozolomide for glioblastoma. *N Engl J Med,* 352**,** 987-96.

STUPP, R., TAILLIBERT, S., KANNER, A., READ, W., STEINBERG, D. M., LHERMITTE, B., TOMS, S., IDBAIH, A., AHLUWALIA, M. S., FINK, K., DI MECO, F., LIEBERMAN, F., ZHU, J. J., STRAGLIOTTO, G., TRAN, D. D., BREM, S., HOTTINGER, A. F., KIRSON, E. D., LAVY-SHAHAF, G., WEINBERG, U., KIM, C. Y., PAEK, S. H., NICHOLAS, G., BURNA, J., HIRTE, H., WELLER, M., PALTI, Y., HEGI, M. E. & RAM, Z. 2017. Effect of Tumor-Treating Fields Plus Maintenance Temozolomide vs Maintenance Temozolomide Alone on Survival in Patients With Glioblastoma: A Randomized Clinical Trial. *JAMA,* 318**,** 2306-2316.

STUPP, R., WONG, E. T., KANNER, A. A., STEINBERG, D., ENGELHARD, H., HEIDECKE, V., KIRSON, E. D., TAILLIBERT, S., LIEBERMANN, F., DBALY, V., RAM, Z., VILLANO, J. L., RAINOV, N., WEINBERG, U., SCHIFF, D., KUNSCHNER, L., RAIZER, J., HONNORAT, J., SLOAN, A., MALKIN, M., LANDOLFI, J. C., PAYER, F., MEHDORN, M., WEIL, R. J., PANNULLO, S. C., WESTPHAL, M., SMRCKA, M., CHIN, L., KOSTRON, H., HOFER, S., BRUCE, J., COSGROVE, R., PALEOLOGOUS, N., PALTI, Y. & GUTIN, P. H. 2012. NovoTTF-100A versus physician's choice chemotherapy in recurrent glioblastoma: a randomised phase III trial of a novel treatment modality. *Eur J Cancer,* 48**,** 2192-202.

SUN, W. Y., KIM, H. M., JUNG, W. H. & KOO, J. S. 2016. Expression of serine/glycine metabolism-related proteins is different according to the thyroid cancer subtype. *J Transl Med,* 14**,** 168.

TIBBETTS, A. S. & APPLING, D. R. 2010. Compartmentalization of Mammalian folate-mediated one-carbon metabolism. *Annu Rev Nutr,* 30**,** 57-81.

TSAI, J. C., GOLDMAN, C. K. & GILLESPIE, G. Y. 1995. Vascular endothelial growth factor in human glioma cell lines: induced secretion by EGF, PDGF-BB, and bFGF. *J Neurosurg,* 82**,** 864-73.

TURCAN, S., ROHLE, D., GOENKA, A., WALSH, L. A., FANG, F., YILMAZ, E., CAMPOS, C., FABIUS, A. W., LU, C., WARD, P. S., THOMPSON, C. B., KAUFMAN, A., GURYANOVA, O., LEVINE, R., HEGUY, A., VIALE, A., MORRIS, L. G., HUSE, J. T., MELLINGHOFF, I. K. & CHAN, T. A. 2012. IDH1 mutation is sufficient to establish the glioma hypermethylator phenotype. *Nature,* 483**,** 479-83.

UNRUH, D., SCHWARZE, S. R., KHOURY, L., THOMAS, C., WU, M., CHEN, L., CHEN, R., LIU, Y., SCHWARTZ, M. A., AMIDEI, C., KUMTHEKAR, P., BENJAMIN, C. G., SONG, K., DAWSON, C., RISPOLI, J. M., FATTERPEKAR, G., GOLFINOS, J. G., KONDZIOLKA, D., KARAJANNIS, M., PACIONE, D., ZAGZAG, D., MCINTYRE, T., SNUDERL, M. & HORBINSKI, C. 2016. Mutant IDH1 and thrombosis in gliomas. *Acta Neuropathol,* 132**,** 917-930.

VAN MEIR, E. G., HADJIPANAYIS, C. G., NORDEN, A. D., SHU, H. K., WEN, P. Y. & OLSON, J. J. 2010. Exciting new advances in neuro-oncology: the avenue to a cure for malignant glioma. *CA Cancer J Clin,* 60**,** 166-93.

VAN SCHAFTINGEN, E., RZEM, R., MARBAIX, A., COLLARD, F., VEIGA-DA-CUNHA, M. & LINSTER, C. L. 2013. Metabolite proofreading, a neglected aspect of intermediary metabolism. *J Inherit Metab Dis,* 36**,** 427-34.

VELPULA, K. K., BHASIN, A., ASUTHKAR, S. & TSUNG, A. J. 2013. Combined targeting of PDK1 and EGFR triggers regression of glioblastoma by reversing the Warburg effect. *Cancer Res,* 73**,** 7277-89.

VERHAAK, R. G., HOADLEY, K. A., PURDOM, E., WANG, V., QI, Y., WILKERSON, M. D., MILLER, C. R., DING, L., GOLUB, T., MESIROV, J. P., ALEXE, G., LAWRENCE, M., O'KELLY, M., TAMAYO, P., WEIR, B. A., GABRIEL, S., WINCKLER, W., GUPTA, S., JAKKULA, L., FEILER, H. S., HODGSON, J. G., JAMES, C. D., SARKARIA, J. N., BRENNAN, C., KAHN, A., SPELLMAN,

P. T., WILSON, R. K., SPEED, T. P., GRAY, J. W., MEYERSON, M., GETZ, G., PEROU, C. M., HAYES, D. N. & CANCER GENOME ATLAS RESEARCH, N. 2010. Integrated genomic analysis identifies clinically relevant subtypes of glioblastoma characterized by abnormalities in PDGFRA, IDH1, EGFR, and NF1. *Cancer Cell,* 17**,** 98-110.

VILLANO, J. L., SEERY, T. E. & BRESSLER, L. R. 2009. Temozolomide in malignant gliomas: current use and future targets. *Cancer Chemother Pharmacol,* 64**,** 647-55.

WAINWRIGHT, D. A., BALYASNIKOVA, I. V., CHANG, A. L., AHMED, A. U., MOON, K. S., AUFFINGER, B., TOBIAS, A. L., HAN, Y. & LESNIAK, M. S. 2012. IDO expression in brain tumors increases the recruitment of regulatory T cells and negatively impacts survival. *Clin Cancer Res,* 18**,** 6110-21.

WANG, Q., HU, B., HU, X., KIM, H., SQUATRITO, M., SCARPACE, L., DECARVALHO, A. C., LYU, S., LI, P., LI, Y., BARTHEL, F., CHO, H. J., LIN, Y. H., SATANI, N., MARTINEZ-LEDESMA, E., ZHENG, S., CHANG, E., SAUVE, C. G., OLAR, A., LAN, Z. D., FINOCCHIARO, G., PHILLIPS, J. J., BERGER, M. S., GABRUSIEWICZ, K. R., WANG, G., ESKILSSON, E., HU, J., MIKKELSEN, T., DEPINHO, R. A., MULLER, F., HEIMBERGER, A. B., SULMAN, E. P., NAM, D. H. & VERHAAK, R. G. W. 2017. Tumor Evolution of Glioma-Intrinsic Gene Expression Subtypes Associates with Immunological Changes in the Microenvironment. *Cancer Cell,* 32**,** 42-56 e6.

WANG, Q., LU, K., DU, H., ZHANG, Q., CHEN, T., SHU, Y., HUA, Y. & ZHU, L. 2014. Association between cytosolic serine hydroxymethyltransferase (SHMT1) gene polymorphism and cancer risk: a meta-analysis. *Biomed Pharmacother,* 68**,** 757-62.

WARD, P. S., CROSS, J. R., LU, C., WEIGERT, O., ABEL-WAHAB, O., LEVINE, R. L., WEINSTOCK, D. M., SHARP, K. A. & THOMPSON, C. B. 2012. Identification of additional IDH mutations associated with oncometabolite R(-)-2-hydroxyglutarate production. *Oncogene,* 31**,** 2491-8.

WATANABE, K., TACHIBANA, O., SATA, K., YONEKAWA, Y., KLEIHUES, P. & OHGAKI, H. 1996. Overexpression of the EGF receptor and p53 mutations are mutually exclusive in the evolution of primary and secondary glioblastomas. *Brain Pathol,* 6**,** 217-23; discussion 23-4.

WATANABE, T., NOBUSAWA, S., KLEIHUES, P. & OHGAKI, H. 2009. IDH1 mutations are early events in the development of astrocytomas and oligodendrogliomas. *Am J Pathol,* 174**,** 1149-53.

WATTERS, J. J., SCHARTNER, J. M. & BADIE, B. 2005. Microglia function in brain tumors. *J Neurosci Res,* 81**,** 447-55.

WEI, J., WU, A., KONG, L. Y., WANG, Y., FULLER, G., FOKT, I., MELILLO, G., PRIEBE, W. & HEIMBERGER, A. B. 2011. Hypoxia potentiates glioma-mediated immunosuppression. *PLoS One,* 6**,** e16195.

WEN, P. Y. & KESARI, S. 2008. Malignant gliomas in adults. *N Engl J Med,* 359**,** 492-507.

WEN, P. Y., SCHIFF, D., KESARI, S., DRAPPATZ, J., GIGAS, D. C. & DOHERTY, L. 2006. Medical management of patients with brain tumors. *J Neurooncol,* 80**,** 313-32.

WOELLER, C. F., ANDERSON, D. D., SZEBENYI, D. M. E. & STOVER, P. J. 2007. Evidence for Small Ubiquitin-like Modifier-dependent Nuclear Import of the Thymidylate Biosynthesis Pathway. *Journal of Biological Chemistry,* 282**,** 17623-17631.

WRENSCH, M., MINN, Y., CHEW, T., BONDY, M. & BERGER, M. S. 2002. Epidemiology of primary brain tumors: current concepts and review of the literature. *Neuro Oncol,* 4**,** 278-99.

WU, S., ZHANG, G., LI, P., CHEN, S., ZHANG, F., LI, J., JIANG, C., CHEN, X., WANG, Y., DU, Y., SUN, Q. & ZHAO, G. 2016. miR-198 targets SHMT1 to inhibit cell proliferation and enhance cell apoptosis in lung adenocarcinoma. *Tumour Biol,* 37**,** 5193-202.

XIAO, M., YANG, H., XU, W., MA, S., LIN, H., ZHU, H., LIU, L., LIU, Y., YANG, C., XU, Y., ZHAO, S., YE, D., XIONG, Y. & GUAN, K. L. 2012. Inhibition of alpha-KG-dependent histone and DNA demethylases by fumarate and succinate that are accumulated in mutations of FH and SDH tumor suppressors. *Genes Dev,* 26**,** 1326-38.

XU, W., YANG, H., LIU, Y., YANG, Y., WANG, P., KIM, S. H., ITO, S., YANG, C., WANG, P., XIAO, M. T., LIU, L. X., JIANG, W. Q., LIU, J., ZHANG, J. Y., WANG, B., FRYE, S., ZHANG, Y., XU, Y. H.,

LEI, Q. Y., GUAN, K. L., ZHAO, S. M. & XIONG, Y. 2011. Oncometabolite 2-hydroxyglutarate is a competitive inhibitor of alpha-ketoglutarate-dependent dioxygenases. *Cancer Cell,* 19**,** 17-30.

XU, X., ZHAO, J., XU, Z., PENG, B., HUANG, Q., ARNOLD, E. & DING, J. 2004. Structures of human cytosolic NADP-dependent isocitrate dehydrogenase reveal a novel self-regulatory mechanism of activity. *J Biol Chem,* 279**,** 33946-57.

YAN, H., BIGNER, D. D., VELCULESCU, V. & PARSONS, D. W. 2009a. Mutant metabolic enzymes are at the origin of gliomas. *Cancer Res,* 69**,** 9157-9.

YAN, H., PARSONS, D. W., JIN, G., MCLENDON, R., RASHEED, B. A., YUAN, W., KOS, I., BATINIC-HABERLE, I., JONES, S., RIGGINS, G. J., FRIEDMAN, H., FRIEDMAN, A., REARDON, D., HERNDON, J., KINZLER, K. W., VELCULESCU, V. E., VOGELSTEIN, B. & BIGNER, D. D. 2009b. IDH1 and IDH2 mutations in gliomas. *N Engl J Med,* 360**,** 765-73.

YAN, K., WU, Q., YAN, D. H., LEE, C. H., RAHIM, N., TRITSCHLER, I., DEVECCHIO, J., KALADY, M. F., HJELMELAND, A. B. & RICH, J. N. 2014. Glioma cancer stem cells secrete Gremlin1 to promote their maintenance within the tumor hierarchy. *Genes Dev,* 28**,** 1085-100.

YANG, H., YE, D., GUAN, K. L. & XIONG, Y. 2012. IDH1 and IDH2 mutations in tumorigenesis: mechanistic insights and clinical perspectives. *Clin Cancer Res,* 18**,** 5562-71.

YE, J., MANCUSO, A., TONG, X., WARD, P. S., FAN, J., RABINOWITZ, J. D. & THOMPSON, C. B. 2012. Pyruvate kinase M2 promotes de novo serine synthesis to sustain mTORC1 activity and cell proliferation. *Proc Natl Acad Sci U S A,* 109**,** 6904-9.

YOSHIDA, K., FURUYA, S., OSUKA, S., MITOMA, J., SHINODA, Y., WATANABE, M., AZUMA, N., TANAKA, H., HASHIKAWA, T., ITOHARA, S. & HIRABAYASHI, Y. 2004. Targeted disruption of the mouse 3-phosphoglycerate dehydrogenase gene causes severe neurodevelopmental defects and results in embryonic lethality. *J Biol Chem,* 279**,** 3573-7.

YOSHIMI, N., FUTAMURA, T., BERGEN, S. E., IWAYAMA, Y., ISHIMA, T., SELLGREN, C., EKMAN, C. J., JAKOBSSON, J., PALSSON, E., KAKUMOTO, K., OHGI, Y., YOSHIKAWA, T., LANDEN, M. & HASHIMOTO, K. 2016. Cerebrospinal fluid metabolomics identifies a key role of isocitrate dehydrogenase in bipolar disorder: evidence in support of mitochondrial dysfunction hypothesis. *Mol Psychiatry,* 21**,** 1504-1510.

YUNG, W. K., SHAPIRO, J. R. & SHAPIRO, W. R. 1982. Heterogeneous chemosensitivities of subpopulations of human glioma cells in culture. *Cancer Res,* 42**,** 992-8.

ZANETTI, K. A. & STOVER, P. J. 2003. Pyridoxal phosphate inhibits dynamic subunit interchange among serine hydroxymethyltransferase tetramers. *J Biol Chem,* 278**,** 10142-9.

ZEISBERGER, S. M., ODERMATT, B., MARTY, C., ZEHNDER-FJALLMAN, A. H., BALLMER-HOFER, K. & SCHWENDENER, R. A. 2006. Clodronate-liposome-mediated depletion of tumour-associated macrophages: a new and highly effective antiangiogenic therapy approach. *Br J Cancer,* 95**,** 272-81.

ZENG, L., MORINIBU, A., KOBAYASHI, M., ZHU, Y., WANG, X., GOTO, Y., YEOM, C. J., ZHAO, T., HIROTA, K., SHINOMIYA, K., ITASAKA, S., YOSHIMURA, M., GUO, G., HAMMOND, E. M., HIRAOKA, M. & HARADA, H. 2014. Aberrant IDH3alpha expression promotes malignant tumor growth by inducing HIF-1-mediated metabolic reprogramming and angiogenesis. *Oncogene*.

ZHAN, C. & LU, W. 2012. The blood-brain/tumor barriers: challenges and chances for malignant gliomas targeted drug delivery. *Curr Pharm Biotechnol,* 13**,** 2380-7.

ZHANG, D., WANG, Y., SHI, Z., LIU, J., SUN, P., HOU, X., ZHANG, J., ZHAO, S., ZHOU, B. P. & MI, J. 2015. Metabolic reprogramming of cancer-associated fibroblasts by IDH3alpha downregulation. *Cell Rep,* 10**,** 1335-48.

ZHANG, K., XU, P., SOWERS, J. L., MACHUCA, D. F., MIRFATTAH, B., HERRING, J., TANG, H., CHEN, Y., TIAN, B., BRASIER, A. R. & SOWERS, L. C. 2017. Proteome analysis of hypoxic glioblastoma cells reveals sequential metabolic adaptation of one-carbon metabolic pathways. *Mol Cell Proteomics*.

ZHANG, W. C., SHYH-CHANG, N., YANG, H., RAI, A., UMASHANKAR, S., MA, S., SOH, B. S., SUN, L. L., TAI, B. C., NGA, M. E., BHAKOO, K. K., JAYAPAL, S. R., NICHANE, M., YU, Q., AHMED, D.

A., TAN, C., SING, W. P., TAM, J., THIRUGANANAM, A., NOGHABI, M. S., PANG, Y. H., ANG, H. S., MITCHELL, W., ROBSON, P., KALDIS, P., SOO, R. A., SWARUP, S., LIM, E. H. & LIM, B. 2012. Glycine decarboxylase activity drives non-small cell lung cancer tumor-initiating cells and tumorigenesis. *Cell,* 148**,** 259-72.

ZHOU, F., XU, X., WU, J., WANG, D. & WANG, J. 2017. NF-kappaB controls four genes encoding core enzymes of tricarboxylic acid cycle. *Gene,* 621**,** 12-20.

ZHU, T. S., COSTELLO, M. A., TALSMA, C. E., FLACK, C. G., CROWLEY, J. G., HAMM, L. L., HE, X., HERVEY-JUMPER, S. L., HETH, J. A., MURASZKO, K. M., DIMECO, F., VESCOVI, A. L. & FAN, X. 2011. Endothelial cells create a stem cell niche in glioblastoma by providing NOTCH ligands that nurture self-renewal of cancer stem-like cells. *Cancer Res,* 71**,** 6061-72.